Rockefeller University
Digital Commons @ RU

Student Theses and Dissertations

2008

Further Insight into the Two Functions of Telomeres: Determining the Role of Tankyrase1 in Telomere Length Regulation and Tin2 in Telomere Protection

Jill Donigian

Follow this and additional works at: http://digitalcommons.rockefeller.edu/student_theses_and_dissertations

 Part of the Life Sciences Commons

Recommended Citation

Donigian, Jill, "Further Insight into the Two Functions of Telomeres: Determining the Role of Tankyrase1 in Telomere Length Regulation and Tin2 in Telomere Protection" (2008). *Student Theses and Dissertations*. Paper 195.

This Thesis is brought to you for free and open access by Digital Commons @ RU. It has been accepted for inclusion in Student Theses and Dissertations by an authorized administrator of Digital Commons @ RU. For more information, please contact mcsweej@mail.rockefeller.edu.

FURTHER INSIGHT INTO THE TWO FUNCTIONS OF TELOMERES: DETERMINING THE ROLE OF TANKYRASE1 IN TELOMERE LENGTH REGULATION AND TIN2 IN TELOMERE PROTECTION

A Thesis Presented to the Faculty of

The Rockefeller University

In Partial Fulfillment of the Requirements for

the Degree of Doctor of Philosophy

by

Jill Donigian

June 2008

© Copyright by Jill Donigian 2008

FURTHER INSIGHT INTO THE TWO FUNCTIONS OF TELOMERES: DETERMINING THE ROLE OF TANKYRASE1 IN TELOMERE LENGTH REGULATION AND TIN2 IN TELOMERE PROTECTION

Jill Donigian, Ph.D.

The Rockefeller University 2008

Tankyrase1 is a multifunctional poly(ADP-ribose) polymerase that can localize to telomeres through its interaction with the shelterin component TRF1. Tankyrase1 poly(ADP-ribosyl)ates TRF1 in vitro, and its nuclear overexpression leads to loss of TRF1 and telomere elongation, suggesting that tankyrase1 is a positive regulator of telomere length. In agreement with this proposal, we showed that tankyrase1 RNA interference results in telomere shortening proportional to the level of knockdown, while a tankyrase1-resistant form of TRF1 enforced normal telomere length control. Thus, in human cells, tankyrase1 appears to act upstream of TRF1, promoting telomere elongation through the removal of TRF1. This pathway appears absent from mouse cells. We demonstrated that murine TRF1, which lacks the tankyrase1-binding motif, is not a substrate for tankyrase1 poly(ADP-ribosyl)sylation in vitro. Furthermore, overexpression of tankyrase1 in mouse nuclei did not remove TRF1 from telomeres and had no detectable effect on other components of mouse shelterin. We propose that the tankyrase1-controlled telomere extension is a human-specific elaboration that allows additional control over telomere length in telomerase positive cells.

TIN2 interacts with the double-stranded telomeric DNA-binding proteins TRF1 and TRF2 independently or simultaneously, acting as a bridge linking TRF1 and TRF2 to TPP1 and POT1, the single-stranded telomeric DNA-binding protein. To gain further insight into the function of the TRF2-TIN2 complex, we created a TRF2 mutant that no longer associates with TIN2. Employing protein overlay assays, we established that TIN2 binds TRF2 within its hinge domain from residues 352 to 367. Deletion of this region led to the production of a TRF2 TIN2-binding mutant, $TRF2^{\Delta T}$, which abrogated TRF2-TIN2 binding in protein overlay assays and in immunoprecipitation analysis. Expression of $TRF2^{\Delta T}$ in MEFs that contain a conditionally null allele of TRF2 resulted in substantial loss of TIN2 from telomeres, the formation of telomere dysfunction induced foci (TIFs), and the appearance of multiple telomeric signals and telomere loss at chromatid ends. We show that the ATM signaling pathway is activated in response to the telomere dysfunction induced by loss of TIN2 from the TRF2 complex, suggesting that TIN2 assists TRF2 in suppressing ATM activation at telomeres.

ACKNOWLEDGEMENTS

Foremost I would like to thank my advisor, Titia de Lange, for her tremendous guidance throughout my *many* years in the lab. Her ability to postulate a question and her know-how to determine its answer is science at its best and what has made her the premier expert in our field. It was both exciting and humbling to go through this process under her mentorship. I would also like to thank her for providing such a clean and organized place to do science!

I would like to thank the members of my thesis committee, Magda Konarska and Mike Young, for the invaluable advice and perspective they have provided over the years. They always challenged and encouraged me at our yearly committee meetings. I would also like to express my appreciation to Carolyn Price, for serving as the external examiner on my thesis committee.

To the past and present members of the de Lange lab, I would like to express my gratitude for making the lab an intellectually stimulating and constructive work environment. I would particularly like to thank Jeffrey Ye, who initially trained me and made my transition into the lab so comfortable, and Hiro Takai, my bay-mate from the beginning. Giulia Celli, Eros Lazzerini-Denchi, Sean Rooney, and Agnel Sfeir were also exceedingly generous with their scientific knowledge, advice, and reagents. I would like to thank the former and current graduate students of the de Lange lab, Josh Silverman, Rich Wang, Jan-Peter Daniels, Wilhelm Palm, Dirk Hockemeyer, Megan van Overbeek, Nadya Dimitrova, and Peng Wu for their camaraderie and generosity with scientific advice and reagents. A special thank you to Kristina Hoke, who has become one of my best friends

over our years together in lab. Our unique ability to talk about telomeres in one sentence and the latest celebrity gossip in the next has helped us both to maintain our sanity during the arduous process of getting our degrees.

I would also like to thank Stew Barnes, Stephanie Blackwood, Heidi Moss, Heather Parsons, Vanessa Marrero, Sarah Hooper, Eliana Forero, Kaori Takai, Diana Argibay, and Rita Rodney for organizing the lab and making it a productive place to do research. Thank you to Devon White for always being my cheerleader and for many great conversations. I am also indebted to Lola MacRae for her help with formatting and proofreading my thesis. Additionally, the Rockefeller University Dean's Office has been extremely helpful during the dissertation process.

To my previous scientific mentors, Dr. Nikola Pavletich, Dr. Michael Finnin, Dr. Nancy Walworth, and Mr. Bennett, thank you for your guidance and encouragement. To my families in New Jersey and Virginia, thank you for all the love and support you have given me throughout my time in graduate school and always. I would especially like to acknowledge my "Gram", Theresa Hettesheimer and my "Pa", Marvin Adler, two of the smartest people, in life and love, I could have ever known. Finally, I would like to thank my husband, Dan, and my son, Max. Over our ten plus years together, Dan and I have worked side by side to help each other achieve our goals. I thank him for his love, patience, and humor. And to Max…he is for sure my most successful experiment! I would like to dedicate this thesis to Dan and Max.

TABLE OF CONTENTS

LIST OF FIGURES

LIST OF ABBREVIATIONS

ATM	Ataxia-Telangiectasia Mutated
ATR	ATM and Rad3-Related
ChIP	Chromatin Immunoprecipitation
DAPI	4,6-Diamidino-2-Phenylindole
DC	Dyskeratosis Congenita
FISH	Fluorescence In Situ Hybridization
GST	Glutathione S-Transferase
HJ	Holliday Junction
HR	Homologous Recombination
IF	Immunofluorescence
IP	Immunoprecipitation
IVT	In Vitro Translated Protein
MEF	Mouse Embryonic Fibroblast
MTS	Multiple Telomeric Signals
NHEJ	Non-Homologous End Joining
NLS	Nuclear Localization Signal
OB	Oligonucleotide/Oligosaccharide Binding
PAR	Poly(ADP-Ribose)
PARP	Poly(ADP-Ribose) Polymerase
PD	Population Doubling
PFGE	Pulsed Field Gel Electrophoresis
PNA	Peptide Nucleic Acid
POT1	Protector of Telomeres 1
RAP1	Repressor and Activator Protein 1
RNAi	RNA Interference
RPA	Replication Protein A
SA b-gal	Senescence Associated b-Galactosidase
shRNA	Short Hairpin RNA
SFE	Signal Free Ends
siRNA	Small Interfering RNA
TANK1	TRF1-Interacting Ankyrin-Related ADP-Ribose Polymerase 1

TBM	TRFH-Binding Motif
TERC	Telomerase Reverse RNA
TERT	Telomerase Reverse Transcriptase
TIF	Telomere Dysfunction Induced Foci
TIN2	TRF1-Interacting Protein 2
TPP1	TINT1, PTOP, PIP1
TRF1	TTAGGG Repeat Binding Factor 1
TRF2	TTAGGG Repeat Binding Factor 2
TRFH	TTAGGG Repeat Binding Factor Homology
T-SCE	Telomere Sister Chromatid Exchange

CHAPTER 1: INTRODUCTION

Telomeric DNA

Telomeres are nucleoprotein complexes that cap the ends of linear chromosomes in eukaryotic cells. This DNA-protein complex allows cells to distinguish between natural chromosome ends and DNA breaks, preventing activation of DNA damage signals and repair pathways and permitting stable replication of chromosome ends.

The DNA component of telomeres is composed of GC-rich repeats that can vary in composition and length depending on the organism. In vertebrates, telomeres are comprised of 5'-TTAGGG-3' tandem repeats that range in size from 2-20 kb for humans[25, 30, 85] (Fig. 1-1), 50-150 kb for laboratory mice[63], and 12-23 kb for canines[90].

The telomere terminus is not blunt-ended; instead, the 3' end extends a G-rich single-stranded overhang, commonly referred to as the 3' overhang or G-overhang[79, 82] (Fig. 1-1). It is likely that the G-overhang is a product of C-strand degradation by a nuclease[79]. In humans, the C-strand preferentially ends with the sequence 3'-CCAATC-5', suggesting that processing of the C strand terminus is tightly regulated. Conversely, the last base of the 3' overhang shows much variation[103] (Fig. 1-1).

The G-overhang is thought to invade the duplex telomeric DNA forming a lariat-like structure termed the t-loop[42] (Fig. 1-1). At the invasion site, the overhang base pairs with the C-strand, displacing the G-strand and forming a displacement loop (D loop). It is possible that recruitment of homologous recombination factors to telomeres is responsible for generating t-loops[122]. Using electron microscopy, t-loops have been visualized at the telomeres of various organisms including vertebrates, worms, plants, trypanosomes, and ciliates[12, 42, 86, 88, 95]. This conserved structure is proposed to play a role in telomere protection and length regulation.

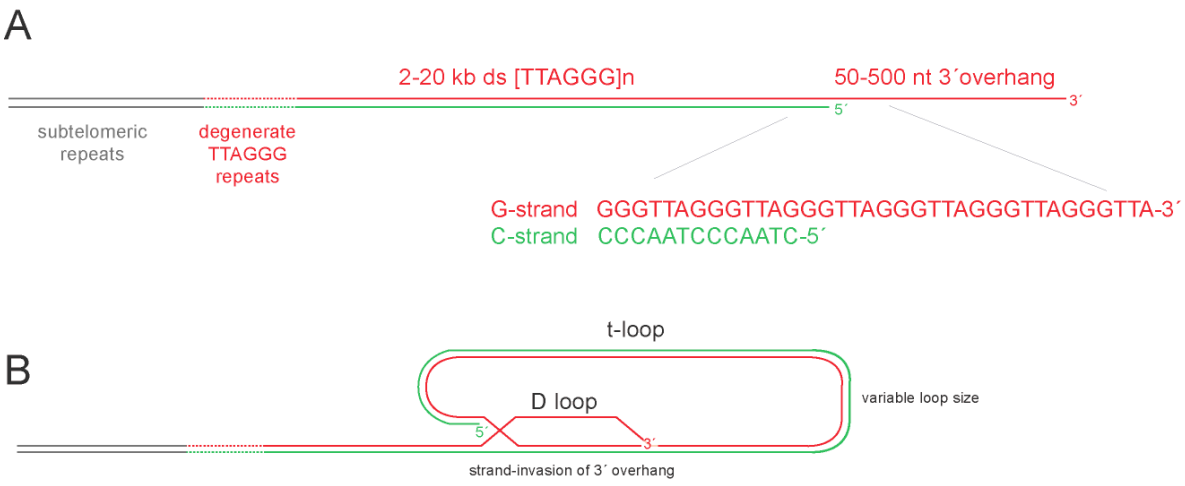

Figure 1-1. The structure of human telomeres.

(A) Human chromosomes end in an array of TTAGGG repeats that varies in length. Proximal to the telomeric repeats is a segment of degenerate repeats and subtelomeric repetitive elements. The telomere terminus contains a long G-strand overhang. The 3' end is not precisely defined whereas the 5' end of human chromosomes nearly always features the sequence ATC-5'. (B) Schematic of the t-loop structure. The size of the loop is variable.

Telomere Maintenance by Telomerase

With each successive cell division, human primary cells suffer a loss of telomeric DNA. A small percentage of this loss is attributable to the "end replication problem"[92, 128]. Initiation of DNA synthesis requires an RNA primer, which is later degraded and filled in by DNA polymerase. However, lack of 3'-5' polymerization activity prevents DNA polymerase from extending the very end of the lagging strand left by the last RNA primer. This gap left by the RNA primer results in loss of telomeric DNA at a rate of about 3 bp/end/cell division. However, the shortening rate of human telomeres is actually around 50-200 bp/end/cell division[52]. Nuclease attack of chromosome ends is likely responsible for such an increased rate of telomere loss.

To counteract telomere attrition, chromosome ends are maintained primarily by the enzyme telomerase[40, 41]. Composed of a telomere-specific reverse transcriptase (TERT) and an RNA subunit (TERC), telomerase uses the 3' end of the chromosome as a primer for reverse transcription of a short template sequence near the 5' end of its RNA[37, 40, 41, 72, 89]. The RNA template is transcribed repeatedly, generating a tandem array of G-rich repeats. Telomere length maintenance is highly regulated at the level of telomerase expression[8].

Catalytically active human telomerase consists of hTERT, hTERC, and the RNA-binding protein dyskerin[18]. Mutations in hTERT, the RNA component of telomerase, dyskerin, or NOP10, a component of H/ACA snoRNP complexes, are associated with the human disease dyskeratosis congenita (DC)[83, 124, 125, 132]. Patients with DC have severe bone marrow failure in addition to abnormal skin pigmentation, leukoplakia, and nail dystophy. Affected individuals also exhibit chromosome instability and a predisposition to develop certain types of malignancy[33, 83]. These phenotypes are thought to result from the inability of telomerase to maintain the telomeres in stem cell compartments[83].

With the exception of germ line and stem cells, most adult human cells do not express telomerase[60]. The telomeres of these cells continue to shorten with each division, and eventually the cells enter an irreversible state of arrested growth called replicative senescence[44, 45]. Limiting the proliferative potential of cells can be viewed as a tumor suppressor mechanism. However, in most tumor cells, this pathway is disabled by telomerase activation, allowing telomeres to be maintained at a length long enough for continued growth[60]. This same phenomenon is seen in cell culture, where expression of hTERT in telomerase-negative human primary fibroblasts leads to telomere elongation and cellular immortalization[8, 84].

The Shelterin Complex

Chromosome ends are protected and regulated by shelterin, a complex of six proteins (TRF1, TRF2, TIN2, TPP1, POT1, and Rap1) found predominately at telomeres[29]. TRF1 and TRF2 bind directly to double-stranded TTAGGG repeats, serving as anchors for other proteins to be recruited to telomeres[5, 7, 9, 17, 122]. Rap1 is a TRF2-interacting partner[70] while TIN2 binds both TRF1 and TRF2, stabilizing their association with chromosome ends[61, 134]. TIN2 also binds TPP1[49, 74, 135], which, in turn, recruits POT1, the single-stranded telomeric DNA binding protein[4, 76]. These six proteins can be found in a single complex or as separate TRF1 and TRF2/Rap1 subcomplexes each linked to TIN2-TPP1-POT1[73, 134].

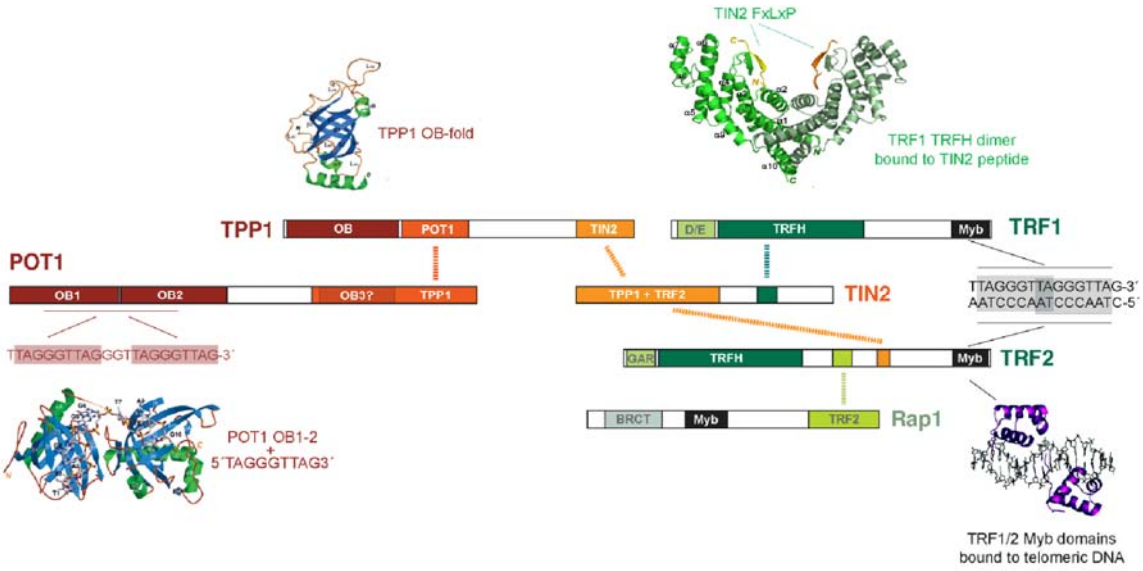

Figure 2-2. The shelterin complex.

The domain structures and interactions among the six components of human shelterin. Domains whose structures have been determined are shown. See text for references.

TRF1 and TRF2

TRF1 was the first human telomeric protein to be discovered, based on its ability to bind telomeric DNA[17]. TRF2 was identified through database searches as a TRF-like protein[7, 9]. The TRF proteins share a similar domain structure except at the N-terminus; TRF1 has an acidic domain, while TRF2 has a basic domain. Adjacent to the N-terminus is the TRF homology (TRFH) domain, which mediates homodimerization of the TRF proteins as well as interactions with binding partners. The three-dimensional structures of the TRFH domains of TRF1 and TRF2 are almost identical, yet heterodimerization does not occur due to steric constraints[36]. TRF1 and TRF2 bind double stranded TTAGGG repeats as homodimers using a conserved Myb domain in their C-terminus. The TRFH and Myb domain is connected by a flexible hinge domain, which allows the two Myb domains of a TRF1 dimer to bind DNA with little constraint on distance or orientation[5, 6].

TRF1 and TRF2 are both implicated in telomere length regulation, although the main function of TRF2 is to protect telomeres from being recognized as sites of DNA damage (discussed in detail below). Overexpression of TRF1 in the fibrosarcoma cell line HT1080 leads to a gradual and progressive shortening of telomeres, while a dominant-negative

mutant allele of TRF1, which lacks the DNA-binding Myb domain, induces telomere elongation[111, 121]. Dissection of these phenotypes led to the conclusion that TRF1 acts as a negative regulator of telomere length in telomerase-positive cells. Overexpression of TRF2 in the same cell line leads to an initial telomere shortening phenotype, implying TRF2 is also a negative regulator of telomere length[111]. Additionally, overexpression of TRF2 in telomerase-inhibited cells increases the rate of telomere shortening[1, 58].

Rap1

Human Rap1 was identified in a yeast two-hybrid screen using TRF2 as bait[70]. This TRF2-interacting protein is comprised of three distinguishable domains including an N-terminal BRCT domain, a central Myb domain, and an acidic RCT domain (Rap1 C-terminus) that mediates the interaction with a small motif in the hinge domain of TRF2. Despite having a Myb domain, Rap1 does not bind TTAGGG repeats, but instead is recruited to telomeres through its association with TRF2[70]. Rap1 is removed from telomeres and destabilized upon deletion of TRF2[10, 70]. Overexpression studies indicate that Rap1 is a negative regulator of telomere length and also imply that the BRCT domain of Rap1 influences telomere

length homogeneity[69]. Rap1 is an essential gene in mice, suggesting a possible role in telomere protection (van Overbeek and de Lange, unpublished).

TIN2

TIN2 was originally identified as a TRF1-interacting protein in a yeast two-hybrid screen[62]. It is now known that TIN2 interacts with both TRF1 and TRF2[49, 61, 134]. Crystallography studies reveal that TIN2 binds the TRFH domain of TRF1 using a small C-terminal peptide that contains a conserved F-X-L-X-P TRFH-docking motif [15]. TRF2 association is mediated through the N-terminus of TIN2 and a small sequence in the hinge domain of TRF2[15]. TIN2 can bind TRF1 and TRF2 independently or simultaneously, stabilizing the association of shelterin with telomeric DNA. Disruption of TIN2 by RNAi or mutation results in a DNA damage response at telomeres[61, 134]. Similar studies also suggest that TIN2 is a negative regulator of telomere length[62, 133]. TIN2 exerts its control over telomere length by protecting TRF1 from poly(ADP-ribosyl)ation (PARsylation) by the telomeric poly(ADP-ribose) polymerase (PARP), tankyrase1, and contributing to the accumulation of the TRF1 complex on telomeres[133]. TIN2 also recruits POT1 to telomeres, which, as discussed below, acts at the telomere terminus to inhibit telomerase[59, 74, 76, 135].

In addition to binding to TRF1 and TRF2, TIN2 interacts with a third partner, TPP1. TPP1 was discovered in biochemical experiments that sought TIN2 and POT1 interacting factors[49, 61, 74, 135]. The N-terminus of TIN2 localizes TPP1 to telomeres, which in turn, recruits POT1 to chromosome ends. Hence, TIN2 is the linchpin of shelterin, mediating interactions between double- and single-stranded telomeric DNA-binding proteins.

TPP1/POT1

TPP1 uses its C-terminus to bind TIN2 and a centrally located domain to interact with POT1[74, 135]. POT1 associates with TPP1 through its C-terminus and contains two oligonucleotide/ oligosaccharide-binding (OB) folds that are highly specific for single-stranded telomeric DNA at its N-terminus[4, 76, 77]. The majority of POT1 is recruited to telomeres through the TPP1/TIN2 link to TRF1 and TRF2, and not through its ability to bind DNA[47, 74, 130, 135]. Data from several different experiments support this claim. The deletion of the first OB fold of POT1 ($POT1^{\Delta OB}$) inhibits it from binding DNA, but does not prevent the recruitment of POT1 to telomeres[76]. Furthermore, ChIP data suggests that longer telomeres recruit more POT1, even though the single-stranded DNA remains unaltered[76]. Additionally,

depletion of TPP1 or expression of TPP1 mutants deficient in POT1 binding leads to removal of all detectable POT1 from telomeres. Finally, human POT1 is only recruited to telomeres when TPP1 is present[47, 74, 130].

POT1 has been implicated in both telomere length regulation as well as telomere protection. Overexpression of a mutant form of POT1 that lacks the DNA-binding domain, POT1$^{\Delta OB}$, or shRNA-mediated reduction in POT1 protein levels abrogates TRF1-mediated control of telomere length and induces significant telomere elongation, suggesting that POT1 is a negative regulator of telomerase[74, 76, 135]. This is supported by in vitro experiments showing POT1, but not POT1$^{\Delta OB}$, has the ability to inhibit telomerase activity[59]. The protective function of POT1 was revealed by loss of POT1 studies in human and mouse cells. Cells depleted of POT1 experience a DNA damage response and a telomere length phenotype[46, 48, 129]. Not surprisingly, disruption of TPP1 function results in the same loss-of-POT1 phenotypes[74, 130, 135].

Shelterin Accessory Factors

Shelterin does not act alone to carry out the functions of telomeres; instead, a number of other proteins are recruited to chromosomes ends to assist in telomere maintenance. Most of these factors have roles independent

of telomere biology and only transiently associate with telomeres. In fact, the majority of these shelterin-associated proteins are DNA damage signaling and repair molecules.

TRF1-associated factors

The acidic N-terminus of TRF1 binds to tankyrase1 and 2, poly(ADP-ribose) polymerases that can modify TRF1. ADP-ribosylation of TRF1 impedes its DNA binding activity in vitro, and tankyrase overexpression removes TRF1 from telomeres and promotes its degradation[21, 54, 97, 98, 108]. TRF1 may also negatively regulate telomere length through its interaction with PINX1, a protein that can inhibit telomerase in vitro[136]. Additionally, TRF1 has been shown to bind Ku[51], the BLM RecQ helicase[71, 93], and the ATM kinase[64].

TRF2-associated factors

The TRF2-Rap1 complex interacts with a number of DNA damage/repair proteins. Pulldown experiments coupled to mass spectrometry analysis revealed that TRF2 associates with the Mre11-Rad50-Nbs1 complex and the ERCC1/XPF nucleotide excision repair endonuclease[137, 138]. The Mre11 complex is thought to be involved in the repair of double-strand breaks through homologous recombination, although its role at

telomeres has not been elucidated[118, 131], while ERCC1/XPF is required for removal of the 3' overhang at deprotected telomeres[138]. TRF2 also associates with the NHEJ factors DNA-PKcs and Ku70/80[26, 50, 91, 112]. Ku acts to stimulate fusion of dysfunctional telomeres, yet protects chromosome ends from homologous recombination[11]. The WRN and BLM helicases are associated with chromosome ends as well, where WRN is required for efficient lagging strand replication of telomeres[23, 71, 78, 93]. Apollo, a putative 5' exonuclease, is also recruited to telomeres through its association with TRF2, where it protects telomeres in S phase[68, 120]. Finally, the interaction of TRF2 with the ATM kinase is implicated in suppressing ATM activation at telomeres[56].

Telomere Protection by TRF2

TRF2 prevents activation of a DNA damage response at telomeres

Removal of TRF2 from telomeres, either by expression of a dominant negative allele of TRF2 in human cells or by genetic deletion in the mouse leads to an ATM-dependent DNA damage response[10, 55, 66, 122]. The ATM kinase is activated by autophosphorylation on S1981, and Chk2, a downstream target of ATM is phosphorylated[10, 66, 117]. Additionally, many of the same factors that localize to double-strand breaks are recruited to

TRF2-deficient telomeres. Proteins such as 53BP1, phosphorylated histone H2AX (γ-H2AX), ATM phosphorylated on S1981, Mre11, Nbs1, and MDC1 colocalize with telomeric DNA forming telomere dysfunction induced foci, or TIFs[27, 117]. Loss of TRF2 also leads to senescence-like arrest or apoptosis, depending on the cell type[55, 122]. The senescence associated with TRF2 deficiency resembles that of replicative senescence. Both lead to the stabilization of p53, induction of p21 and p16, hypophosphorylation of Rb, and positive staining for SA-β-galactosidase[109, 117, 122]. How TRF2 inhibits ATM from activating a DNA damage response at telomeres remains to be determined, but several models will be discussed in chapter four of this thesis.

TRF2 inhibits non-homologous end joining at telomeres

Another consequence of TRF2 inhibition is the formation of telomere end-to-end fusions[10, 122]. These fusion events are ATM-dependent and do not occur in the absence of DNA Ligase IV or Ku, indicating that they are generated by the NHEJ pathway[10, 11, 66, 110]. A prerequisite to the fusion event is cleavage of the 3' single-stranded overhang by the ERCC1/XPF nuclease[138]. In mouse cells, overhang cleavage and end-joining are coupled, while in human cells the two processes occur independently[10, 32].

Inhibition of TRF2 using a temperature-sensitive allele of TRF2 ($TRF2^{ts}$) gives further insight into the NHEJ process at telomeres[65]. The inactivation of $TRF2^{ts}$ at 37ºC is rapid and reversible, permitting induction of short periods (3-6 hours) of telomere dysfunction in the G_0, G_1, and S/G_2 phases of the cell cycle. This has shown that NHEJ occurs primarily in G_1, explaining the predominance of chromosome-type fusions and lack of sister fusions, which generally occur after replication in G_2. Furthermore, it has been shown that NHEJ is repressed in S/G_2 in a CDK-dependent manner[65].

TRF2 has been proposed to inhibit NHEJ at telomeres by mediating the formation of t-loops. The structure of the t-loop may execute this function by protecting the overhang from degradation as well as preventing the Ku70/80 complex, which requires a free double-stranded DNA end, from loading onto the telomere[11]. Alternatively, just the presence of TRF2/Rap1 at the telomere end may be enough to block NHEJ. This is supported by in vitro data showing that Rap1 could prevent end-joining of short telomere arrays[2].

TRF2 prevents homologous recombination at telomeres

As described above, Ku is required to fuse telomeres by the NHEJ pathway in TRF2-inhibited cells. However, this is not the only telomeric

function attributed to Ku. In parallel with TRF2, Ku acts to prevent homologous recombination (HR) between telomeres on sister chromatids (telomere-sister chromatid exchange, T-SCE)[11]. Loss of Ku alone did not cause significant changes in the structure of the telomeric DNA or activate a DNA damage response at telomeres. Only when both TRF2 and Ku are deleted is there an increase in the number of T-SCEs[11]. This process can shorten and elongate individual telomeres when the exchanged segments are not equal, perhaps generating critically short telomeres that can threaten the viability of the cell.

Experiments using a mutant allele of TRF2 that lacks the basic domain, TRF2$^{\Delta B}$, also implicate TRF2 in protecting telomeres from inappropriate HR[127]. Expression of TRF2$^{\Delta B}$ leads to the induction of TIFs and the onset of senescence, but does not cause telomere fusions. Instead, TRF2$^{\Delta B}$ cells experience telomere shortening and the formation of t-loop sized extrachromosomal telomeric circles, suggesting t-loop HR[127]. T-loop HR requires formation of a Holliday junction (HJ), which is then resolved by a resolvase. The finding that t-loop HR is dependent on XRCC3, a proposed HJ resolvase, is consistent with this model[20, 75, 127].

Telomere Protection by POT1

Loss of POT1 by RNAi in human cells and by genetic deletion in the mouse has shown that POT1 functions in telomere protection. In human cells, POT1 deficiency leads to a transient DNA damage response in G_1, causing the formation of TIFs and a reduction in the 3' overhang[48]. Mouse cells require two POT1 proteins, POT1a and POT1b, to protect telomeres. Deletion of POT1a results in a more severe telomere deprotection phenotype, while POT1b is mainly responsible for regulating exonucleolytic degradation of the C-rich telomere strand[46].

While TRF2 safeguards telomeres by inhibition of the ATM kinase, POT1 does so by repression of the ATR kinase[66]. It is speculated that POT1 competes with RPA for binding to single-stranded telomeric DNA, thus preventing the recruitment and activation of ATR.

Telomere Length Regulation

In telomerase-expressing cells, the average length of telomeres is kept within a narrow species-specific range by maintaining a balance between telomerase-mediated elongation and the processes that lead to telomere shortening. Several experiments have shown that telomere length is regulated in cis at each individual chromosome end[1, 3, 43, 104, 113, 114]. As such,

cis-acting length control cannot be exerted through changes in the expression of telomerase. Instead, shelterin modulates how telomerase acts at the telomere terminus through a negative feedback loop.

The mechanism by which shelterin exerts its negative effect on telomerase-mediated telomere elongation can be explained using a protein-counting model[80, 121]. In this model the accumulation of shelterin on the telomere depends on its length. Shorter telomeres can accept less negative regulators of telomere length, and as a consequence, the telomere has a greater chance of being elongated by telomerase. The telomere will continue to lengthen until it has become long enough to recruit sufficient amounts of shelterin to inhibit telomerase. The length of a telomere is therefore measured based on the amount of bound inhibitor. Support for this model is provided by numerous telomere length regulation studies in human cells. Overexpression of TRF1 leads to the gradual and progressive shortening of telomeres, while a dominant negative allele of TRF1, which removes endogenous TRF1 from telomeres, causes telomere elongation[121]. Similarly, disruption of TRF2, TIN2, TPP1, or POT1 by RNAi or by expression of mutant alleles results in telomere elongation, defining these proteins as negative regulators of telomere length (Takai, K and de Lange, unpublished)[62, 74, 133, 135].

The shelterin-mediated negative regulation of telomerase must be relayed from the double-stranded telomeric DNA to the 3' single-stranded overhang where POT1 has the potential to block telomerase. Evidence that POT1 is the terminal transducer of this inhibitory signal comes from experiments using POT1$^{\Delta OB}$. This mutant allele of POT1 fails to bind the telomere terminus and causes rapid and extensive telomere elongation[76]. Additionally, direct competition between POT1 and telomerase for the 3' single-stranded overhang was observed in vitro[59, 67]. These findings suggest a model to explain how the signal is transduced from duplex DNA to the end of the telomere. As a telomere gets longer, more shelterin molecules are loaded onto double-stranded TTAGGG repeats, increasing the amount of TIN2/TPP1 recruited to the telomere. Since the majority of POT1 is localized to telomeres through its association with TIN2/TPP1[47, 74, 130], the possibility that POT1 will bind the telomere terminus and inhibit telomerase are substantially raised[24, 59].

Although most studies have focused on negative regulation of telomerase, not much is known about how telomerase is actually recruited to telomere ends. The fact that there are only 20-50 molecules of telomerase per cell raises the question of how such a small number of molecules can find its low abundant substrate[18]. Recent data indicates that the TPP1/POT1

complex may contribute to recruiting telomerase. In fact, TPP1 has a direct interaction with telomerase and has been shown to increase the activity and processivity of the enzyme when complexed with POT1[126, 130]. This posits TPP1/POT1 as both negative and positive regulators of the telomerase pathway[126, 130].

CHAPTER 2: TANKYRASE1 IS AN UPSTREAM NEGATIVE REGULATOR OF TRF1 AND A POSITIVE REGULATOR OF TELOMERE LENGTH

Introduction

Telomeres can be elongated by the telomere specific reverse transcriptase telomerase and shortened through the effects of DNA replication and nucleolytic attack[40, 41, 92, 128]. The TTAGGG repeat array of vertebrate telomeres has a species-specific length setting, suggesting that these forces are balanced in the germ line[22]. Telomere length control has been primarily studied in human tumor cells that express telomerase. Such cells often maintain the length of their telomeres within a set range. This telomere length homeostasis is achieved through a negative feedback loop involving shelterin, the telomere-specific protein complex[29, 121]. Shelterin is comprised of six proteins (TRF1, TRF2, POT1, TPP1, TIN2, and Rap1) whose abundance at chromosome ends is dictated by the length of the duplex telomeric repeat array[29]. All shelterin components behave as negative regulators of telomere elongation by telomerase. Inhibition of TRF1, TPP1, TIN2, and POT1 results in telomere elongation whereas overexpression of several shelterin components shortens the length of the

telomeres[72, 121, 133, 134]. Telomere healing experiments demonstrated that cells have the ability to monitor and regulate telomerase at individual telomeres, and tethering of TRF1 at subtelomeric sites showed that TRF1 can modulate telomere length in cis[1, 3, 43, 104, 113, 114]. These findings have resulted in a model for shelterin dependent telomere length homeostasis whereby long telomeres contain more shelterin and thus have a diminished chance of being elongated further by telomerase[80, 121]. A key player in this negative feedback loop is POT1, whose binding to the single-stranded telomeric DNA appears to block telomerase in vivo[72, 76, 135] and in vitro[59, 67, 126, 130].

The length of human telomeres can be reset by manipulating tankyrase1, a TRF1-associated poly(ADP-ribose) polymerase (PARP). Tankyrase1 (TRF1-interacting, ankyrin-related ADP-ribose polymerase) consists of four domains: an N-terminal His, Pro, Ser (HPS) rich region, a central ankyrin domain containing 24 ankyrin repeats, a region homologous to the sterile alpha module (SAM) motif, and a C-terminal domain with homology to the catalytic domain of PARPs[108]. The ankyrin domain of tankyrase1 is composed of five conserved subdomains, which all serve as binding sites for TRF1[31, 101, 102]. TRF1 interacts with tankyrase1 using a conserved motif its N-terminal acidic domain[97]. Tankyrase1 lacks a nuclear

localization signal and is only found at telomeres through its association with TRF1[108]. In addition to telomeres, tankyrase1 associates with a diverse set of proteins in different subcellular compartments[16, 106].

Tankyrase1 is a fully functional PARP, capable of poly(ADP-ribosyl)ating (PARsylating) itself and TRF1. Using nicotinamide adenine dinucleotide (NAD^+) as a substrate, tankyrase1 catalyzes the formation of poly(ADP-ribose) (PAR) onto its protein acceptors[108]. In vitro, tankyrase1-mediated modification of TRF1 causes a decrease in the DNA binding affinity of TRF1, while in vivo targeting of tankyrase1 to the nucleus promotes TRF1 delocalization from telomeres and degradation by ubiquitin-mediated proteolysis[14, 108]. Furthermore, overexpression of nuclear tankyrase1 leads to a telomere elongation phenotype that requires the catalytic activity of the PARP domain of tankyrase 1[21, 100, 107], although a recent report from the Seimiya group suggests otherwise[87]. TRF1 can be protected from the effect of tankyrase1 by TIN2, which forms a ternary complex with tankyrase1 and TRF1 and blocks the PARsylation of TRF1 in vitro[133]. When TIN2 is inhibited in vivo, TRF1 appears more sensitive to the endogenous tankyrase1 and telomere elongation occurs.

Collectively, these results implicate tankyrase1 as a positive regulator of telomere elongation by telomerase. Several approaches have been used to

provide further evidence for such a role of endogenous tankyrase1. PARP inhibitors were shown to induce telomere shortening, but it has been difficult to ascribe this phenotype to inhibition of tankyrase1 rather than one of the other PARPs[100]. Dominant negative alleles of tankyrase1 have largely failed to yield the expected telomere shortening phenotypes[21, 107], although success with one allele has been reported[100]. Here we investigate this issue further by examining the telomere dynamics of cells targeted with tankyrase1 shRNAs and through the use of a tankyrase1-resistant allele of TRF1. The following results were published by Donigian and de Lange in the Journal of Biological Chemistry[34].

Results

Tankyrase1 shRNAs affect telomerase-mediated telomere elongation

To further address the role of tankyrase1 as a positive regulator of telomere length, we examined the telomere length of cells treated with tankyrase1 shRNAs. Since tankyrase1 deficiency is known to induce a mitotic arrest[13, 35] and thus incompatible with long-term culturing, we aimed for shRNAs that would generate partial knockdown. We tested shRNAs for the residual tankyrase1 protein levels by quantitative western blotting (Fig. 2-1A, D) and identified two shRNAs that lowered the

tankyrase1 level about two-fold. A third shRNA had a very modest effect, and a fourth shRNA did not affect tankyrase1 and served as a control. None of these shRNAs affected the proliferation of the cells (Fig. 2-1B).

Since the knockdown of tankyrase1 is partial, we anticipated that its effect would be most easily monitored under conditions where telomerase is not in excess, since high levels of telomerase can mask regulatory pathways[24]. Our BJ-hTERT cells showed gradual telomere shortening, despite the fact that they were expressing telomerase. Their shortening rate was 25-30 bp/end/population doubling (PD) which is significantly less than for telomerase negative BJ cells (80 bp/end/PD)[58], indicating that telomerase is active at a significant but low level. If tankyrase1 contributes to the telomerase pathway in these cells, we would expect to detect an increase in the shortening rate from 25-30 bp/end/PD to the maximal rate of 80 bp/end/PD. In order to be able to determine such changes accurately, BJ-hTERT cells expressing the various shRNAs were cultured in parallel with the vector control for approximately 130 PDs, and the telomere shortening rates were determined based on multiple genomic blots at various PDs (Fig. 2-1C, D). The results indicated that tankyrase1 shRNAs sh1 and sh5 resulted in a significant increase in the shortening rate to 43±2.2 and 46±2.5 bp/end/PD, respectively. The less effective sh3 had a minor effect

(shortening at 35±0.5 bp/end/PD) and as expected, cells expressing the ineffective sh4 had a similar shortening rate as the vector control cells (31±3.1 bp/end/PD). Together with previous data indicating that tankyrase1 does not affect telomere dynamics in telomerase negative cells[21], our results confirm the role for tankyrase1 as a positive regulator of the telomerase pathway.

Mutation of the tankyrase1 binding motif of TRF1

In the simplest model for the effect of tankyrase1 on telomere maintenance, the enzyme binds and PARsylates TRF1, removing TRF1 from telomeres. Here, tankyrase1 only acts upstream of TRF1 and is not required for the ability of TRF1 to function as a negative regulator of telomere length. However, the data do not exclude the possibility that tankyrase1 may also have a role downstream of TRF1, affecting the negative regulation of telomere length by TRF1[133]. In order to examine this possibility, we generated a TRF1 mutant that lacks a functional tankyrase1 interaction motif and determined whether it was still capable of negatively regulating telomere length. In characterizing the minimal tankyrase-binding motif, it was shown that the first residue in the hexapeptide RXXADG is critical for tankyrase-binding, while substitution of the second residue had no effect on

binding[97]. Using site-directed mutagenesis, a mutation was made in the N-terminal $_{13}$RGCADG$_{18}$ motif of hTRF1 by converting arginine 13 to an

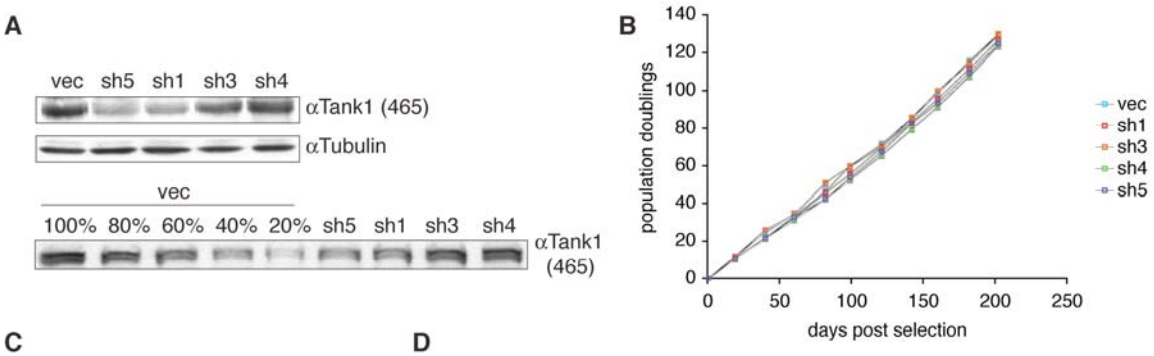

C

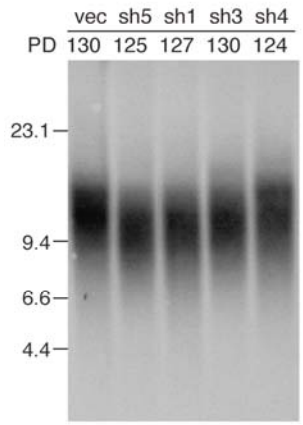

D

shRNA	Rel. Tank 1 Level (%)	Tel. Short. Rate (bp/end/PD) *At Indicated PD*	*Mean*
vec	100	27 (PD 53) 30 (PD 116) 28 (PD 130)	28±1.2
sh5	53	45 (PD 50) 49 (PD 110) 43 (PD 125)	46±2.5
sh1	57	44 (PD 52) 45 (PD 112) 40 (PD 127)	43±2.2
sh3	89	35 (PD 54) 35 (PD 115) 34 (PD 130)	35±0.5
sh4	99	29 (PD 49) 35 (PD 108) 28 (PD 124)	31±3.1

Figure 2-1. Tankyrase1 suppression causes telomere shortening.

(A) Western blots showing tankyrase1 protein levels in BJ-hTERT cells expressing shRNA-encoding retroviruses and the vector control. Total cellular proteins were analyzed by immunoblotting using antibodies to tankyrase1 (465) and to γ-tubulin. (B) Graph of growth curves of BJ-hTERT cells infected with tankyrase1 shRNAs and the vector control. Cells were selected with puromycin for 5 days and then proliferation was monitored over several months. (C) Genomic blot of telomeric restriction fragments in four BJ-hTERT cell lines infected with the indicated tankyrase1 shRNA retroviruses and the vector control. DNA agarose plugs were prepared at ~PD 130, digested with AluI and MboI, and analyzed by Southern blotting using a double-stranded TTAGGG repeat probe. (D) Table summarizing the relative tankyrase1 protein levels and the telomere shortening rates of BJ-hTERT cells expressing tankyrase1 shRNAs.

alanine (Fig. 2-2A). Additionally, glycine 14 was inadvertently mutated to an arginine. The ability of this hTRF1$^{\Delta Tank}$ allele to bind tankyrase1 was tested by far western assay. Baculovirus-derived TIN2, tankyrase1, and Rap1 (as a negative control) were probed with in vitro translated ^{35}S-labeled hTRF1 and hTRF1$^{\Delta Tank}$. The results showed that wild type hTRF1 was able to bind tankyrase1 while hTRF1$^{\Delta Tank}$ failed to do so. On the other hand, the mutation did not affect the TRF1-TIN2 association, as demonstrated by the robust signal in the TIN2 lane for both wild type hTRF1 and the mutant (Fig 2-2B). Co-immunoprecipitation experiments also indicated that hTRF1$^{\Delta Tank}$ no longer bound tankyrase1. MYC-tagged hTRF1 and hTRF1$^{\Delta Tank}$ were transiently co-transfected with FLAG-NLS-tagged tankyrase1 (FN-tankyrase1) into 293T cells, and TRF1 was precipitated from the cells using an antibody against MYC. The immunoblot shows that wild type hTRF1 was able to pull down tankyrase1 while hTRF1$^{\Delta Tank}$ failed to do so (Fig. 2-2C).

hTRF1$^{\Delta Tank}$ is resistant to tankyrase1 activity in vitro and in vivo

We next tested whether the hTRF1$^{\Delta Tank}$ mutant could be PARsylated by tankyrase1 in an in vitro PARP assay (Fig. 2-3). The PARsylation of hTRF1$^{\Delta Tank}$ by tankyrase1 was reduced by 4-5-fold compared to wild type

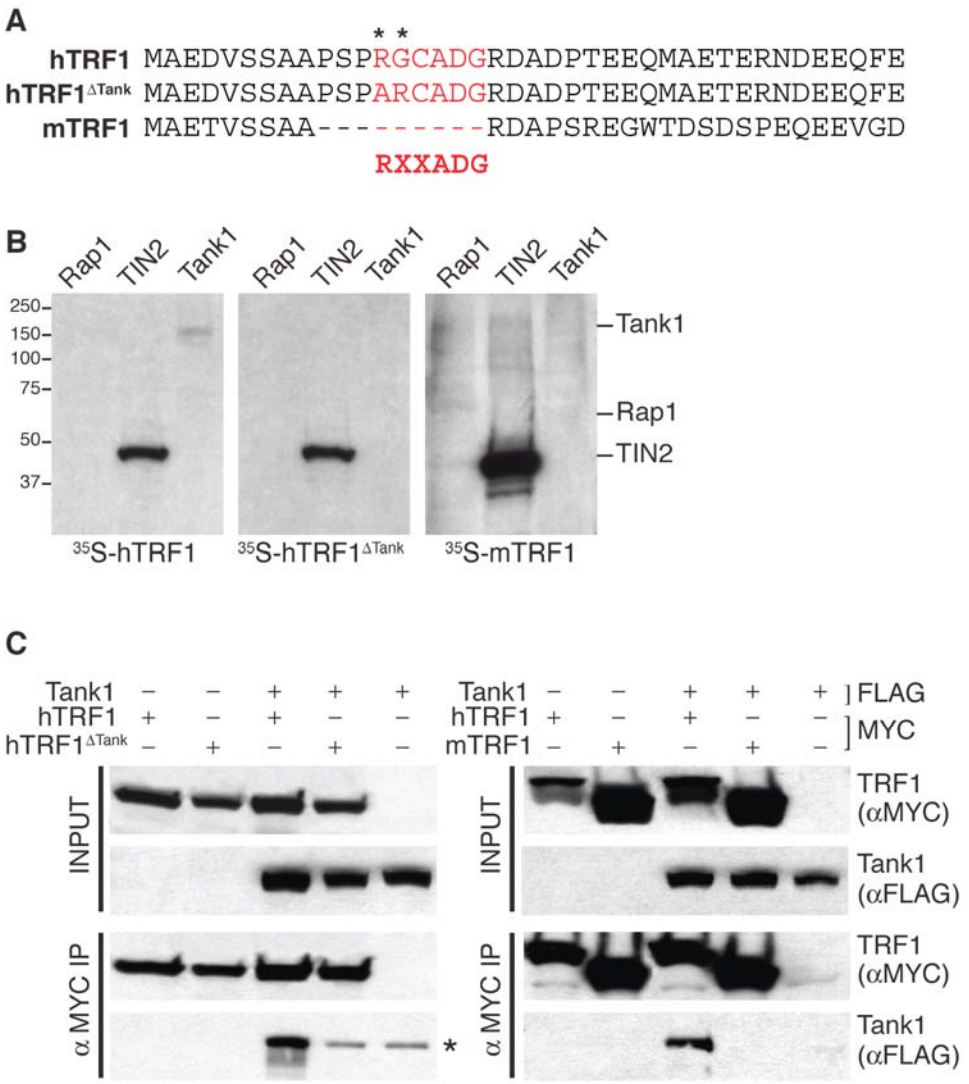

Figure 2-2. hTRF1$^{\Delta Tank}$ and mTRF1 do not bind tankyrase1.

(A) Alignment of the N-terminal acidic domain of hTRF1, hTRF1$^{\Delta Tank}$, and mTRF1. The TRF1 tankyrase1-binding consensus sequence is also shown. (B) Far-western analysis of the tankyrase1-binding ability of hTRF1, hTRF1$^{\Delta Tank}$, and mTRF1. Each lane contains 2 μg of purified recombinant protein derived from insect cells using a His-tag. The proteins were subjected to SDS-PAGE, blotted onto nitrocellulose, and incubated with the indicated ^{35}S-labeled IVT protein. (C) Co-immunoprecipitations from transfected 293T cells. MYC-tagged hTRF1, hTRF1$^{\Delta Tank}$, mTRF1 and FN-tankyrase1 were transiently transfected into 293T cells in the combinations shown. Whole-cell extracts (input) were immunoprecipitated (IP) using an antibody to MYC (9E10). A small fraction of FN-tankyrase1 is recovered non-specifically in the IPs resulting in the band indicated with an asterisk.

hTRF1 (22±7.6% of wild type in 3 experiments). The discrepancy between the ability of hTRF1$^{\Delta Tank}$ to bind tankyrase1 and to be modified by tankyrase1 may lie in the sensitivity of the assays used. It is possible that hTRF1$^{\Delta Tank}$ can still loosely associate with tankyrase1 outside of its acidic domain[101], allowing for modest PARsylation of hTRF1$^{\Delta Tank}$. In fact, this is the case with chicken TRF1, which binds tankyrase1 even though it lacks the RXXADG tankyrase-binding motif[31].

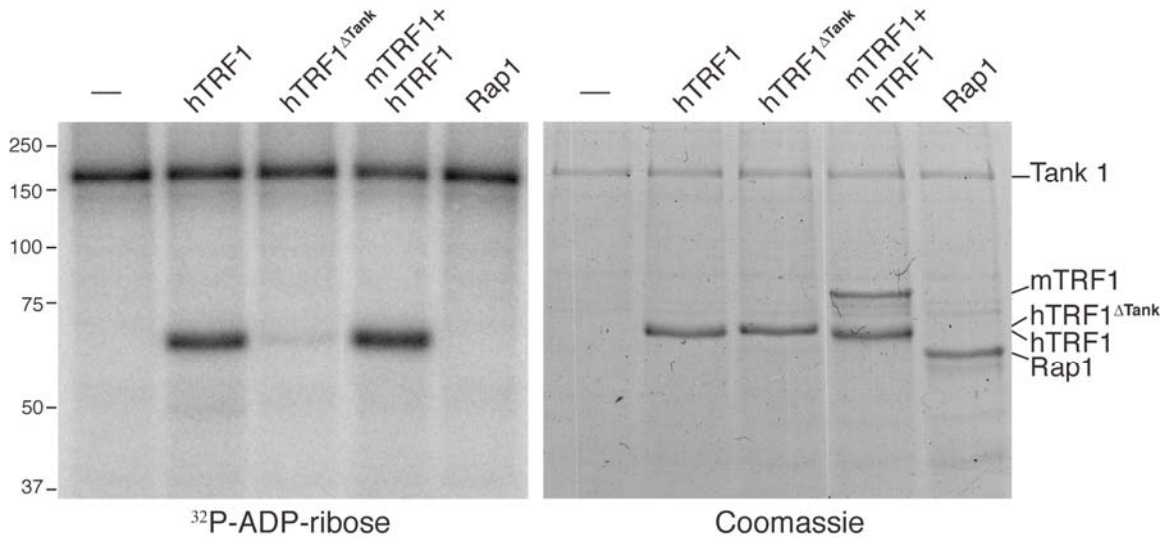

Figure 2-3. hTRF1$^{\Delta Tank}$ and mTRF1 are not readily PARsylated by tankyrase1.

The autoradiograph (left) and Coomassie blue-stained gel (right) from a tankyrase1 PARP assay. Each lane contains 4 μg of the indicated proteins derived from insect cells or *E. coli* cells (GST-mTRF1) in a reaction with ^{32}P-β-NAD^{+}. Products from each reaction were subjected to SDS-PAGE and processed for autoradiography or Coomassie blue staining. The blot shown here yielded a hTRF1$^{\Delta Tank}$ signal that was 12% of the band intensity of wild type hTRF1.

Finally, we tested the ability of hTRF1$^{\Delta Tank}$ to resist removal from the telomere in the presence of excess nuclear tankyrase1 in vivo. HeLa cells expressing MYC-tagged hTRF1 or hTRF1$^{\Delta Tank}$ were transiently transfected with FN-tankyrase1, and the removal of TRF1 was monitored by indirect immunofluorescence. As expected, hTRF1 was no longer detectable at telomeres in the nuclei that expressed tankyrase1 (Fig. 2-4A). In contrast, hTRF1$^{\Delta Tank}$ retained its punctuate pattern in tankyrase1-expressing cells (Fig. 2-4B). We conclude that hTRF1$^{\Delta Tank}$ has largely lost tankyrase1 interaction in vitro and in vivo.

hTRF1$^{\Delta Tank}$ behaves as a negative regulator of telomere length

In order to evaluate the effect of the diminished tankyrase1 interaction on the telomere length regulatory activity of TRF1, we analyzed telomere length in BJ-hTERT and HTC75 cells overexpressing wild type hTRF1 and hTRF1$^{\Delta Tank}$. Both proteins were expressed at the same level (Fig. 2-5A). Their overexpression was such that only ~15% of the total TRF1 in the cells was derived from the endogenous (wild type) locus. The TRF1 mutant allele had no effect on the viability of the cells, and they proliferated at the same rate as cells expressing hTRF1 or the vector control (Fig. 2-5B and data not shown). As seen in the tankyrase1 shRNA experiment, the BJ-hTERT vector

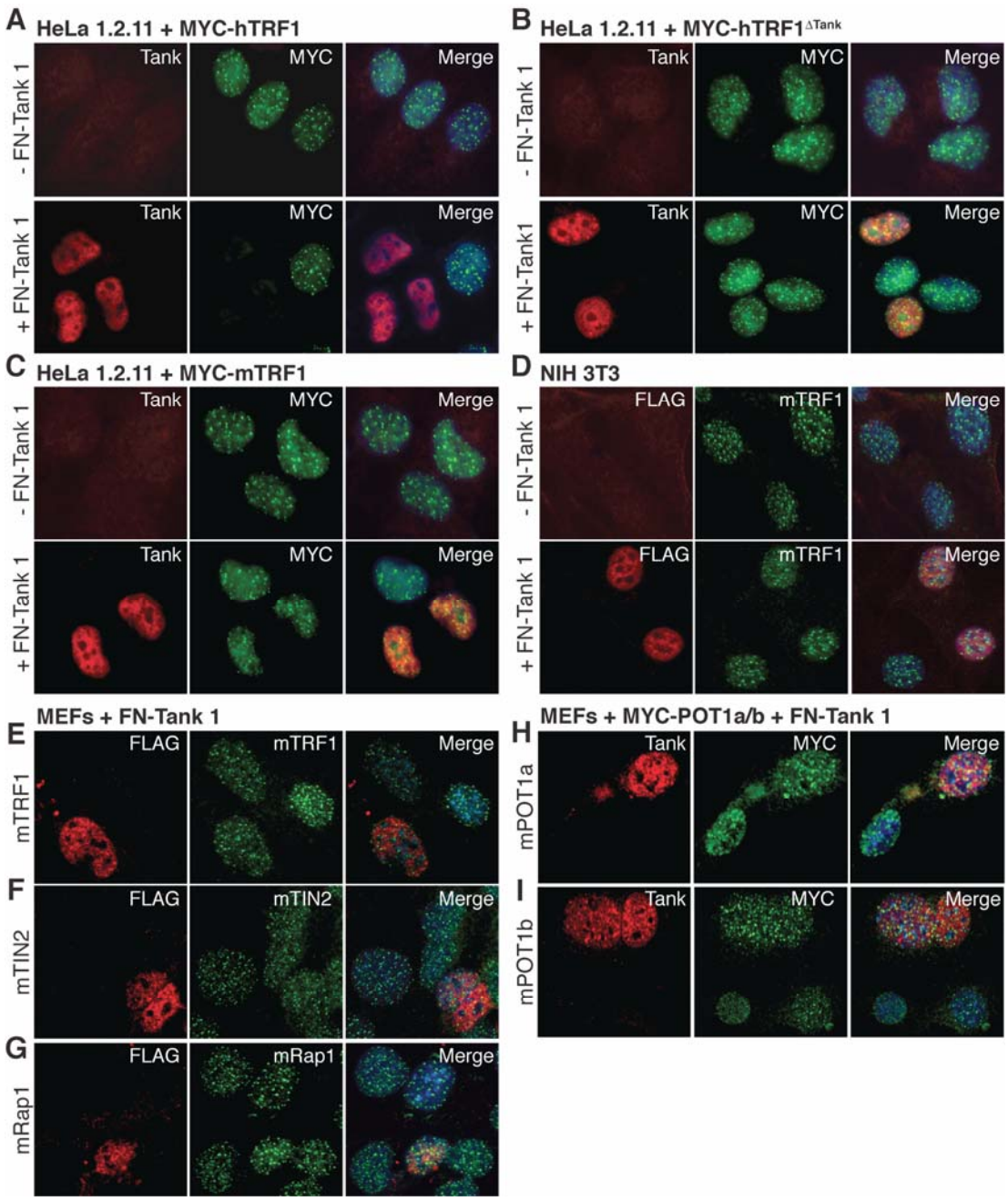

Figure 2-4. Overexpression of tankyrase1 in the nucleus releases hTRF1, but not hTRF1$^{\Delta Tank}$, mTRF1, or other mouse shelterin proteins.

Indirect immunofluorescence of TRF1 localization in (A-C) HeLa1.2.11 cells stably expressing (A) MYC-hTRF1, (B) MYC-hTRF1$^{\Delta Tank}$ or (C) MYC-mTRF1, or in (D) mouse NIH 3T3 cells transiently transfected with FN-tankyrase1 or mock transfected. (E-I) Indirect immunofluorescence of mouse shelterin proteins (E) mTRF1, (F) mTIN2, (G) mRap1, (H) mPOT1a, and (I) mPOT1b in immortalized MEFs transiently transfected with FN-tankyrase1. For H and I, immortalized MEFs stably expressing MYC-mPOT1a and MYC-mPOT1b were used, respectively.

control cells experienced mild telomere shortening (21±9.5 bp/end/PD) while the HTC75 vector control cells remained at a stable telomere length setting. Overexpression of hTRF1 led to telomere shortening at a rate of 66±3.5 bp/end/PD in BJ-hTERT cells and 11±1.0 bp/end/PD in HTC75 cells (Fig. 2-5C, D; data not shown). A similar shortening phenotype was evident for the cells expressing hTRF1$^{\Delta Tank}$, which induced a shortening rate of 68±7.0 bp/end/PD in BJ-hTERT cells and 12±0.5 bp/end/PD in HTC75 cells (Fig. 2-5C, D; data not shown). This result implies that diminished recruitment of tankyrase1 does not have a strong impact on the ability of TRF1 to negatively regulate telomere length. Thus, tankyrase1 appears to primarily act upstream of TRF1 in the telomere length regulation pathway.

Mouse TRF1 does not interact with tankyrase1 in vitro and in vivo

Interestingly, the N-terminus of mouse TRF1 lacks the RGCADG motif (Fig. 2-2A), and does not bind tankyrase1[97]. This would suggest that the wild type mTRF1 would resemble the hTRF1$^{\Delta Tank}$ mutant. To test this idea, we asked whether full-length mTRF1 could interact with and be modified by tankyrase1. Human and mouse tankyrase1 are 98% identical overall with most differences occurring in the N-terminus, which is not implicated in the interaction with TRF1 or its PARP activity. We therefore

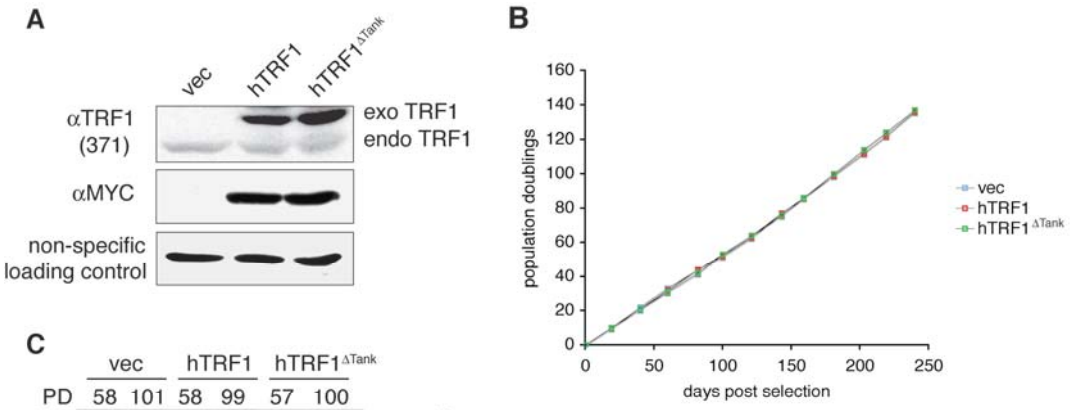

D

	BJ-hTERT Tel. Short. Rate (bp/end/PD)		HTC75 Tel. Short. Rate (bp/end/PD)	
	At Indicated PD	*Mean*	*At Indicated PD*	*Mean*
vec	30 (PD 58) 11 (PD 101)	21±9.5	-3 (PD 45) 3 (PD 104)	0±3.0
hTRF1	63 (PD 58) 70 (PD 99)	66±3.5	10 (PD 45) 12 (PD 106)	11±1.0
hTRF1$^{\Delta Tank}$	61 (PD 57) 75 (PD 100)	68±7.0	11 (PD 45) 12 (PD 105)	12±0.5

Figure 2-5. Overexpression of hTRF1$^{\Delta Tank}$ causes telomere shortening.

(A) Western blots of endogenous TRF1 and exogenously expressed MYC-tagged hTRF1 and hTRF1$^{\Delta Tank}$ in BJ-hTERT cells. Total cellular proteins were analyzed by immunoblotting using antibodies to TRF1 (371), MYC (9E10), and γ-tubulin. (B) Graph of growth curves of BJ-hTERT cells infected with hTRF1, hTRF1$^{\Delta Tank}$, and the vector control. Cells were selected with puromycin for 5 days and then proliferation was monitored over 100 PDs. (C) Genomic blot of telomeric restriction fragments in BJ-hTERT cell lines infected with hTRF1 and hTRF1$^{\Delta Tank}$ retroviruses and the vector control. DNA agarose plugs were prepared at the indicated PDs, digested with AluI and MboI, and analyzed by Southern blotting using a double-stranded TTAGGG repeat probe. (D) Table summarizing the telomere shortening rates of BJ-hTERT and HTC75 cells expressing hTRF1, hTRF1$^{\Delta Tank}$, and the vector control.

used the available human tankyrase1 constructs for these tests because this approach allowed comparison of human and mouse TRF1 in the same experiment. In the far western assay, mTRF1 behaved similarly to hTRF1$^{\Delta Tank}$, forming a complex with TIN2, yet failing to interact with tankyrase1 (Fig. 2-2B). Furthermore, mTRF1 did not bind tankyrase1 based on their lack of co-IP from transfected 293T cells (Fig. 2-2C). Additionally, GST-mTRF1 was not PARsylated by tankyrase1 in an in vitro PARP assay (Fig. 2-3). The reaction was validated by showing that hTRF1 and tankyrase1 were still modified in the presence of GST-mTRF1. This control was included to rule out that GST-mTRF1, the only protein prepared from bacteria, did not contain a fortuitous inhibitor of the PARP reaction. The effect of tankyrase1 on mTRF1 telomere localization was also examined. HeLa 1.2.11 cells infected with MYC-mTRF1 (Fig. 2-4C), NIH 3T3 cells (Fig. 2-4D), and MEFs (Fig. 2-4E) were transfected with FN-tankyrase1, and the distribution of mTRF1 was assessed by IF. As with hTRF1$^{\Delta Tank}$, tankyrase1 failed to remove mTRF1 from telomeres. We also examined the effect of nuclear overexpression of tankyrase1 on the telomeric localization of other shelterin components, including mTIN2 (Fig. 2-4F), mRap1 (Fig. 2-4G), mPOT1a (Fig. 2-4H), and mPOT1b (Fig. 2-4E). For none of these shelterin proteins was tankyrase1 found to affect their localization.

Discussion

Reduction of tankyrase1 protein levels by shRNA resulted in telomere shortening that was proportional to the level of knockdown while a tankyrase1-resistant form of TRF1 had no effect on the ability of TRF1 to regulate telomere length. These findings suggest that tankyrase1 is a positive regulator of telomere length and does not function downstream of TRF1. Furthermore, we showed that mouse TRF1 does not interact with tankyrase1, is not PARsylated by tankyrase1 in vitro, or is not removed from telomeres when tankyrase1 is overexpressed in mouse nuclei. Similarly, all mouse shelterin proteins were resistant to tankyrase1 overexpression and remained bound to telomeres. Consistent with these results, tankyrase1 knockout mice do not have defects in telomere length maintenance (Chiang et al., unpublished).

Collectively, the data imply that tankyrase1 does not have the same role at mouse telomeres as it does at human telomeres. This is not the first time a difference has been observed between human and mouse telomeres. Recently, it was discovered that rodent shelterin is comprised of two functionally distinct POT1 proteins, both of which are required to protect telomeres, whereas human shelterin only includes a single POT1 protein[46]. The use of tankyrase1 as a shelterin accessory factor is another example of

the rapid evolution of the telomere/telomerase system. Tankyrase1 presumably provides an additional level of control over telomere elongation by telomerase. Perhaps the tankyrase1 pathway allows the subset of telomerase-positive human somatic cells to control the rate of telomere shortening.

CHAPTER 3: TIN2 PREFERENTIALLY BINDS THE TRFH DOMAIN OF TRF1 AND THE HINGE DOMAIN OF TRF2

Introduction

The TTAGGG repeat arrays of mammalian telomeres associate with two related telomeric DNA-binding proteins, TRF1 and TRF2[7, 9, 17]. These factors have closely related C-terminal Myb-type DNA binding domains and bind TTAGGG sequences as dimers or higher order oligomers. Dimerization is mediated by the TRF-homology (TRFH) domain, the signature motif of this family of telomeric proteins[5, 36]. The crystal structure of the TRFH domains of TRF1 and TRF2 shows that the heterodimerization of TRF1 and TRF2 is impeded by crucial amino acid differences in the main dimerization interface[5, 36], and TRF1/TRF2 heterodimers are not formed in vitro or in vivo[9]. Therefore, before this study, the prevailing view had been that TRF1 and TRF2 form separate complexes at telomeres.

The two-complex model was reinforced by functional studies revealing distinct roles for TRF1 and TRF2 at telomeres. Originally, TRF1, TIN2, TPP1, and POT1 were mainly implicated in telomere-length homeostasis, a process that regulates the maintenance of telomeric DNA by telomerase[19, 62, 74, 76, 121, 133, 135]. It was not until after this study that we

learned of the protective function of POT1/TPP1 in mammalian cells[46-48, 129]. On the other hand, TRF2 has always been associated with telomere protection. Its inhibition leads to dysfunctional telomeres that are detected and processed by the DNA damage response machinery[10, 27, 55, 117, 122]. However, targeted deletion of TRF1 in mice results in early embryonic lethality, and ES cells deprived of TRF1 function die rapidly[53, 57]. The cell-lethal phenotype of TRF1 loss would not be expected if these proteins acted solely to regulate telomere length and suggests that TRF1 may be contributing to telomere protection. Interestingly, TRF1-deficient ES cells show diminished presence of TRF2 at chromosome ends[53], suggesting a link between these two complexes.

This chapter reveals that TIN2 is the connecting factor between the TRF1 and TRF2 complexes. We show that the C terminus of TIN2 binds the TRFH domain of TRF1, while the N terminus of TIN2 interacts with a small motif in the hinge domain of TRF2. This allows TIN2 to bind TRF1 and TRF2 independently or simultaneously, bridging the TPP1-POT1 complex not only to TRF1, but also to TRF2 and stabilizing shelterin proteins at telomeres.

Results

Shelterin and its subcomplexes

Several experiments led to the conclusion that TRF1 and TRF2 exist in independent complexes as well as a comprehensive shelterin unit with all six components. One clue that there was a link between the TRF1 and TRF2 complexes came from an experiment in which TRF1 was targeted by RNAi and analyzed by IF. Knockdown of TRF1 in HeLa cells resulted not only in loss of TRF1 from telomeres, but a reduction in the amount of TRF2 and Rap1 at chromosome ends[134]. A possible explanation for the effect of TRF1 siRNA on TRF2 is the presence of a proteinaceous link between these two complexes that stabilizes TRF2 on telomeres. To find TRF1- and TRF2-interacting factors that might represent such a linking factor, my colleagues performed mass spectrometry on isolated TRF1 and TRF2 complexes from HeLaS3 cells. Found in association with the TRF2-associated protein, Rap1, were peptides derived from TRF1, PIP1, and POT1[134], and conversely, peptides derived from TRF2 and Rap1 were identified in the TRF1-TIN2 complex[135]. My own data were consistent with these findings. When FLAG-tagged TRF1 was overexpressed and precipitated from BJ-hTERT cells, TRF2 and Rap1 were pulled down as well (Fig. 3-1). Treatment of lysates with ethidium bromide or RNase A did not affect the recovery of

TRF2 and Rap1 in the TRF1/TIN2 IPs, suggesting that these proteins were not tethered by nucleic acids. The interaction between the TRF1 and TRF2 complexes was, however, sensitive to high salt concentrations[134]. This can explain why TRF1 and its associated factors were not recovered in a previously analyzed TRF2 complex that was isolated from a high salt heparin chromatography fraction[137, 138].

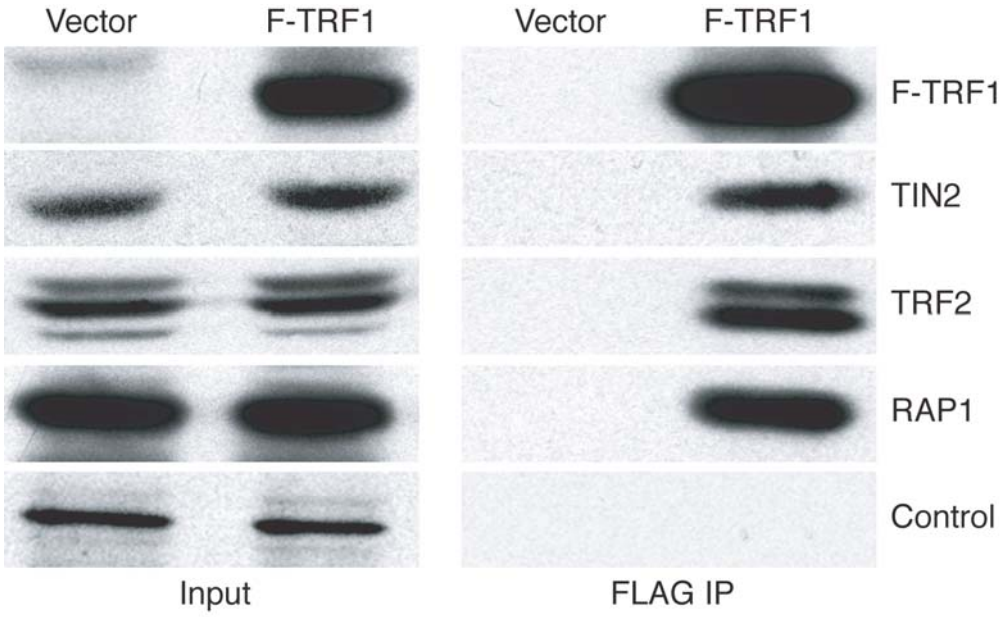

Figure 3-1. Co-IP of the TRF1 and TRF2 complexes.

Immunoblot of extracts from retrovirally infected BJ-hTERT cells expressing FLAG-tagged TRF1 or vector alone immunoprecipitated with FLAG beads and eluted with FLAG peptide. Antibodies used: anti-FLAG, M2; anti-TIN2, 864; anti-TRF2, 647; and anti-Rap1, 765; control is a nonspecific band that reacted with the Rap1 antibody.

Gel filtration was used to gain further insight into the interaction between the TRF2 complex and the TRF1 complex. Endogenous telomeric protein complexes of HeLa cells were size-fractionated and constituent

proteins were identified by immunoblotting (Fig. 3-2; experiment done by Jeffrey Ye). A TRF2-Rap1 complex (complex III) was detected in the lower molecular mass range that appeared to lack the other telomeric proteins. This is consistent with the direct interaction between these two factors. The fractions in the 2 MDa range (the exclusion limit of the column) contained tankyrase 1, TRF1, TIN2, POT1, TRF2, and hRap1. Although the co-elution of these proteins could be due to the presence of a single large complex, it is also possible that these high molecular mass fractions contain multiple complexes that each have a molecular mass in the 2-MDa range or that they are held together by DNA. The most informative complex was recovered in fractions 24–26 (complex II), which contained TRF2, Rap1, TIN2, and POT1 but lacked TRF1 and tankyrase 1. The reduced presence of TRF1 in these fractions suggested that the association of TIN2 and POT1 with TRF2/Rap1 is not mediated by TRF1. The lack of requirement for TRF1 in this association further confirmed that DNA tethering is an unlikely source of the connection between the telomeric complexes and points to an association of either TIN2 or POT1 or one of their interacting partners with the TRF2-Rap1 complex.

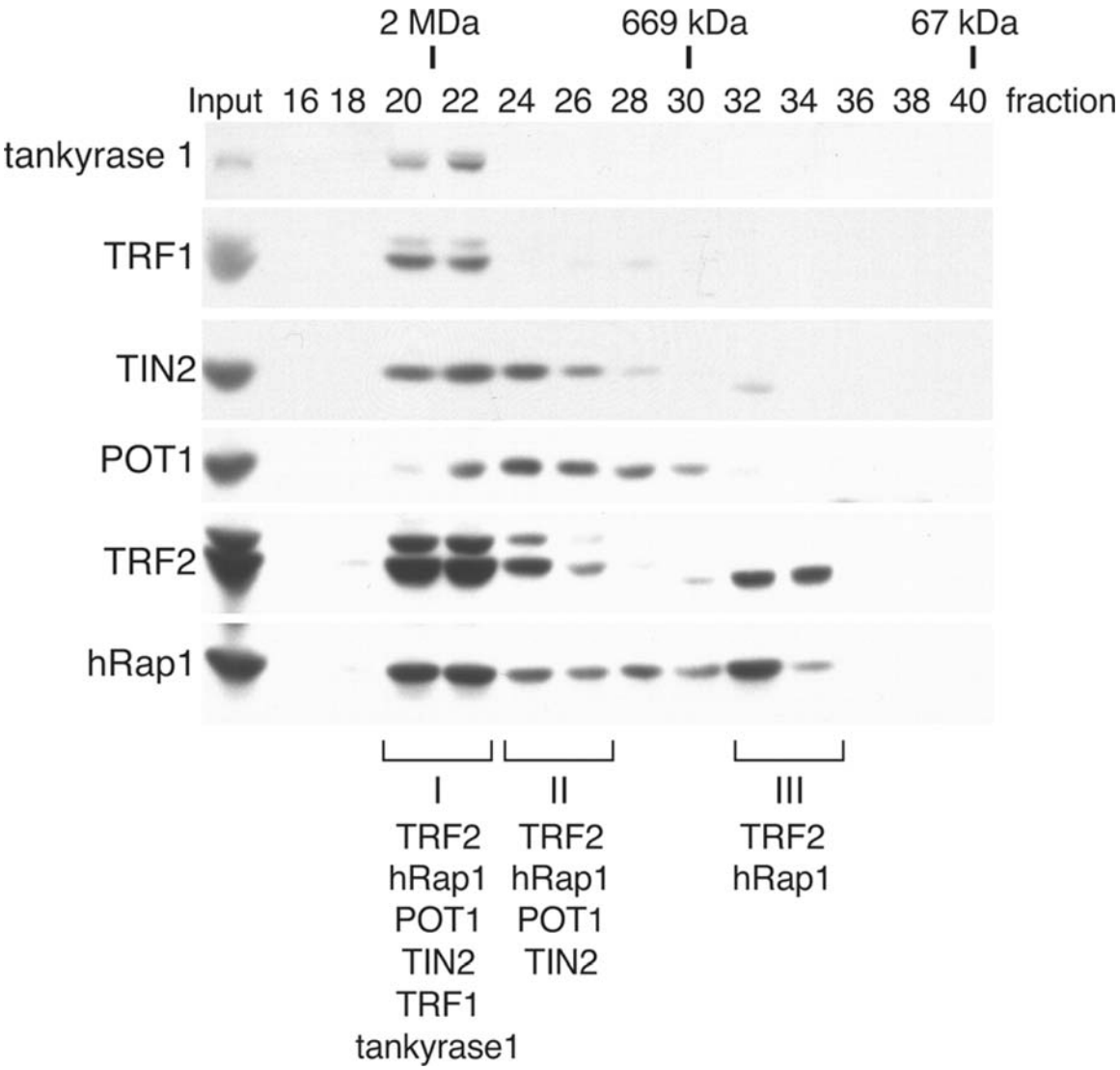

Figure 3-2. Gel-filtration analysis of telomeric complexes.

Immunoblotting analysis of endogenous telomeric proteins in HeLa nuclear extract fractionated on Sephacryl S-300. 10 µl of the indicated fractions were loaded per lane. Antibodies used: anti-tankyrase 1, number 465; anti-TRF1, 371; anti-TIN2, 864; anti-POT1, 978; anti-TRF2, 647; and anti-Rap1, 765. Molecular mass markers used were blue dextran (2 MDa), thyroglobulin (669 kDa), and bovine serum albumin (67 kDa). (Figure done by Jeffrey Ye)

Direct Binding of TIN2 to TRF1 and TRF2

Because TIN2 appeared to be shared between the TRF1 and TRF2 complexes, we tested its ability to interact with TRF2 and/or Rap1 by far western assaying. When purified baculovirus-derived telomeric proteins were probed with [^{35}S]methionine-labeled in vitro translated (IVT) TIN2, a robust interaction of TIN2 with TRF2 was detected, and the basic domain of TRF2 was dispensable for this association (Fig. 3-3A). TIN2, however, failed to bind Rap1, POT1, TRF1, or itself. The fact that TIN2 did not interact with TRF1 was surprising, but it is possible that the denaturing conditions of the far western assay prevented filter-bound TRF1 from being a good substrate for TIN2 because the reverse reaction proved successful; native IVT TRF1 was able to interact with filter-bound TIN2. We next asked which region of TIN2 was responsible for binding TRF2. TIN2–13, a C-terminal fragment of TIN2 that retains its TRF1 interacting domain, was used to probe blotted TRF2 with negative results (data not shown). These data corroborate the yeast two-hybrid data indicating that TIN2 interacts with TRF2 and that this interaction requires sequences present in the N terminus of TIN2[134].

Having established that TIN2 binds to TRF2 as well as to TRF1, we wanted to determine whether TIN2 can link TRF1 to TRF2. To address this

issue, we performed a modified Far-Western assay in which unlabeled TIN2 was tested for its ability to mediate binding of labeled TRF1 to filter-bound TRF2 (Fig. 3-3B). As expected, in the absence of TIN2, IVT TRF1 associated with filter-bound TIN2 but did not bind to TRF2. However, when the same assay with labeled TRF1 was performed in the presence of unlabeled TIN2 in a binding mixture, TRF1 had the ability to associate with TRF2. This result suggested that TIN2 can tether TRF1 to TRF2.

As discussed earlier, depletion of TRF1 from telomeres leads to partial removal of TRF2 as well. The finding that TIN2 can form a proteinaceous link between TRF1 and TRF2 suggested that TIN2 loss would also destabilize TRF2 at telomeres. To test this, siRNA depletion of TIN2 was implemented. As previously shown, loss of TIN2 diminished the abundance of TRF1at telomeres, in part because of the tankyrase-mediated modification of TRF1[133]. Along with TRF1, the telomeric accumulation of TRF2 and Rap1 was also strongly reduced by TIN2 knockdown[134]. Thus, loss of TIN2 affects the presence of TRF2 at chromosome ends.

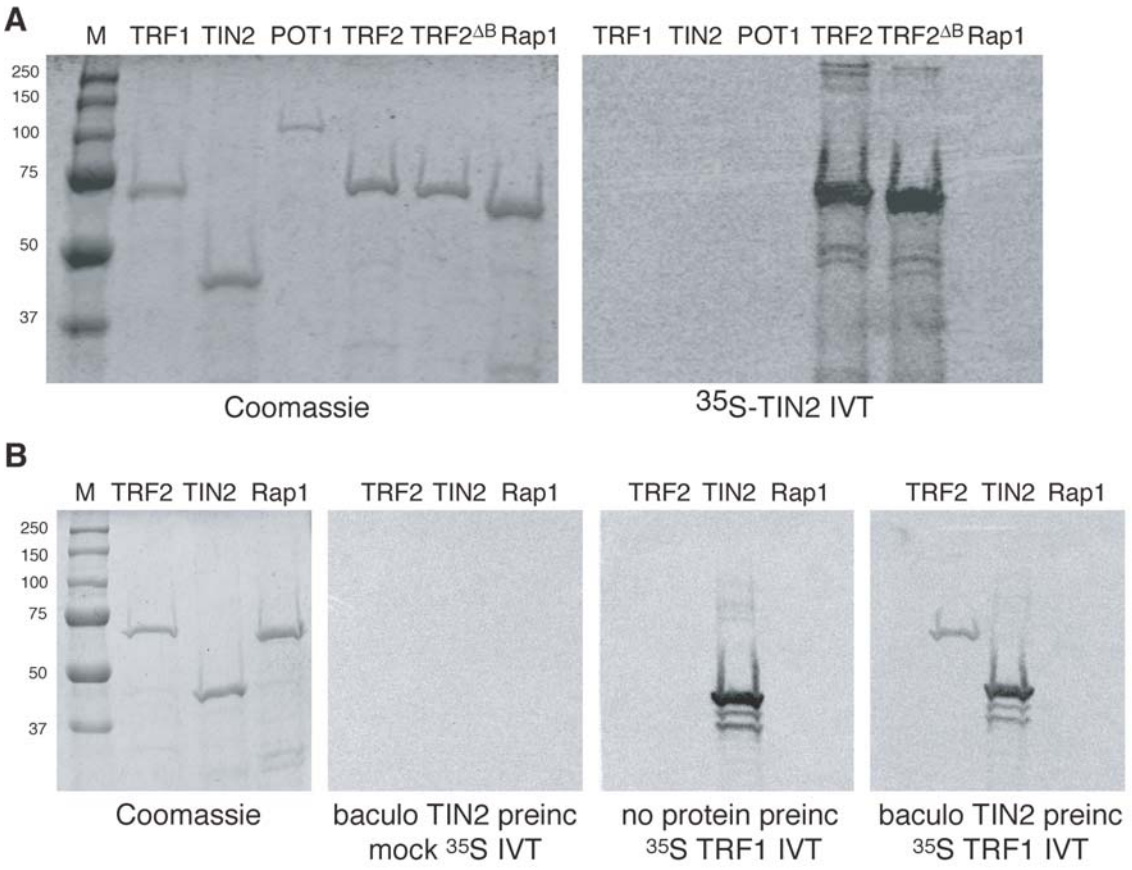

Figure 3-3. TIN2 interacts with TRF1 and TRF2 simultaneously.

(A) Far-western analysis of indicated telomeric proteins with [^{35}S]TIN2 IVT protein. Each lane contains 2 μg of purified protein derived from *E. coli* (using glutathione *S*-transferase; POT1) or Sf21 cells (using a His-tag; all other proteins). The proteins were subjected to SDS-PAGE, stained with Coomassie Blue (left), or blotted onto nitrocellulose and incubated with [^{35}S]TIN2 IVT protein (right). (B) Modified far-western analysis of the ability of TIN2 to bridge TRF1 to TRF2. From left to right, Coomassie blue-stained gel loaded with 2 μg of purified baculovirus TRF2, TIN2, and Rap1; nitrocellulose blot of the same proteins preincubated with baculovirus TIN2 followed by incubation with mock ^{35}S-labeled IVT protein (no DNA was added to the IVT reaction); blot preincubated without protein followed by incubation with ^{35}S-labeled TRF1 IVT protein; blot preincubated with baculovirus TIN2 followed by incubation with ^{35}S-labeled TRF1 IVT protein.

Mapping of the TRF2 TIN2-binding domain

Having shown that TIN2 can bind to both TRF1 and TRF2, we set out to create a separation-of-function mutant whereby we could examine the role of TIN2 when it is bound exclusively to TRF2. To do this, the region in TRF2 that associates with TIN2 needed to be determined. We once again used far westerns to map the TIN2-binding motif in TRF2. In these experiments, lysates from induced *E. coli* BL21 bacterial cultures that expressed various GST-fused TRF2 constructs were used as the filter-bound protein source while [^{35}S]methionine-labeled IVT TIN2 was used as the probe[15]. We first tested the known domains of TRF2 (Fig. 3-4A). TIN2 failed to interact with the TRFH or Myb domains, but showed a strong interaction with full-length TRF2, TRF2$^{\Delta B}$, and, most informative, the hinge or linker region in TRF2 (Fig. 3-5B). The hinge domain was then broken down into smaller GST-fused constructs to narrow in on the area of interaction. TIN2 only bound to the GST fusion containing aa 352-406 of TRF2. Further analysis of this short amino acid stretch revealed that TIN2 preferentially interacted with the N-terminal portion of this region from residue 352 to 385 (Fig. 3-5B). Finally, the minimal TRF2 TIN2-binding motif was mapped to aa 352-365 of the hinge domain. Deletion of this region from GST-TRF2 completely abrogated TIN2 binding in the far

western assay[15] (Fig. 3-5B). For cloning simplicity, the deletion was made from residues 352-367. TRF2$^{\Delta 352\text{-}367}$ will be referred to as TRF2$^{\Delta T}$ (for deletion of TIN2) from here on out.

The inability of TIN2 to bind TRF2$^{\Delta T}$ was further verified by co-IP in 293T cells[15]. Myc-tagged TRF2^{WT} and TRF2$^{\Delta T}$ were co-transfected with FLAG-HA-tagged TIN2 into 293T cells, and TRF2 was precipitated from the cells 24 hours later using a Myc antibody. So as to not disrupt the salt sensitive TRF2-TIN2 interaction, the lysates were prepared under physiological salt conditions. The western blot reveals that TRF2^{WT} was able to pull down TIN2, while very little TIN2 was associated with TRF2$^{\Delta T}$ (Fig. 3-5C). In fact, TRF2$^{\Delta T}$ may dimerize with endogenous TRF2, and the small amount of TIN2 seen in the IP could be a result of its interaction with this population of TRF2. The decrease in the amount of TIN2 in the TRF2$^{\Delta T}$ lysate compared to the wild type control suggests that the interaction between TRF2 and TIN2 improves the stability of TIN2.

Previous studies have shown that the TRF1-TIN2 interaction is mediated by the TRFH domain of TRF1 and the C terminus of TIN2[62]. Considering that the TRFH domains of TRF1 and TRF2 have almost

identical three-dimensional structures[36], we were surprised that TIN2 did not associate with the TRFH domain of TRF2, but instead used its N terminus to bind the hinge region of TRF2.

Figure 3-4. TIN2 binds a small motif in the hinge domain of TRF2.

(A) Schematic of human TRF2. The minimal Rap1 and TIN2 binding domains are indicated. Relevant TRF2 sequences from the indicated organisms surrounding the TIN2-interacting domain were aligned with ClustalW. Boxes indicate identical amino acids. A conserved SQ site is shaded in pink. (B) Far western mapping the TRF2 TIN2-binding domain. Each lane contains lysate from induced *E. coli* BL21 bacterial cultures that express the indicated GST-fused TRF2 constructs. The lysates were subjected to SDS-PAGE, stained with Coomassie blue (left), or blotted onto nitrocellulose and incubated with [^{35}S]TIN2 IVT protein (right). UN, uninduced control; FL, full-length TRF2; ΔB, TRF2Δ1-42. (C) Co-IP of TIN2 with cotransfected wild-type and mutant TRF2. TRF2 proteins are Myc-tagged and TIN2 proteins are HA-tagged. Myc 9E10 antibody was used for the IP.

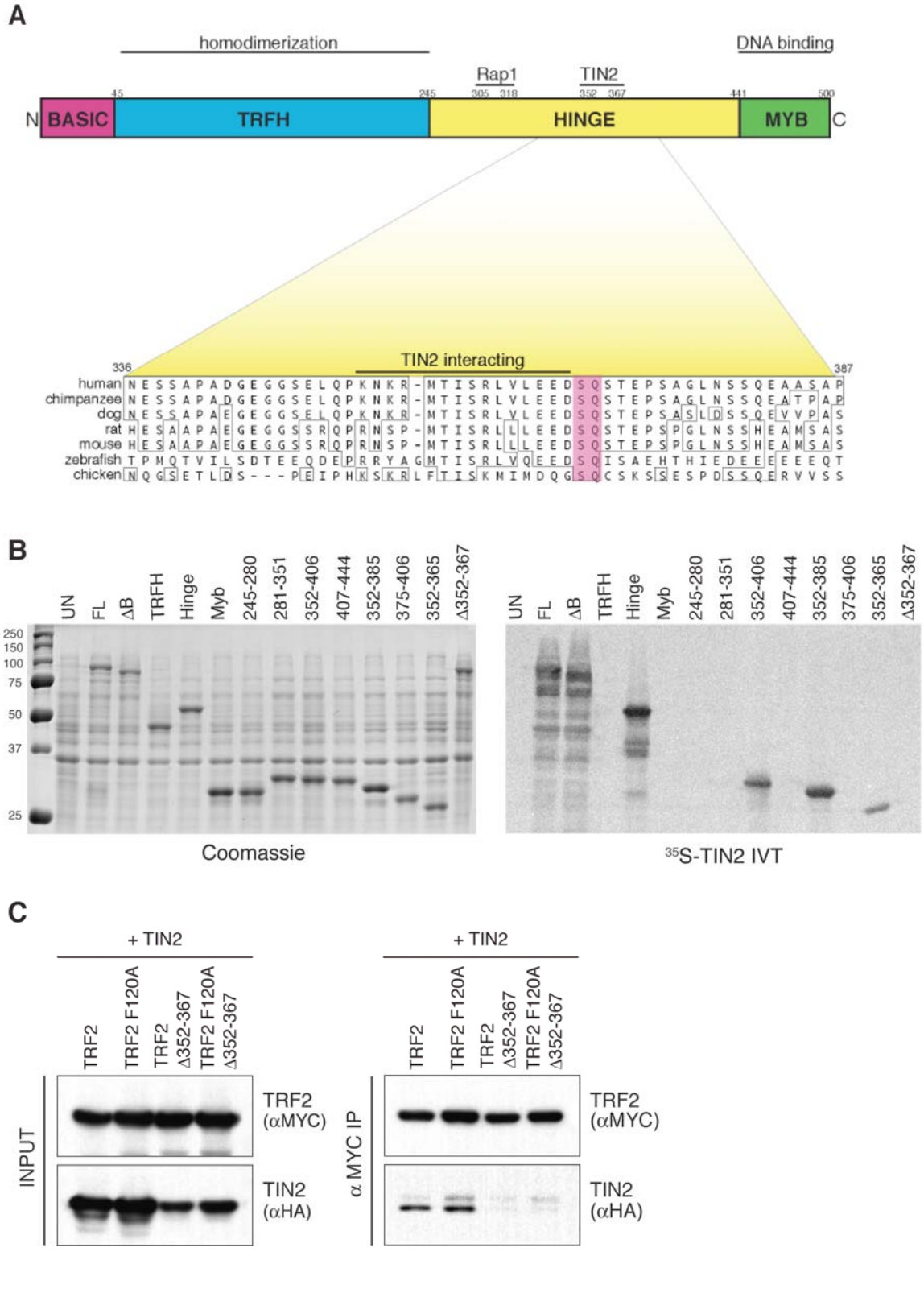
A
homodimerization
DNA binding
Rap1
TIN2
45
245
305 318
352 367
441
500
N
BASIC
TRFH
HINGE
MYB
C
TIN2 interacting
336
387
human
chimpanzee
dog
rat
mouse
zebrafish
chicken
B
UN
FL
ΔB
TRFH
Hinge
Myb
245-280
281-351
352-406
407-444
352-385
375-406
352-365
Δ352-367
250
150
100
75
50
37
25
Coomassie
35S-TIN2 IVT
C
+ TIN2
TRF2
TRF2 F120A
TRF2 Δ352-367
TRF2 F120A Δ352-367
INPUT
α MYC IP
TRF2 (αMYC)
TIN2 (αHA)

In collaboration with the Lei laboratory (University of Michigan Medical School), we examined the TRF1^{TRFH}-TIN2 and TRF2^{TRFH}-TIN2 interfaces to determine why TIN2 prefers the TRFH domain of TRF1 over that of TRF2. In doing so, we learned that TRF1-interacting proteins contain an F-X-L-X-P TRFH docking motif, while TRF2-interacting proteins have a Y-X-L-X-P TRFH localization sequence[15].

Structural analysis of the TRF1^{TRFH}-TIN2 interaction

To understand how TIN2 is recognized by TRF1^{TRFH}, Lei and his colleagues first mapped the TIN2 TRFH-binding motif, TIN2^{TBM}, to a short sequence (aa 256-276) in the C terminus of TIN2. They then crystallized the TRF1^{TRFH}-TIN2^{TBM} complex and solved its structure at 2.0 Å resolution[15]. The electron density map shows that residues 257 to 268 of TIN2^{TBM} assume a well-defined conformation. TRF1^{TRFH} forms homodimers, and each TRF1^{TRFH} interacts with one TIN2^{TBM} peptide (Fig. 3-5A). TRF1^{TRFH} exhibits essentially the same conformation as unliganded TRF1^{TRFH} except for loop L34 (Fig. 3-5B). Loop L34 is partially disordered in the peptide-free structure. However, once TIN2^{TBM} is bound, loop L34 folds back upon helices 3 and 4, sandwiched between the helices and TIN2^{TBM}.

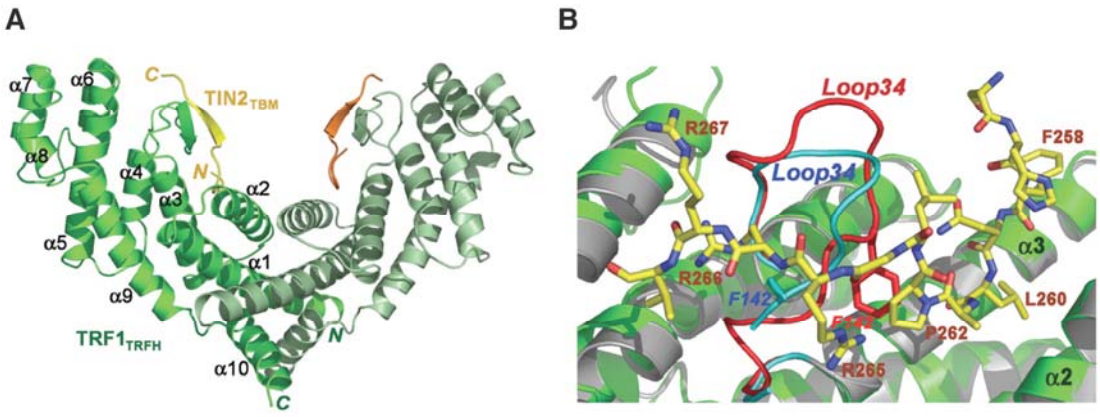

Figure 3-5. Structure of the TRF1^{TRFH}-TIN2^{TBM} complex.

(A) Overall structure of the dimeric TRF1^{TRFH}-TIN2^{TBM} complex. TRF1^{TRFH} and TIN2^{TBM} are colored in green and yellow, respectively, in one complex, and dark green and orange, respectively, in the other. (B) Superposition of the TRF1^{TRFH}-TIN2^{TBM} complex on the unliganded structure of TRF1^{TRFH}. Loop L34 in the complex is in red and that of unliganded TRF1^{TRFH} is in cyan, whereas the rest of TRF1$_{TRFH}$ is in green (TIN2^{TBM}-bound) or gray (peptide-free). (Figure done by Lei group)

The structure of the complex reveals two adjacent but structurally distinct interaction modes (Fig. 3-6A, B). The N terminus of TIN2^{TBM} (H257-F-N-L-A-P262) adopts an extended conformation stabilized by an extensive intermolecular hydrogen-bonding network. The side chain of L260 is therefore positioned into a deep hydrophobic pocket of TRF1^{TRFH}. In addition, F258 and P262 also make hydrophobic contacts with TRF1^{TRFH}: F258 sits on a concave hydrophobic surface, whereas P262 stacks with TRF1-F142. In contrast, the C terminus of TIN2^{TBM} (L263-G-R-R-R-V268) is positioned on the surface of loop L34 through formation of an antiparallel β sheet with D139-A-Q141 of TRF1^{TRFH} so that R265-R-R267 of TIN2^{TBM} contacts TRF1^{TRFH} through electrostatic interactions. In particular, R266 is

nested within an acidic depression on the surface of loop L34 through a network of salt bridges and hydrogen bonds[15].

To investigate the importance of this TRF1-TIN2 interface, I performed co-IPs from 293T cells transiently expressing wild type and mutant forms of TIN2 and TRF1[15] (Fig 3-6C). Substitution of TIN2 L260 with either an alanine or a glutamate abolished the interaction. By contrast, TIN2-P262A, designed to eliminate a stacking interaction with TRF1-F142, had a wild-type binding affinity, indicating that loss of this interaction is not essential for binding. However, substitution of TRF1-F142 with an alanine completely abrogated the binding to TIN2. These results were consistent with the in vitro isothermal titration calorimetry (ITC) binding data as measured by Lei and his colleagues[15].

Structural analysis of the TRF2^{TRFH}-TIN2 interaction

As discussed above, far western mapping of the TRF2-TIN2 interaction suggested that binding of TIN2 to TRF2 is only mediated through the hinge domain of TRF2 and not the TRFH domain as is the case for TRF1. This result was consistent with co-IP studies; while mutation of TRF1-F142 to an alanine abolished TIN2 binding, TRF2-F120A (the structural equivalence of TRF1-F142A) interacted with TIN2 to the same

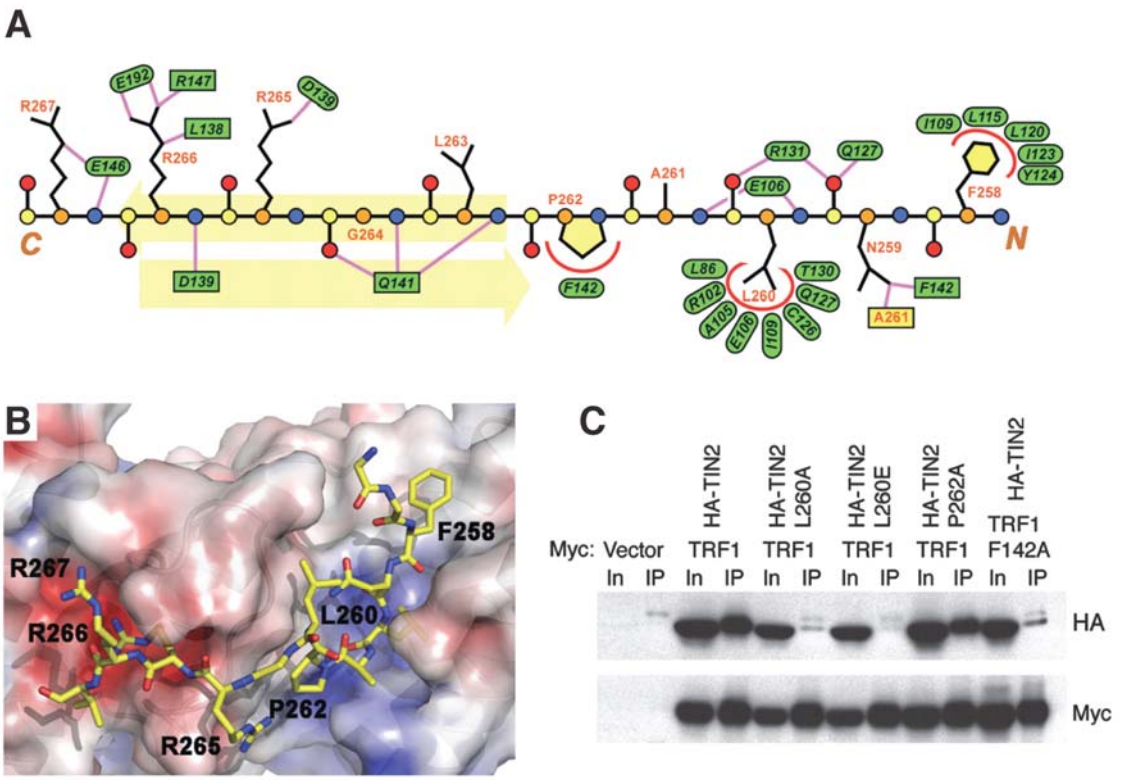

Figure 3-6. The TRF1^{TRFH}-TIN2^{TBM} interface.

(A) Schematic depiction of the TRF1^{TRFH}-TIN2^{TBM} interaction. The main-chain atoms of TIN2^{TBM} are shown as circles [carbon in yellow (Cα in orange), oxygen in red, and nitrogen in blue]. Residues of TRF1^{TRFH} are shown as green ovals (side-chain interaction) and square boxes (main-chain interaction). Hydrophilic and hydrophobic interactions are shown as straight magenta lines and curved red lines, respectively. The pale yellow arrows denote the intermolecular β sheet. (B) Electrostatic surface potential of the TIN2^{TBM} binding site of TRF1^{TRFH}. Positive potential, blue; negative potential, red. (Figures A and B done by Lei group) (C) Co-IP of wild type and mutant TRF1-TIN2 interactions. TRF1 proteins are Myc-tagged and TIN2 proteins are HA-tagged. Myc 9E10 antibody was used for the IP.

extent as wild type TRF2[15] (Fig. 3-4C). Therefore, TRF2^{TRFH} is not required for the stable association with TIN2 in vivo. ITC measurements showed that TIN2^{TBM} interacts with TRF2^{TRFH} in vitro, but with a much lower affinity (6.49 μM) than with TRF1^{TRFH} (0.31 μM). The distinctive specificity of the TRFH domains of TRF1 and TRF2 suggested that subtle

structural differences are responsible for the ability of TIN2 to distinguish between these two paralogous proteins. To understand this binding specificity, the Lei lab solved the crystal structure of the $TRF2^{TRFH}$-$TIN2^{TBM}$ complex at 2.15 Å resolution[15]. Although the overall conformations of $TIN2^{TBM}$ bound to $TRF1^{TRFH}$ and $TRF2^{TRFH}$ are very similar (Fig. 3-7A), subtle differences can explain the difference in affinities of the two complexes. In the $TRF1^{TRFH}$-$TIN2^{TBM}$ complex, TIN2-F258 sits snugly on a hydrophobic surface of $TRF1^{TRFH}$ (Fig. 3-7B). In contrast, F258 rotates away from the interface and packs less efficiently with $TRF2^{TRFH}$, because the edge of the interaction surface is partially occupied by polar residues S98 and R102 (Fig. 3-7B). In addition, TRF1-E192, which is key for $TIN2^{TBM}$ binding, is replaced by a lysine residue in TRF2 (K173), resulting in loss of two ion-pairing interactions and an electrostatically unfavorable contact between TIN2-R266 and TRF2-K173[15].

Discussion

The data in this chapter show that TIN2 mediates an interaction between the TRF1 and TRF2 telomeric complexes. TIN2 binds the TRFH domain of TRF1 using a sequence that contains an F-X-L-X-P docking motif in its C terminus. Shelterin-associated proteins that bind the TRFH domain

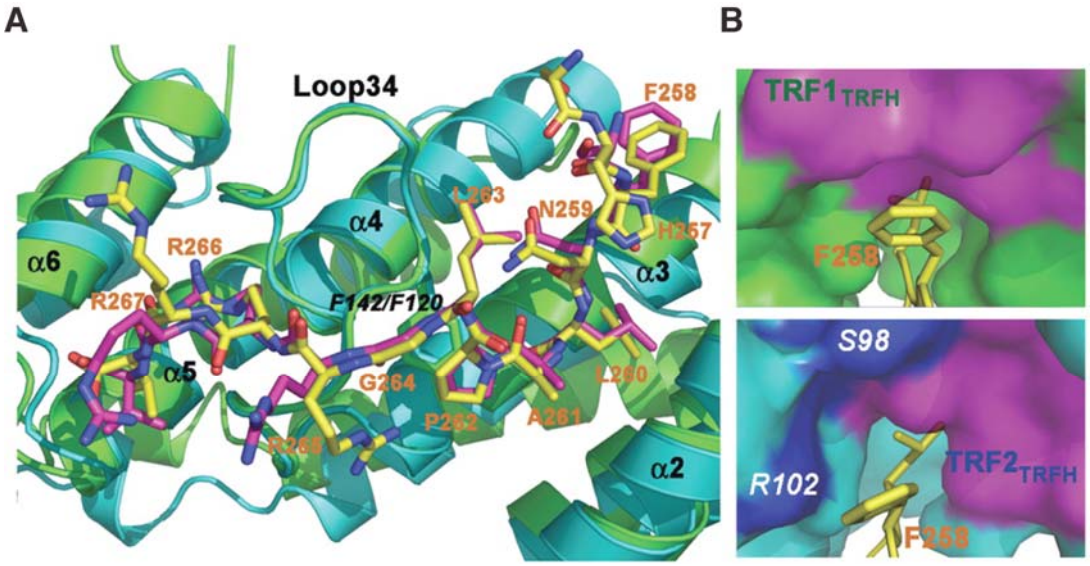

Figure 3-7. Structure of the TRF2^{TRFH}-TIN2^{TBM} complex.

(A) Superposition of the TIN2^{TBM} binding sites in the TRF1^{TRFH}-TIN2^{TBM} and TRF2^{TRFH}-TIN2^{TBM} complexes. TRF1^{TRFH} and TRF2^{TRFH} are in green and cyan, respectively. The TIN2^{TBM} peptides bound to TRF1^{TRFH} and TRF2^{TRFH} are shown in stick model format and in yellow and magenta, respectively. (B) TIN2-F258 interacts less efficiently with TRF2 than with TRF1. The F258 binding surfaces of TRF1^{TRFH} (top panel) and TRF2^{TRFH} (bottom panel) are shown in magenta (hydrophobic patch) and blue (hydrophilic patch). The rest of TRF1^{TRFH} and TRF2^{TRFH} is in green and cyan, respectively. (Figure done by Lei group)

of TRF2, such as Apollo, preferentially use a Y-X-L-X-P TRFH-docking motif. Hence, TIN2 has only a weak interaction with the TRFH domain of TRF2 in vitro[15]. Instead, the major TRF2/TIN2 interface was mapped to the N terminus of TIN2 and a small region in the hinge domain of TRF2. With its separate TRF1 and TRF2 binding domains, TIN2 can interact with both of these shelterin proteins individually or simultaneously.

The removal of TIN2 or TRF1 from telomeres leads to a concomitant loss of TRF2 and Rap1, suggesting that TIN2 plays an important role in stabilizing the TRF2 complex by tethering it to the TRF1 complex. Interactions between two DNA-binding proteins bound to neighboring sites will decrease the off rate of each and increase their affinity for DNA. Thus, the TIN2 link between TRF1 and TRF2 could increase the specificity of both proteins for telomeres. This effect may be particularly important with regard to TRF2, which has interactions with a number of abundant non-telomeric proteins, such as ATM, the Mre11 complex, and ERCC1/XPF. These interactions could lead to an inappropriate localization of TRF2 at non-telomeric sites, for instance, when these factors accumulate at sites of DNA damage. The stabilization of the TRF2 complex by TIN2 tethering to TRF1 may also explain the lethal phenotype of TRF1 and TIN2 deficiency in the mouse. A diminished TRF2 binding to telomeres in the absence of the TRF1/TIN2 stabilizing factor might result in telomere deprotection, which would impede cell proliferation.

In addition to binding to TRF1 and TRF2, TIN2 also interacts with TPP1, which serves to recruit POT1 to the telomeric complex. Because of its protein interactions, TIN2 connects the three main DNA binding activities at telomeres, two double-stranded DNA-binding proteins and the single single-

stranded DNA binding factor. Furthermore, TIN2 tethers POT1 to TRF2 independent of its interaction with TRF1, creating two separate protein interaction pathways by which POT1 can arrive at telomeres. Consistent with this, the binding of POT1 to telomeres is diminished by the inhibition of TRF2 as well as TRF1[76]. We had previously suggested that the loss of POT1 from the telomeres after impaired TRF2 function could be because of the degradation of the single-stranded telomeric overhang[76]. However, the current data suggest the loading of POT1 on telomeres could be affected by TRF2 inhibition in a manner that is not dependent on overhang degradation, but rather due to diminished loading of TIN2[47].

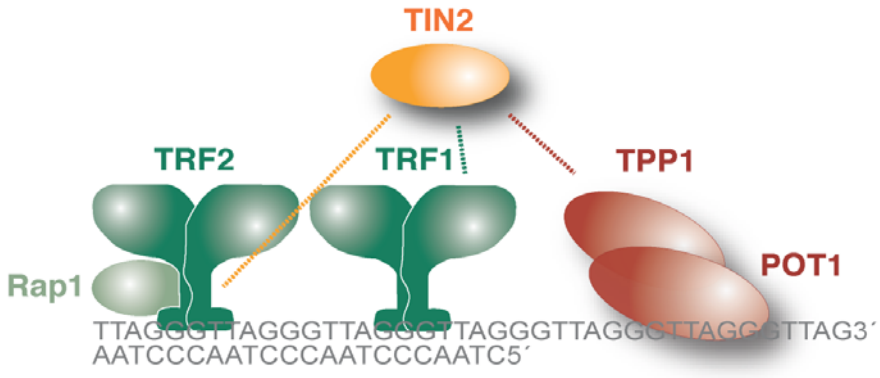

Figure 3-8. TIN2 connects the three main DNA binding activities at telomeres.

Schematic of how shelterin might be positioned on telomeric DNA, highlighting the duplex telomeric DNA interactions of TRF1 and TRF2 and the binding of POT1 to the single-stranded TTAGGG repeats.

Creation of the TRF2 TIN2-binding mutant, TRF2$^{\Delta T}$, provides a reagent for exclusively studying the function of the TRF2-TIN2-TPP1-POT1 complex at telomeres. This surgical mutation in the hinge domain of TRF2 is predicted to affect the TRF2-TIN2 connection while not interfering with the recruitment of TRF2-Rap1 or the TRF1-TIN2-TPP1-POT1 complex to chromosome ends. The experiments in the next chapter examine the phenotype of TRF2$^{\Delta T}$ in mouse cells and provide insight into the function of the TRF2/TIN2 interaction.

CHAPTER 4: TIN2 ASSISTS TRF2 IN SUPPRESSING THE ATM-DEPENDENT DNA DAMAGE RESPONSE AT TELOMERES

Introduction

This chapter describes the phenotype of the mouse TRF2 TIN2-binding mutant, mTRF2$^{\Delta T}$. Disruption of the association between TRF2 and the TIN2-TPP1-POT1 complex results in a unique ATM-dependent telomere damage response that leads to the induction of telomere dysfunction induced foci (TIFs) and changes in the status of the telomeric DNA. The nature of this response differs from that seen by loss of TRF2 or POT1 from telomeres.

Telomere Protection by TRF2

TRF2 plays a key role in protecting telomeres from being recognized as sites of damaged DNA. This function of TRF2 was first elucidated in human cells using a dominant negative allele of TRF2, which lacks the N-terminal basic domain and the C-terminal Myb DNA-binding domain (TRF2$^{\Delta B \Delta M}$). Uncapping of telomeres by TRF2$^{\Delta B \Delta M}$[122], RNAi[117], or by replicative telomere shortening[109] results in a myriad of consequences. One outcome of TRF2 loss is the accumulation of DNA damage response factors,

such as 53BP1, γ-H2AX, Rad17, phosphorylated ATM, and Mre11, at chromosome ends[28, 117]. These entities are referred to as telomere dysfunction induced foci (TIFs)[117]. Activation of the DNA damage response machinery at telomeres also triggers the induction of p53-mediated apoptosis or senescence, depending on cell type[55, 122]. Additionally, deprotected telomeres cause degradation of the G-strand overhang by the nuclease ERCC1/XPF[122, 138]. This event is a prerequisite for DNA Ligase IV-dependent nonhomologous end joining (NHEJ) at telomeres, resulting in end-to-end fusions and formation of dicentric and multicentric chromosomes[110, 122].

While TRF2$^{\Delta B \Delta M}$ and RNAi were used to study the loss-of-TRF2 phenotype in human cells, a novel system was developed in mouse cells. TRF2$^{F/-}$ mouse embryo fibroblasts (MEFs) were generated by deleting one allele of TRF2 and flanking the second TRF2 allele with LoxP sites, allowing inactivation of the TRF2 gene with Cre recombinase. Removal of TRF2 from these MEFs generates the same phenotypes as described above, including TIF formation, loss of the 3' overhang, NHEJ-mediated telomere fusions, and cell cycle arrest[10].

The DNA damage response elicited by deletion of TRF2 from mammalian cells is dependent on the ATM kinase. Ablation of TRF2 leads to autophosphorylation of ATM on S1981, a hallmark of ATM activation, and phosphorylation of the ATM target, Chk2[10, 66, 117]. This response is thwarted when TRF2 is deleted from $ATM^{-/-}$ cells. The formation of TIFs and phosphorylation of Chk2 is largely abrogated[66].

How TRF2 inhibits ATM at telomeres remains to be determined. One possibility is that TRF2 promotes t-loop formation which tucks the 3' overhang into the duplex region of the telomere, perhaps preventing it from being recognized and processed as a DNA break by ATM. In vitro t-loop assays using electron microscopy have shown that TRF2 is able to catalyze t-loop formation or to stabilize loops[42, 115], supporting this model. Another possibility is that TRF2 directly inhibits ATM activation. Evidence in favor of this model comes from the fact that TRF2 can actually binds ATM. Furthermore, overexpression of TRF2 hinders the response of ATM to DNA damage. TRF2 prevents autophosphorylation of ATM on S1981 and subsequent events associated with ATM activation such as phoshorylation of Nbs1, induction of p53 and its targets, and cell cycle arrest[56]. Finally, it is possible that the suppression of ATM at telomeres is mediated by TRF2 binding partners, such as Rap1, the Mre11 complex, or TIN2.

Telomere Protection by TPP1/POT1

Protecting chromosome ends is not solely the responsibility of TRF2. Shelterin's single-stranded DNA binding protein, POT1, along with its recruiter, TPP1, are also major players in carrying out this function of telomeres[46-48, 129]. Using RNAi studies in human cells, it was determined that POT1 loss leads to a transient DNA damage response that differs from that seen by TRF2 inhibition. Cells treated with POT1 shRNA have a reduction of the 3' overhang and induce TIFs in G_1, but lack a significant level of chromosome end fusions and fail to arrest[48].

In mouse cells, two POT1 proteins are required to fully protect telomeres. When both POT1a and POT1b are deleted, 70-80% of the nuclei contain DNA damage response factors at their telomeres, the cells experience a rapid proliferative arrest, and a mild telomere fusion phenotype is evoked. Single knockouts and complementation experiments indicate that POT1a is mainly responsible for repressing this DNA damage signal, while POT1b has a more specific role in regulating the structure of the telomere terminus[46].

Unlike TRF2, which represses the ATM kinase pathway at telomeres, POT1 is implicated in preventing ATR activation at chromosome ends. In agreement with this, POT1 deficiency initiates phosphorylation of Chk1 and

Chk2, downstream targets of ATR, while RNAi-mediated downregulation of ATR protein levels abolishes the damage response. Consistent with ATR as the mediator of this response, ATM deficiency has no effect on the outcome of POT1 loss[66].

The repression of ATR activation by POT1 is speculated to be the result of POT1 preferentially binding to single-stranded telomeric DNA instead of RPA. RPA recognizes and localizes to single-stranded DNA at sites of damage and recruits the ATRIP/ATR complex[139]. The 3' G-overhang or D-loop can serve as a substrate for RPA binding. However, according to the model, the sequence specificity and high abundance of POT1 at chromosome ends allows POT1 to compete with RPA for these DNA sites.

Telomere Protection by TIN2

TIN2 interacts with TRF1 and TRF2 independently or simultaneously, acting as a bridge linking TRF1 and TRF2 to TPP1 and POT1. Removal of TIN2 from telomeres by RNAi or expression of TIN2 mutants that fail to bind TRF1 or TRF2 results in a DNA damage response[61, 134]. However, these methods for depleting TIN2 result in the destabilization of TRF1 and TRF2, and presumably TPP1/POT1 from telomeres, thus masking the

phenotype of a DNA damage response initiated exclusively by TIN2. To circumvent this problem, a surgical mutation was made in the hinge domain of TRF2 that prevents TIN2 binding. This TRF2 mutant, $TRF2^{\Delta T}$, still localizes to telomeres, as does Rap1 and TRF1. The experiments in this chapter were designed to examine the phenotype of $TRF2^{\Delta T}$ and shed light on a novel ATM-dependent TIN2-mediated DNA damage response.

Results

Expression of $TRF^{\Delta T}$ in $TRF2^{F/-}$ $p53^{-/-}$ MEFs

Amino acids 350-365 in the hinge domain of mouse TRF2 were deleted using the same strategy that was employed to create human $TRF2^{\Delta T}$. Far western assaying verified that mouse $TRF2^{\Delta T}$ does not bind TIN2 whereas $TRF2^{WT}$ showed a strong interaction with the ^{35}S-labeled protein (Fig. 4-1).

To study the phenotype of $TRF2^{\Delta T}$ in vivo, Myc-tagged $TRF2^{\Delta T}$, along with Myc-tagged wild type TRF2 and empty vector, were introduced into $TRF2^{F/-}$ $p53^{-/-}$ MEFs by retroviral infection. p53-deficient MEFs were used to overcome the senescence-like arrest associated with TRF2 loss, allowing for analysis of mitotic chromosomes. Examination of $TRF2^{\Delta T}$ cells

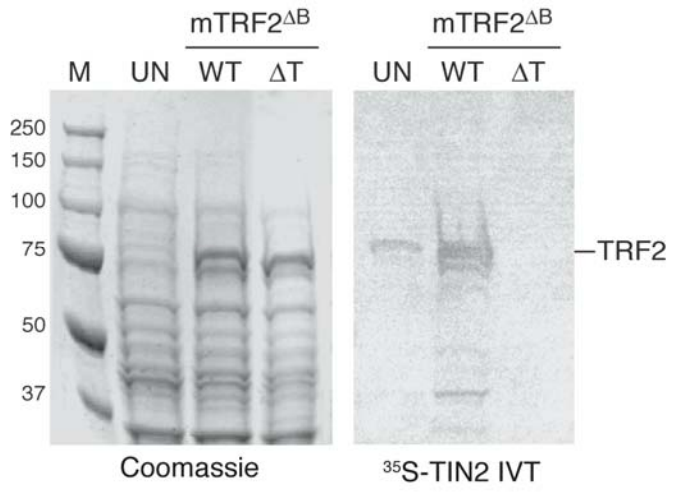

Figure 4-1. mTRF2$^{\Delta T}$ does not bind TIN2.

Far western analysis of mTRF2$^{\Delta T}$ with [^{35}S]TIN2 IVT protein. Each lane contains lysate from induced *E. coli* BL21 bacterial cultures that express the indicated GST-fused mTRF2$^{\Delta B}$ constructs. The lysates were subjected to SDS-PAGE, stained with Coomassie blue (left), or blotted onto nitrocellulose and incubated with [^{35}S]TIN2 IVT protein (right). ΔB, mTRF2Δ1-45; UN, uninduced control; WT, wild type mTRF2; ΔT, mTRF2Δ350-365.

by Myc IF revealed a mixed population of cells, with some exhibiting a mild to robust punctate staining that localized to telomeres and others presenting a diffuse nuclear staining (data not shown). The latter cells clearly were not localizing TRF2$^{\Delta T}$ to telomeres. It became evident that abating the interaction between TIN2 and TRF2 was destabilizing TRF2 at telomeres. Use of these batch cells for analysis of the TRF2$^{\Delta T}$ phenotype would be troublesome, as some of the cells would exhibit a loss-of-TRF2 phenotype. In order to circumvent this problem, we created clonal cell lines that

homogeneously expressed TRF2$^{\Delta T}$ at a moderate to high level. After two rounds of cloning, one from retrovirally-infected cells and one from cells infected with lentivirus, four TRF2$^{\Delta T}$ clones (TRF2$^{\Delta T\text{-}6}$, TRF2$^{\Delta T\text{-}21}$, TRF2$^{\Delta T\text{-}13}$, and TRF2$^{\Delta T\text{-}16}$) were chosen for further examination based on their western blot and IF profiles (Fig. 4-2B, C). The following experiments were done in a setting where the floxed allele of TRF2 was deleted from cells by retroviral expression of Cre recombinase. This technology allows for analysis of the TRF2$^{\Delta T}$ phenotype in the absence of endogenous TRF2. Indeed, western blotting showed that endogenous TRF2 was deleted from cells 96 hours post Cre infection in the TRF2$^{\Delta T}$ clones as well as in vector and wild type cells (Fig. 4-2A, B).

TRF2$^{\Delta T}$ MEFs do not arrest

The majority of the experiments conducted in this chapter were done in the time frame of 72-120 hours post Cre expression. During this time frame, TRF2$^{F/-}$ p53$^{-/-}$ MEFs devoid of TRF2 experience growth defects with cells becoming large and flattened, eventually ending in death of the culture. At 120 hours, there was no evidence of growth arrest or changes in the morphology of the TRF2$^{\Delta T}$ cells. We continued to grow the cells for an

Figure 4-2. TRF2$^{F/-}$ p53$^{-/-}$ clonal cell lines expressing TRF2$^{\Delta T}$.

(A) Experimental timeline. (B) Western blot of cell lysates derived from TRF2$^{\Delta T}$ clones. Cells were infected with Cre retrovirus and harvested 96 hours later. Anti-TRF2, 1254 antibody was used; TRF2 and non-specific bands are indicated. (C) IF of TRF2$^{\Delta T}$ clones. Antibodies used: anti-c-Myc, Sigma and anti-mTRF1, 644.

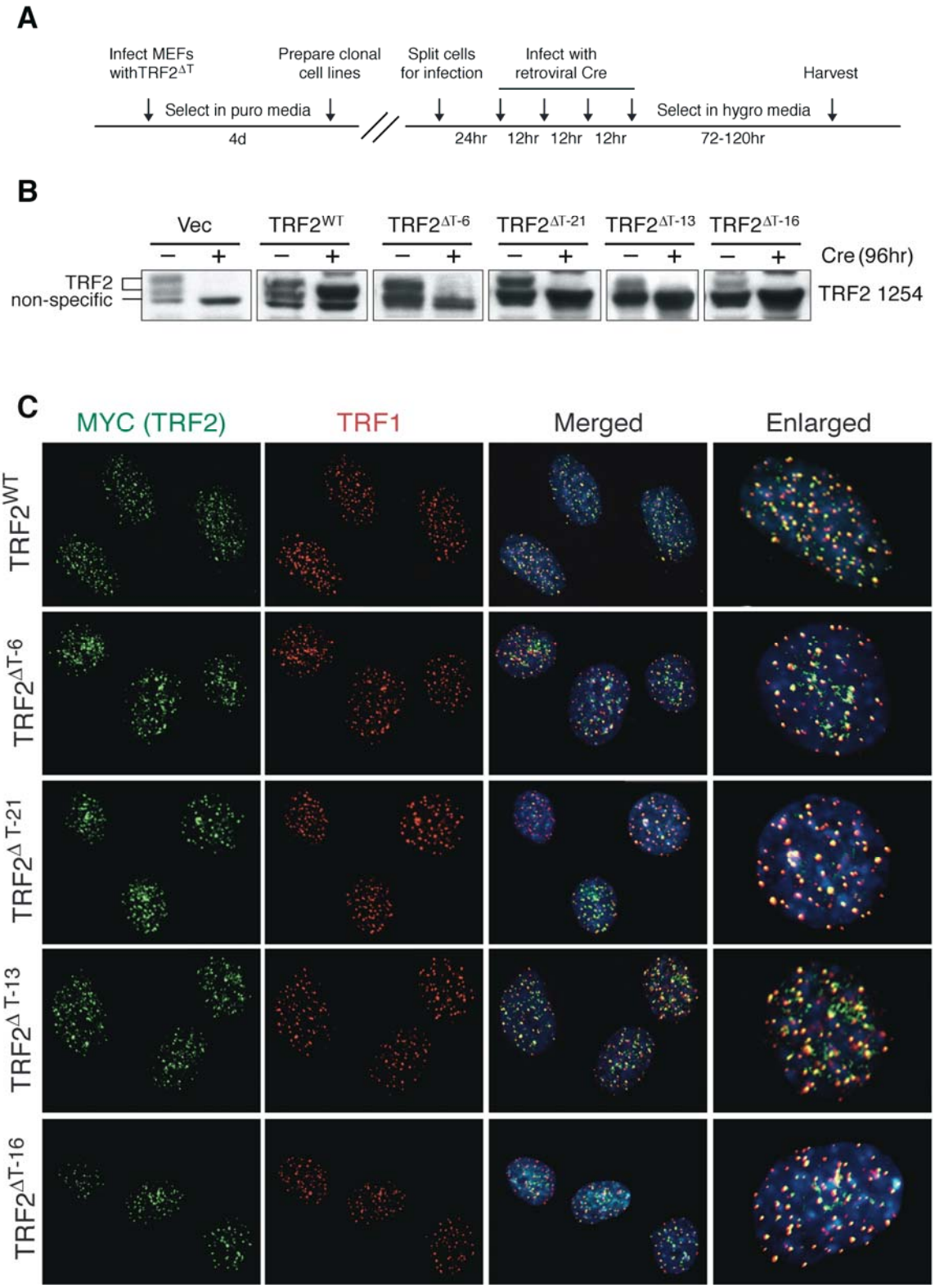
A
Infect MEFs withTRF2ΔT
Prepare clonal cell lines
Split cells for infection
Infect with retroviral Cre
Harvest
Select in puro media
Select in hygro media
4d
24hr
12hr
12hr
12hr
72-120hr
B
Vec
TRF2WT
TRF2ΔT-6
TRF2ΔT-21
TRF2ΔT-13
TRF2ΔT-16
Cre (96hr)
TRF2
non-specific
TRF2 1254
C
MYC (TRF2)
TRF1
Merged
Enlarged
TRF2WT
TRF2ΔT-6
TRF2ΔT-21
TRF2ΔT-13
TRF2ΔT-16

extended period of time to evaluate the proliferative potential of these MEFs. However, a western blot performed approximately two weeks post Cre infection revealed expression of endogenous TRF2 (data not shown). This suggested that there was a positive selection for cells that had not been exposed to Cre. To circumvent this problem, secondary clones of $TRF2^{\Delta T\text{-}13}$ and $TRF2^{\Delta T\text{-}16}$ were made after the cells had been treated with Cre. Two clones for each were chosen for growth analysis. Western blotting revealed that after 42 days from the start of the growth curve, endogenous TRF2 was still deleted from these clones, while exogenous Myc-tagged $TRF2^{\Delta T}$ continued to be expressed (Fig. 4-3). As the growth curve shows, there were no major growth defects in any of the clones analyzed (Fig. 4-3). The $TRF2^{\Delta T\text{-}13}$ clones, regardless of their Cre status, grew at similar rates, while the $TRF2^{\Delta T\text{-}16}$ Cre-positive clones proliferated somewhat slower than the Cre-negative control. It is possible that these clones were expressing such a high level of Cre that it was slightly toxic to the cells.

Shelterin localization in $TRF2^{\Delta T}$ MEFs

Based on far western assaying and 293T co-immunoprecipitation, it was shown that the association of $TRF2^{\Delta T}$ with TIN2 was hindered. In order to determine the amount of TIN2 localizing to telomeres, the $TRF2^{\Delta T}$ clones

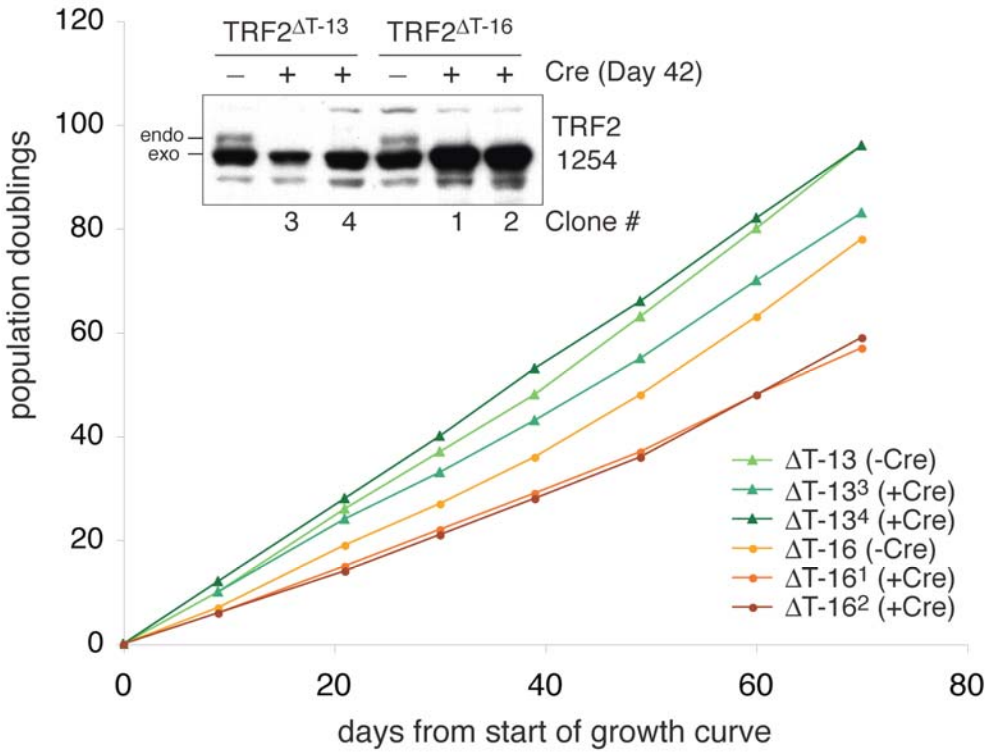

Figure 4-3. TRF2$^{\Delta T}$ clones do not have growth defects.

Graph of growth curves of Cre-positive secondary TRF2$^{\Delta T}$ clones and the Cre-negative controls. TRF2$^{\Delta T\text{-}13}$ TRF2$^{\Delta T\text{-}16}$ clones were infected with retroviral Cre, selected in hygromycin for 5 days, clonal populations were isolated, and Cre-positive clones were chosen. Growth of the secondary clones was monitored for 70 days. Western blot shows that endogenous TRF2 was still inhibited after 42 days from the start of the growth curve, while exogenous TRF2$^{\Delta T}$ was still expressed. endo, endogenousTRF2; exo, exogenous Myc-tagged TRF2$^{\Delta T}$.

were examined by IF. This required the production of an antibody against mouse TIN2. TIN2 was cloned from a mouse cDNA library into a GST-tagged *E. coli* protein expression vector. GST-mTIN2 was affinity-purified from induced BL21 bacterial cultures (Fig. 4-4A) and sent to Covance for polyclonal antibody production in rabbits. Upon receipt of the serum, the antibody was affinity-purified and tested by western blotting and IF. The

western blot revealed that mTIN2 1447 recognizes overexpressed Myc-tagged mTIN2 and recombinant GST-mTIN2 protein, but not a discernable band for the endogenous protein (Fig. 4-4B). There was no reduction in proteins levels around the 50 kD marker in the lanes of MEFs treated with mTIN2 shRNAs compared to the lane of cells treated with the control luciferase shRNA (Takai, K and de Lange, unpublished). On the contrary, the antibody was successful in distinguishing endogenous mTIN2 by IF. TIN2 1447 elicited a robust punctate signal that co-localized with telomeric DNA at telomeres (Fig. 4-4C). This signal was greatly reduced in many of the cells treated with the same TIN2 shRNAs that were used for the western blot (data not shown) (Takai, K and de Lange, unpublished).

With this reagent in hand, we investigated the effect of $TRF2^{\Delta T}$ expression on TIN2 localization to telomeres after deletion of endogenous TRF2. The $TRF2^{\Delta T}$ clones, along with the $TRF2^{WT}$ control, were infected with Cre retrovirus four times every twelve hours, selected in media containing hygromyocin, and then harvested for immunofluorescence-fluorescence in-situ hybridization (IF-FISH) analysis 96 hours post Cre infection. In the cells expressing $TRF2^{WT}$, there was a strong TIN2 signal

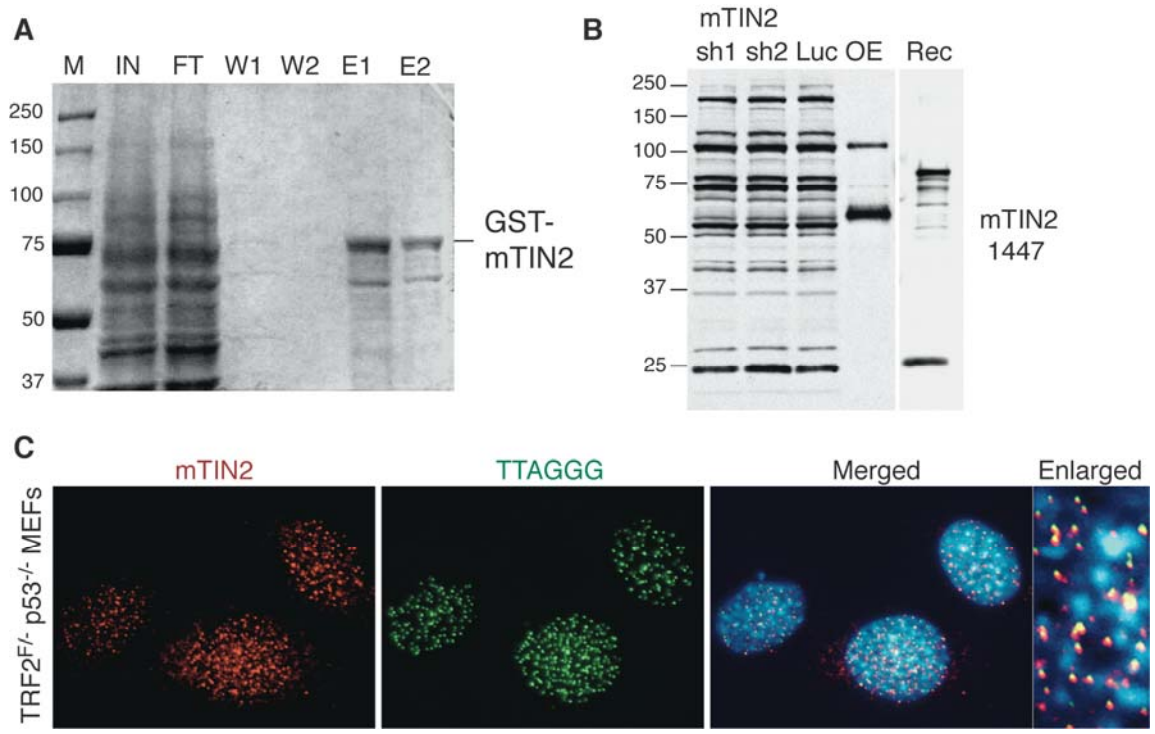

Figure 4-4. Antibody against mouse TIN2.

(A) Coomassie-gel of affinity-purified GST-mTIN2. UN, uninduced; IN; input; FT, flow-through; W, wash; E, elution. (B) Western blot using mTIN2 1447. Endogenous mTIN2, with shRNA-mediated knockdown (sh1 and sh2) or without (Luc, luciferase shRNA), overexpressed Myc-tagged mTIN2 (OE), and recombinant GST-mTIN2 (Rec) were tested. (C) IF of endogenous mTIN2 at telomeres. Telomeres were detected by FISH using a PNA probe specific for telomeric repeats (TTAGGG).

that completely localized to telomeres based on the merged image with the telomeric TTAGGG PNA probe. However, a different pattern of TIN2 signals was evident for the TRF2$^{\Delta T}$ clones. In these cells, TIN2 gave a diffuse nuclear staining, with several dampened telomeric signals, suggesting that some TIN2 remains at telomeres through its interaction with TRF1 (Fig. 4-5). Similarly, the majority of POT1a did not localize to telomeres in cells expressing TRF2$^{\Delta T}$. In fact, the nucleus of these cells

appeared almost vacant, with little to no POT1a staining, except for a few extremely weak telomeric signals (Fig. 4-6A). It is important to point out that this POT1a antibody is suboptimal for IF procedures; as such, it is possible that the amount of POT1a remaining at telomeres was below the detection level of the antibody.

Although TIN2 was substantially destabilized at telomeres in TRF2$^{\Delta T}$ cells, we verified by IF-FISH that TRF1 and Rap1 are still localized to telomeres using TRF2$^{\Delta T\text{-}13}$ as an example (Fig. 4-6B, C). However, there was a noticeable increase in the amount of nucleoplasmic Rap1, and to a much lesser extent, TRF1, suggesting that some Rap1 and TRF1 is displaced from chromosome ends. We used telomere-specific ChIP to quantify the percentage of shelterin components at telomeres in the wild type and mutant settings. TRF2^{WT} and TRF2$^{\Delta T\text{-}13}$ MEFs were infected with Cre and processed for ChIP analysis 120 hours later. The results indicated that there was approximately a 30-50% reduction in the amount of TRF1, TRF2, TIN2, and Rap1 at telomeres in TRF2$^{\Delta T\text{-}13}$ cells (Fig. 4-6D, E). For TPP1, POT1a, and POT1b, the overall amounts of precipitated proteins were too low to determine whether there was a significant difference between wild type and mutant cells. Combining the findings of the IF and ChIP experiments, we could presume that all components of shelterin are present at telomeres to

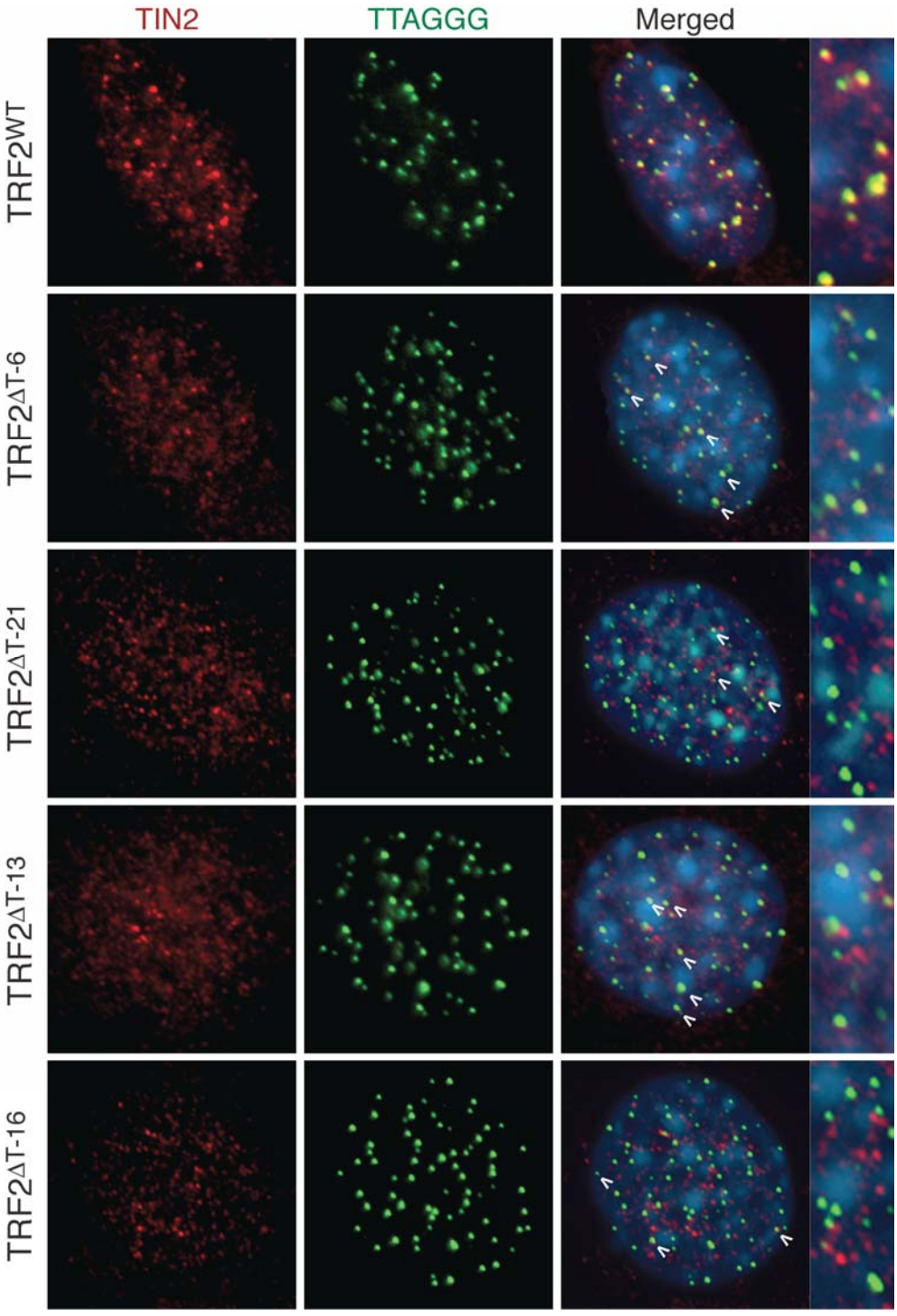

Figure 4-5. Less TIN2 is localized to telomeres in TRF2$^{\Delta T}$ clones.

IF of TIN2 localization to telomeres in TRF2$^{\Delta T}$ clones and the wild-type control 96 hours post Cre infection. TIN2 was detected with anti-TIN2, 1447 and telomeres were detected by FISH using a PNA probe specific for telomeric repeats (TTAGGG). White arrows indicate the few TIN2 signals that co-localize with telomeres in TRF2$^{\Delta T}$ cells.

some degree except for the TIN2-TPP1-POT1 complex that associates with TRF2. This makes TRF2$^{\Delta T}$ an attractive reagent for studying the function of this complex. Although, it cannot be ruled out that the reduction in TRF1, TRF2, or Rap1 may contribute to the phenotype of this mutant.

TRF2$^{\Delta T}$ MEFs induced TIFs

We treated TRF2^{WT} and TRF2$^{\Delta T}$ MEFs with retroviral Cre and examined the cells for TIFs, using 53BP1 staining, 96 hours later. Whereas the MEFs rescued with wild type TRF2 presented only a small background percentage of cells with five or more TIFs (6%), TRF2$^{\Delta T\text{-}6}$, TRF2$^{\Delta T\text{-}21}$, and TRF2$^{\Delta T\text{-}13}$ elicited TIFs in 86%, 71%, and 42% of the cells scored, respectively (Fig. 4-7). These TIFs varied in morphology and frequency when compared to TIFs induced by loss of TRF2. The 53BP1 foci in the TRF2$^{\Delta T}$ clones appeared much larger, extending far beyond the telomeres, and TIFs occurred at fewer telomeres. Cells suffering from loss of TRF2 have approximately 80% TIF-positive telomeres, while TRF2$^{\Delta T}$ cells gave an average of 21% TIF-positive telomeres (Fig. 4-7).

Although the majority of 53BP1 foci co-localized with telomeres 96 hours post Cre expression, some foci were present in regions of nuclei completely devoid of telomeric signals. These telomere-less foci became

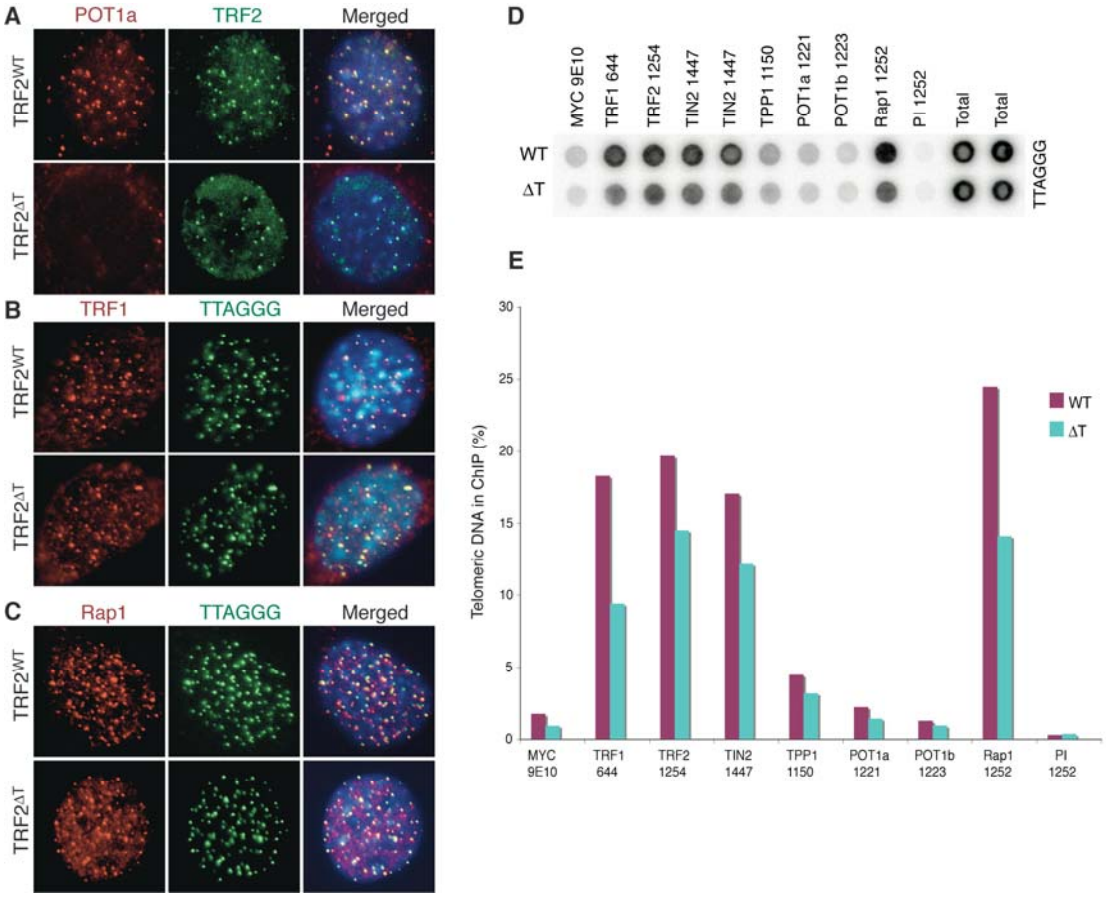

Figure 4-6. Localization of shelterin components to telomeres in TRF2$^{\Delta T}$ clones.

IF of POT1a (A), TRF1 (B), and Rap1 (C) localization to telomeres in TRF2$^{\Delta T\text{-}13}$ cells and the wild type control 96 hours post Cre infection. Antibodies used: mouse anti-POT1a; anti-TRF1, 644; anti-Rap1, 1252. Telomeres were detected by FISH using a PNA probe specific for telomeric repeats (TTAGGG). (D) ChIP of shelterin proteins at telomeres in TRF2^{WT} and TRF2$^{\Delta T\text{-}13}$ cells. ChIP was performed on the indicated cell lines 96 hours after introduction of Cre. Immunoprecipitated DNA was blotted onto a membrane and probed with the telomere specific γ-^{32}P end-labeled oligonucleotide probe $(CCCTAA)_4$. Antibodies used: anti-c-Myc, 9E10 (Calbiochem); anti-TRF1, 644; anti-TRF2, 1254; anti-TIN2, 1447; anti-TPP1, 1150; anti-POT1a, 1221; anti-POT1b, 1223; anti-Rap1, 1252; PI, Pre-Immune serum (from animal used to generate Rap1 antibody 1252). (E) Quantification of signals in (A).

even more prevalent at later time points. In fact, seven to ten days post Cre expression, the majority of 53BP1 foci were lacking a telomeric signal, thus rendering the number of TIF-positive cells insignificant.

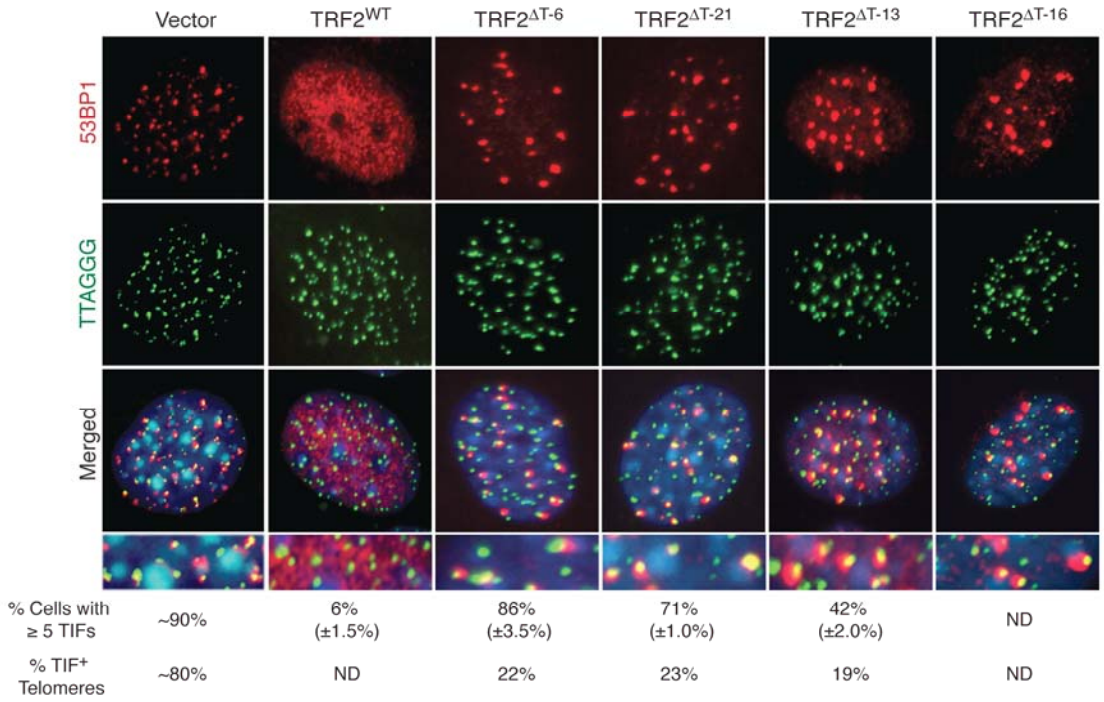

Figure 4-7. TRF2$^{\Delta T}$ cells induce TIFs.

IF of 53BP1 localization to telomeres in TRF2$^{\Delta T}$ clones, TRF2^{WT} cells, and the vector control. IF was preformed for 53BP1 (Novus) in conjunction with FISH using a PNA probe specific for telomeric repeats (TTAGGG) 96 hours after Cre infection. The percentage of cells with 5 or more TIFs and the percentage of TIF-positive telomeres are indicated for each. ND, not determined.

ATM-mediated telomere damage response in TRF2$^{\Delta T}$ MEFs

TRF2 and POT1 function independently to repress the activation of ATM and ATR kinases at natural chromosome ends. We asked whether the telomere damage response caused by expression of TRF2$^{\Delta T}$ was ATM-dependent. TRF2$^{F/-}$ ATM$^{+/+}$ and TRF2$^{F/-}$ ATM$^{-/-}$ cell lines expressing TRF2$^{\Delta T}$ were infected with Cre retrovirus and harvested for TIF and telomeric FISH analysis 72-120 hours later. Western blotting showed that TRF2$^{\Delta T}$ was highly overexpressed compared to endogenous TRF2 and Cre deletion of the floxed allele was successful (Fig. 4-8A). In TRF2$^{F/-}$ ATM$^{+/+}$ cells, expression of TRF2$^{\Delta T}$ induced TIFs in approximately 30% of the nuclei scored (Fig. 4-8B). The number of TIF-positive cells was reduced by more than half to 13% in TRF2$^{F/-}$ ATM$^{-/-}$ MEFs expressing TRF2$^{\Delta T}$, suggesting the DNA damage response caused by TIN2 loss from the TRF2 complex is, to some extent, an ATM-mediated event. This was supported by the fact that Chk2 was phosphorylated in TRF2$^{\Delta T}$ TRF2$^{F/-}$ ATM$^{+/+}$ cells after Cre treatment, but not in cells deficient in ATM. On the other hand, the MTS phenotype seemed to persist in the absence of ATM. These results were recapitulated, albeit to a lesser extent, in the TRF2$^{\Delta T\text{-}13}$ clone targeted with shRNA against ATM (Fig. 4-8D). In control cells treated just with an empty

vector, approximately 38% of the nuclei contained TIFs. When ATM protein levels were knocked down in the TRF2$^{\Delta T\text{-}13}$ MEFs, there was a mild reduction to 27% TIF-positive cells. It should be noted, however, that the shRNA-mediated decrease of ATM protein levels was not complete, and thus some ATM signaling was still occurring (Fig. 4-8C).

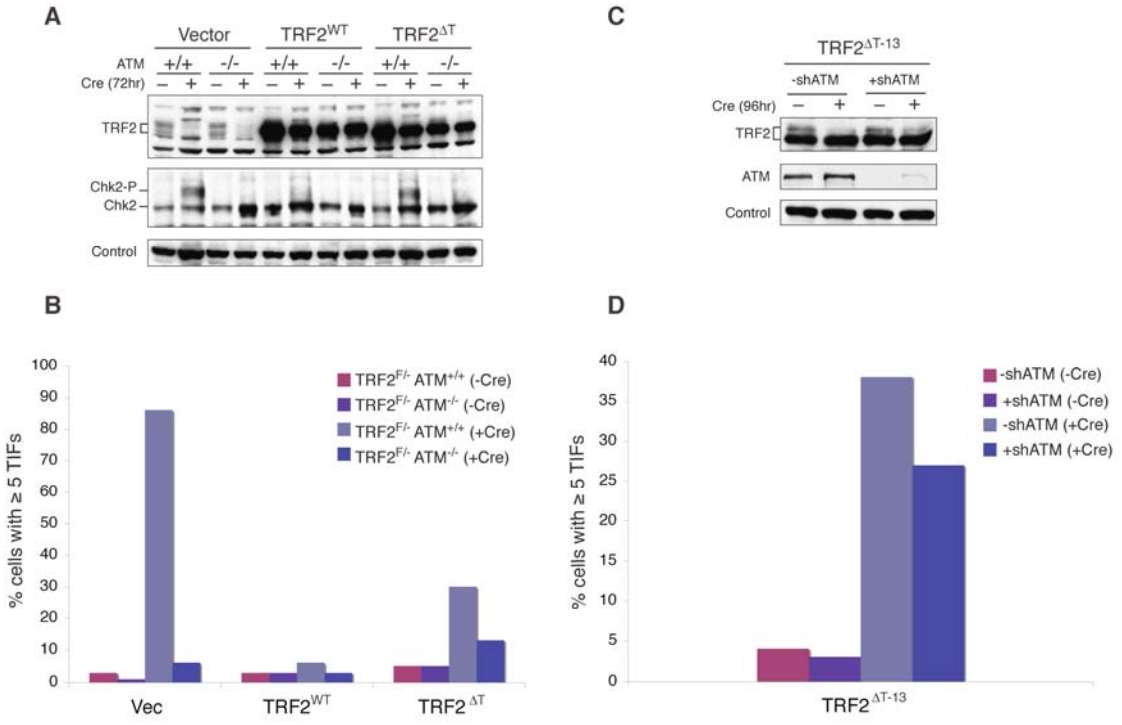

Figure 4-8. Telomere dysfunction induced by loss of TIN2 from the TRF2 complex is partly ATM-dependent.

(A) Immunblots for TRF2 and Chk2-P in TRF2$^{F/-}$ ATM$^{+/+}$ and TRF2$^{F/-}$ ATM$^{-/-}$ MEFs expressing TRF2$^{\Delta T}$, TRF2^{WT}, or the vector control. Cells were infected with Cre retrovirus and harvested 72 hours later. Antibodies used: anti-TRF2, 1254; anti-Chk2 (BD Trans. Lab) (B) Quantification of TIF-positive cells in the indicated cell lines. (C) Immunblots for TRF2 and ATM in TRF2$^{\Delta T\text{-}13}$ cells treated with shATM or a vector control. Cells were infected with Cre retrovirus and harvested 96 hours later. Antibodies used: anti-TRF2, 1254; anti-ATM, MAT3 (Sigma) (B) Quantification of TIF-positive cells in the indicated cell lines. TIF-positive cells = cells with ≥ 5 TIFs.

Multiple telomeric signals and telomere loss at the ends of TRF2$^{\Delta T}$ chromosomes

The induction of a DNA damage response at telomeres in TRF2$^{\Delta T}$ MEFs prompted us to examine the status of the telomeric DNA. The condition of the telomeric overhang as well as the duplex telomeric DNA was evaluated using the in-gel hybridization method. Unlike the telomeres of the empty vector control cells, TRF2$^{\Delta T}$ telomeres did not show signs of overhang loss or fusion events (Fig. 4-9).

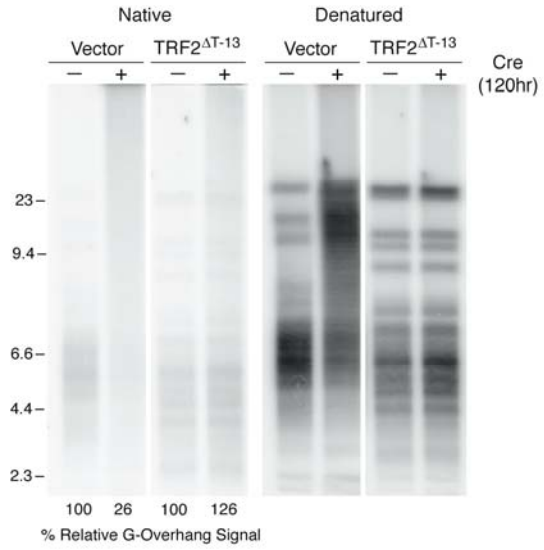

Figure 4-9. TRF2$^{\Delta T}$ cells prevent overhang loss and fusions.

In-gel hybridization assay examining single-stranded and duplex telomeric DNA in TRF2$^{\Delta T\text{-}13}$ cells. Cells were harvested 120 hours post Cre infection; DNA was digested with MboI restriction endonuclease and subjected to PFGE. In-gel hybridization was performed under native conditions and the telomeric overhang was detected with the γ-^{32}P end labeled oligonucleotide probe $(CCCTAA)_4$ (Left). DNA was denatured in situ and reprobed (Right). Overhang signal was quantitated using ImageQuant software and normalized to the total telomeric signal obtained after denaturation. The high molecular weight smearing seen in the denatured gel for the Cre-positive vector cells indicates fusion events.

Concomitantly, analysis of the metaphase spreads of these cells by fluorescence in-situ hybridization (FISH) failed to reveal any significant chromosomal aberrations such as telomere fusions. We did, however, observe an approximately two-fold increase in the number of chromatid ends with two or more telomeric FISH signals (Fig. 4-10A, B). The number and intensity of these multiple telomeric signals (MTS) at a particular end varied, although the FISH signal we observed on a chromatid with multiple signals was roughly the sum of the sister signal, indicating that there was no loss or gain in the telomeric DNA content. Some MTS appeared as distinct doublets or multiples of equal or unequal intensity, while others failed to have a discrete shape, instead appearing as a spray or smear of signal at the chromatid end (Fig. 4-10A). Along with MTS, TRF2$^{\Delta T}$ chromosomes also experienced a loss of telomeric signal (Fig. 4-10A, B) that was heightened under prolonged exposure to Cre, similarly to what was seen in interphase cells examined by IF-FISH. The number of signal-free ends (SFE) 96 hours post Cre expression was approximately five times higher in TRF2$^{\Delta T}$ MEFs than in cells rescued by wild type TRF2 and approximately eight times higher one week post Cre expression (data not shown). It is not unlikely that MTS are a precursor to SFE.

Figure 4-10. TRF2$^{\Delta T}$ cells have an increase in the occurrence of multiple telomeric signals and signal loss at chromatid ends.

(A) Metaphase spreads illustrating the presence of multiple telomeric signals (MTS) and signal free ends (SFE) 96 hours post Cre expression. Metaphase spreads were obtained from the indicated cell lines and processed for telomeric FISH (green). DNA was stained with DAPI (false-colored in red). Enlarged images show examples of various MTS and SFE. (B) Quantification of MTS and SFE for the indicated cell lines.

A

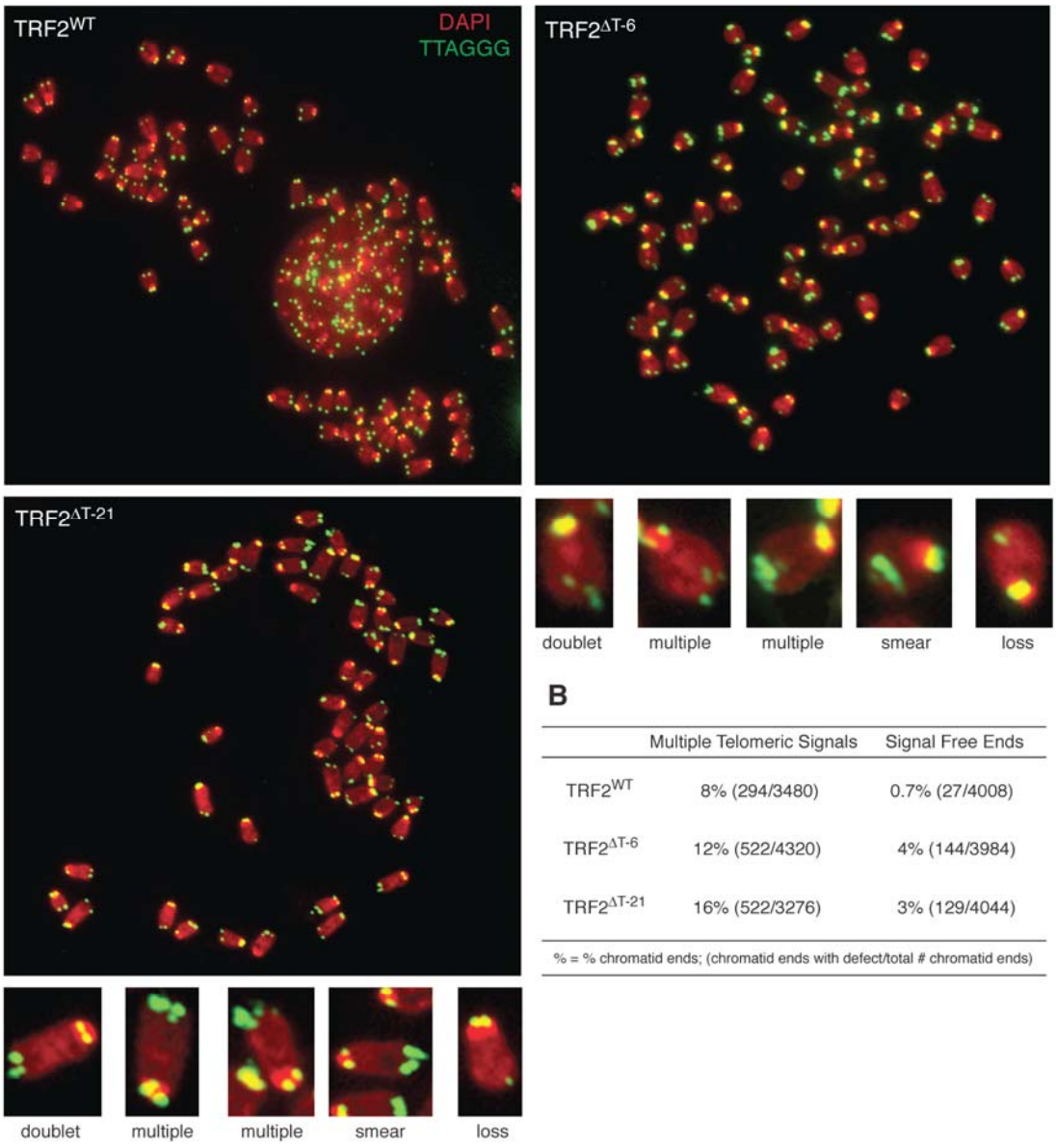

B

	Multiple Telomeric Signals	Signal Free Ends
$TRF2^{WT}$	8% (294/3480)	0.7% (27/4008)
$TRF2^{\Delta T-6}$	12% (522/4320)	4% (144/3984)
$TRF2^{\Delta T-21}$	16% (522/3276)	3% (129/4044)

% = % chromatid ends; (chromatid ends with defect/total # chromatid ends)

Discussion

TIN2 binds TRF1 and TRF2 independently or simultaneously and serves as a linchpin, helping to anchor the shelterin complex at telomeres[61, 134]. We set out to determine the function of TIN2 in the TRF2 complex by creating a TIN2-binding TRF2 mutant, $TRF2^{\Delta T}$. The phenotype of $TRF2^{\Delta T}$ was explored in vivo by expression of $TRF2^{\Delta T}$ in $TRF2^{F/-}$ $p53^{-/-}$ MEFs. Since TRF2 is destabilized in the absence of TIN2, we initially encountered problems localizing $TRF2^{\Delta T}$ to telomeres in batch-prepared cells. Clonal cell lines that homogenously expressed $TRF2^{\Delta T}$ at relatively high levels at telomeres were created to study this TRF2 mutant. Shelterin protein levels were examined by telomere-specific IF and ChIP. IF analysis revealed that recruitment of TIN2 and POT1a to chromosome ends was severely dampened compared to wild type cells, whereas localization of TRF1 and Rap1 to telomeres seemed comparable to the wild type control, although some nucleoplasmic staining was apparent. ChIP data showed a reduction in all shelterin components, particularly TRF1, TRF2, and Rap1. It is possible that a reduction in these protein levels could contribute to the phenotype of $TRF2^{\Delta T}$. Both $TRF2^{\Delta T}$ cells and $TRF1^{-/-}$ MEFs see an increase in multiple telomeric signals at their chromatid ends (Sfeir and de Lange, unpublished), suggesting this phenotype could be attributed to the decrease in TRF1 at

telomeres. A reduction of TRF2/Rap1 is less likely to have an effect, considering that shRNA-mediated knockdown of TRF2, which also causes a decrease in Rap1 levels, has no effect on the ability of TRF2 to protect telomeres from an ATM-dependent DNA damage response (Takai, K and de Lange, unpublished). Hence, $TRF2^{\Delta T}$ is a useful tool for studying the function of the TRF2-TIN2-TPP1-POT1 complex.

Depletion of TRF2 or POT1a/b from mouse cells results in proliferative arrest, changes to the telomeric overhang, and induction of a DNA damage response[10, 46]. $TRF2^{\Delta T}$ MEFs did not exhibit any overt growth defects or alterations in the single-stranded overhang. These cells did, however, elicit a DNA damage response that was monitored by TIF formation. The number of TIF-positive cells was subject to clonal variations. Three $TRF2^{\Delta T}$ clones were scored for localization of 53BP1 foci to telomeres and had an average of 66% TIF-positive cells. Unlike TRF2-loss telomeres, not every $TRF2^{\Delta T}$ telomere was decorated with 53BP1 foci, but for those that were, the foci extended far beyond the telomere.

The DNA damage response elicited by expression of $TRF2^{\Delta T}$ is, in part, ATM-dependent. Loss of TIN2 from the TRF2 complex resulted in phosphorylation of Chk2 and a 2-fold reduction in the number of TIF-positive cells in $TRF2^{F/-}$ $ATM^{-/-}$ cells. This suggests that TIN2 assists TRF2

in suppressing ATM at telomeres. We speculate that TRF2 may indirectly inhibit ATM by maintaining the chromosome end in a t-loop configuration, thus hiding the telomere from activating a DNA damage response. It is possible that TIN2 has a role in helping TRF2 carry out this function. Without TIN2, TRF2 may become promiscuous at maintaining the t-loop in its most protective state. In TRF2$^{\Delta T}$ cells, the t-loop may be "loosened" occasionally, which may be enough to trigger a damage response, but not enough to lose the overhang or cause fusions, as when TRF2 is deleted. This might explain why only 15-20% of input DNAs are able to assemble into t-loops by TRF2 in vitro[115]. Perhaps the addition of TIN2 to this assay would increase the propensity of TRF2 to form t-loops.

TRF2 may also directly inhibit ATM. It has been shown that TRF2 interacts with ATM, and overexpression of TRF2 has the ability to dampen the activation of the ATM kinase[56]. It is possible that TIN2 strengthens this interaction between TRF2 and ATM, thus without TIN2, TRF2 fails to exert as much inhibitory pressure on ATM. Alternatively, ATM may bind TRF2 in or around the same region as TIN2. As such, deletion of this small motif in the hinge domain of TRF2 could weaken or abrogate the TRF2/ATM interaction. Both of these possibilities are easily testable by co-IP analysis.

Cells deficient in TRF2 also exhibit NHEJ-mediated telomere fusions. FISH analysis of metaphase spreads from TRF2$^{\Delta T}$ MEFs did not yield fusions, but instead showed an increase in amount of MTS at chromatid ends as well as telomere loss. The occurrence of MTS has been reported previously in ATM$^{-/-}$ mouse cells[119], in unperturbed human fibroblasts and other human cells[94], in cells where the shelterin accessory factor, Apollo, has been knocked down[120], and in TRF1$^{-/-}$ MEFs (Sfeir and de Lange, unpublished). The nature and origin of these aberrant telomere structures has not been established. One hypothesis is that the MTS are recombined t-loops that are still attached to telomeres. However, preliminary experiments by van Overbeek and Sfeir to prove this have failed (unpublished data). Our current thinking is that MTS structures represent fragile sites. Fragile sites are loci, or regions, that are especially sensitive to forming gaps or breaks on metaphase chromosomes when DNA replication is perturbed[99, 116]. They are frequently deleted or rearranged in many cancer cells[38]. This deletion of the fragile site might be represented by the signal-free end.

CHAPTER 5: DISCUSSION

Telomeres prevent the ends of linear chromosomes from being recognized and processed as damaged DNA and are maintained by the enzyme telomerase. The six-protein complex that binds telomeric DNA, shelterin, is responsible for carrying out many of the functions of telomeres. Originally, shelterin components were viewed as members of separate complexes with the TRF1 complex acting to regulate telomere length and the TRF2 complex serving to protect telomeres. My research and that of others suggest that these two complexes do not only operate as individual units, but can also function as a single complex, with their connection mediated by the shelterin protein, TIN2.

In this thesis, I first examined the role of tankyrase1, a TRF1-associated PARP, in telomere length regulation. I then set out to determine the role of TIN2 in the TRF2 complex after discovering that TIN2 was not only a TRF1-interacting protein, but was also bound to TRF2. My results implicate TIN2 in telomere protection. The discussion that follows below highlights my findings and their relevance to telomere biology.

The role of the poly(ADP-ribose) polymerase, tankyrase1, in telomere length control

Tankyrase1 RNAi resulted in telomere shortening that was proportional to the level of knockdown, validating that tankyrase1 is a positive regulator of telomere length. We also showed that a tankyrase1-resistant form of TRF1 has no effect on the ability of TRF1 to regulate telomere length, implying tankyrase1 is not required downstream of TRF1. Finally, it was shown that tankyrase1 does not seem to have a role at mouse telomeres. It is possible that human cells evolved to include an additional level of control over telomere length that mice may not need because of their increased telomerase activity in somatic cells and their longer telomeres.

Interestingly, a divergence between human and mouse telomeres has also been seen for POT1. The mouse requires two POT1 proteins to properly protect the telomere and to regulate its length, while humans only have one POT1 protein that fulfills these functions[46]. It is conceivable that as more shelterin-associated factors are discovered, there may be further examples of the rapid evolution of the telomere/telomerase system.

The role of TIN2 in the TRF2-TIN2-TPP1-POT1 Complex

TIN2 interacts with TRF1 and TRF2

Co-IP experiments revealed there was a link between the TRF1 and TRF2 complexes, and RNAi studies showed that a reduction in the amount of TRF1 or TIN2 protein levels leads to a concomitant loss of TRF2 and Rap1 from telomeres[134]. Gel filtration verified these results demonstrating that telomeric proteins exist in a single complex and that TIN2/POT1 is a component of the TRF2 complex. Far western analysis revealed that TIN2 directly binds TRF2, and TIN2 can associate with TRF1 and TRF2 simultaneously[134]. This interaction is thought to stabilize shelterin on telomeres[61, 134]. This stabilization is particularly important for TRF2 given the number of interactions this protein has with non-telomeric factors, especially DNA damage/repair proteins.

Crystallography studies and far western mapping determined that TIN2 binds the TRFH domain of TRF1 using an F-X-L-X-P docking motif in its C-terminus while the N-terminus of TIN2 associates with a small sequence in the hinge domain of TRF2[15]. TIN2 has only a weak interaction with the TRFH domain of TRF2, despite the fact that the TRFH domains of TRF1 and TRF2 have almost identical three-dimensional structures[15, 36].

Instead, many proteins that associate with TRF2 contain a Y-X-L-X-P TRFH-docking motif, including Apollo, ERCC1/XPF, ATM, ATR, PARP1, and Nbs1. Except for Apollo, which was shown to have a strong affinity for the TRF2-TRFH domain[15], it remains to be determined whether these factors actually use this motif to bind TRF2. Co-IP analysis coupled with mutational and structural studies would be useful in this regard. Once it is determined which proteins use this motif to bind TRF2, the interactions can be disrupted and the phenotypes associated with loss of these TRF2-associating factors can be evaluated. The same experiments can be implemented for TRF1 and the proteins that potentially bind TRF1 using the F-X-L-X-P docking sequence.

It would also be interesting to see if swapping of the TRF1 TRFH-binding motif ($TRF1^{TBM}$) for the $TRF2^{TBM}$ forces proteins that usually associate with TRF1 to now bind TRF2, or vice-versa. Determining whether these factors are still recruited to telomeres and examining the consequences of switching their binding partners may provide insight into these TRF1/TRF2 protein interactions. It would also be important to establish whether these artificial associations disrupt other naturally occurring interactions at this interface. It is conceivable that a protein forced to interact with TRF2 instead of TRF1 could compete for TRF2 TRFH binding sites

that would normally be available to known TRF2 binding partners, or vice-versa.

Expression of TRF2$^{\Delta T}$ induces a DNA damage response

After mapping the major TIN2-binding domain in TRF2, this small sequence was deleted from TRF2, creating the mutant, TRF2$^{\Delta T}$. The phenotype of this mutant was examined in TRF2$^{F/-}$ p53$^{-/-}$ MEFs, where endogenous TRF2 could be deleted by infection with Cre recombinase. By co-IP and IF analysis, there was a significant reduction in the amount of TIN2 bound to TRF2 and localized to telomeres. Expression of TRF2$^{\Delta T}$ also elicited a DNA damage response that was characterized by telomere dysfunction induced foci (TIF) formation, but not overhang loss or growth arrest. These TIFs appeared at fewer telomeres and were much larger than the TIFs induced upon inhibition of TRF2 or POT1. All of the TIF analysis done in this study used 53BP1 as an indicator of damaged DNA. Upon deletion of TRF2, a number of DNA damage response factors have been shown to localize to telomeres, including γ-H2AX, phosphorylated Rad17, phosphorylated ATM, MDC1, and members of the Mre11 complex[27, 117]. Determining which damage/repair proteins localize to telomeres would be informative in distinguishing the type of damage induced by TRF2$^{\Delta T}$.

The TIFs induced by expression of TRF2$^{\Delta T}$ are, in part, ATM-dependent. The number of TIF-positive cells is reduced by more than half when TRF2$^{\Delta T}$ is expressed in ATM$^{-/-}$ cells. However, the fact that TIF formation is not completely abrogated suggests another DNA damage signaling pathway is at play in these cells. ChIP and IF data revealed that in addition to a decrease in TIN2, TRF2$^{\Delta T}$ telomeres also suffer a reduction in the number of Rap1, TRF1, and POT1 molecules. Loss of TRF1 or POT1 induces a DNA damage response that is dependent on ATR[66] (Sfeir and de Lange, unpublished). Perhaps the reduction in TRF1/POT1 in the TRF2$^{\Delta T}$ MEFs is enough to trigger this response, and thus the TIFs persisting in the ATM$^{-/-}$ cells are a result of ATR activation. Expression of an ATR shRNA in the TRF2$^{\Delta T}$ ATM$^{-/-}$ cells or inhibition of both ATM and ATR by caffeine or wortmannin would address this matter. Similarly, TRF1/POT1 could be overexpressed in the TRF2$^{\Delta T}$ ATM$^{-/-}$ cells to see if this rescues the remaining TIFs.

How does the TRF2-TIN2 interaction inhibit ATM?

Having shown that the DNA damage response elicited by TRF2$^{\Delta T}$ is, to a certain extent, ATM-dependent, we hypothesized how TIN2 could assist TRF2 in suppressing ATM activation at telomeres. One possibility is that

TRF2 needs TIN2 for efficient t-loop maintenance. TIN2 stimulates the ability of TRF1 to induce pairing or higher-order interactions between telomeric DNA tracts by causing a conformational change in TRF1. It is possible that TIN2 can also stimulate the ability of TRF2 to rearrange telomeric DNA into t-loops. The structure of the t-loop is proposed to hide the 3' overhang, preventing a DNA damage response. In $TRF2^{\Delta T}$ cells, the t-loop may be compromised to some extent, triggering a damage response. TIN2 could be added to an in vitro t-loop formation assay to see if there is an increase in the number TRF2-promoted t-loops.

TIN2 may also work with TRF2 to inhibit ATM directly. TRF2 has been shown to bind ATM, and overexpression of TRF2 suppresses ATM activation[56]. TIN2 may enhance this interaction between TRF2 and ATM, or it plausible that ATM binds TRF2 in the same region as TIN2, thus expression of $TRF2^{\Delta T}$ would alleviate the inhibitory pressure on ATM and activate a damage response. One final possibility is that TIN2 directly inhibits ATM. Co-IP analysis could be implemented to test these models.

TRF2$^{\Delta T}$ MEFs do not yield telomere fusions, but multiple telomeric signals and telomere loss

Loss of TRF2 results in the formation of telomere end-to-end fusions that are mediated by the NHEJ pathway[10, 11, 66, 110, 122]. TRF2$^{\Delta T}$ MEFs, on the other hand, did not yield chromosome fusions. It is possible that the presence of TRF2/Rap1 at telomeres was enough to block NHEJ. This is supported by in vitro data showing that Rap1 could prevent end-joining of short telomere arrays[2]. Although no fusions were observed, we did detect a significant increase in the number of multiple telomeric signals (MTS) at chromatid ends as well as telomere loss in cells expressing TRF2$^{\Delta T}$. MTS have also been seen in cells where the TRF2-interacting protein, Apollo, has been knocked down as well as in TRF1$^{-/-}$ MEFs[120] (Sfeir and de Lange, unpublished). It remains to be determined what exactly these MTS structures represent, but one possibility is that they are fragile sites. Fragile sites are chromosomal regions that are particularly sensitive to forming gaps or breaks on metaphase chromosomes after partial inhibition of DNA replication[99, 116]. Treatment with the DNA replication inhibitor aphidicolin induces the expression of fragile sites[39]. It would be interesting to see if the addition of aphidicolin to TRF2$^{\Delta T}$ cells increases the number of MTS. Moreover, fragile sites are frequently deleted or rearranged in many cancer

cells[38]. A similar fragile site-induced deletion might be occurring in TRF2$^{\Delta T}$ cells, which may be represented as signal-free ends. What causes these deletions remains to be determined, but one possibility is they are a result of unequal or faulty homologous recombination of stalled replication forks.

There is no discernable difference between ATM-deficient cells and control cells in spontaneous or aphidicolin-induced chromosome gaps or breaks at fragile sites. However, ATR-deficient cells show a highly significant increase in gaps and breaks at fragile sites both with or without the addition of replication inhibitors[38]. The fact that the TRF2$^{\Delta T}$ MTS phenotype remained unchanged in ATM$^{-/-}$ cells supports the claim that these structures are fragile sites. To further support this claim, the TRF2$^{\Delta T}$ MTS phenotype should be examined in the absence of ATR. Without ATR to stabilize the fragile site, it is likely that the severity of MTS would increase.

Is the TRF2-TIN2 interaction determined by TRF2's phosphorylation status?

Recent work by Hoke and de Lange revealed that TRF2 is phosphorylated at Serine 368 (S368) by the ATR kinase, and phosphorylation of this site plays a role in relieving replication stress at the telomere (unpublished). S368 lies directly adjacent to the TRF2 TIN2-

binding motif (352-367) (Fig. 3-4A), suggesting that the phosphorylation status of TRF2 might regulate its interaction with TIN2. In fact, it was shown that the phosphomimetic mutation, S368E, causes a slight reduction in the amount of TIN2 associated with TRF2 while the S368G mutant, which mimics the unphosphorylated state of TRF2, leads to increased binding to TIN2 (Hoke and de Lange, unpublished). Considering that a residual amount of TIN2 still interacts with $TRF2^{\Delta T}$ (Fig. 3-4C), it may be worthwhile to make the double mutation, $TRF2^{\Delta T\text{-}S368E}$, to diminish this interaction even further, if not completely. Perhaps this double mutation would have a stronger DNA damage phenotype than $TRF2^{\Delta T}$ alone.

TIN2 and Dyskeratosis Congenita

Dyskeratosis congenita (DC) is an inherited bone marrow failure syndrome characterized by nail atrophy, skin hyperpigmentation, and oral leukoplakia. Patients with DC have abnormally short telomeres, chromosome instability, and a predisposition to develop certain cancers[33, 83]. DC has been correlated to mutations in hTERT, hTERC, dyskerin, and NOP10, a component of H/ACA snoRNP complexes[83, 124, 125, 132], however, approximately 60% of DC patients lack an identifiable mutation[81]. A linkage scan was performed on a family with autosomal-dominant DC that

lacked mutations in telomerase, and interestingly, mutations were linked to TIN2[96]. These mutations were mapped to a highly conserved region of TIN2, just outside of the TRFH-binding motif (aa 256-276)[15], and include the following substitutions: K280E, R282S, and R282H. Given the close proximity of these mutations to the TRF1-TRFH binding motif, it is conceivable that altering these amino acids could affect the ability of TIN2 to bind TRF1. This would lead to the destabilization of shelterin and telomere dysfunction. However, our preliminary co-IP data suggests that these TIN2 mutants interact with TRF1 to the same extent as the wild-type control (unpublished). The three-dimensional structure of mutated TIN2 with TRF1 would be useful for reconciling this model.

Despite the fact that TPP1 associates with the N terminus of TIN2 and not near the mutation sites, it may be possible that the mutated TIN2 has an aberrant interaction with TPP1. Recent data indicates that the TPP1/POT1 complex may contribute to the recruitment of telomerase. In fact, TPP1 has a direct interaction with telomerase and has been shown to increase the activity and processivity of the enzyme when complexed with POT1[126, 130]. Perhaps, mutation of TIN2 affects the recruitment or stability of TPP1. Consequently, TPP1 may fail to properly recruit telomerase, thus causing the short telomere phenotype associated with DC. Co-IP analysis of the TIN2-

TPP1 interaction would shed light on this possibility. It also cannot be ruled out that TIN2 itself has a role in recruiting telomerase, and these mutations may inhibit this function.

One final explanation is that TIN2 associates with a yet-to-be identified protein, and mutation of this region in TIN2 disrupts the interaction, leading to telomere instability and the onset of DC. While the reason these TIN2 mutants cause DC remains to be determined, it should be noted that TIN2 is the first shelterin component to be mutated in human disease.

MATERIALS AND METHODS

Cell culture

Phoenix ecotropic and amphotrophic packaging cell lines, 293T cells, HeLa 1.2.11 cells, and $p53^{-/-}$ and SV40 transformed MEFs were grown in DMEM supplemented with 100 U/ml penicillin (Sigma), 0.1 μg/ml of streptomycin (Sigma), 2.0 mM L-glutamine (Invitrogen), 0.1 mM non-essential amino acids (Invitrogen), and 10% Fetal Bovine Serum. BJ fibroblasts (Clontech) were grown in 4:1 DMEM/199 media supplemented with 15% fetal bovine serum, 100 U/ml penicillin (Sigma), 0.1 μg/ml of streptomycin (Sigma), 2.0 mM L-glutamine (Invitrogen), 0.1 mM non-essential amino acids (Invitrogen), and 1 mM sodium pyruvate (Sigma). All cells were grown at 37°C, 5% CO_2, and 95% relative humidity. Cells were passaged by pre-rinsing with room temperature Trypsin-EDTA (Gibco, 0.25%) followed by incubation in Trypsin-EDTA for 2-5min. Cells were seeded as indicated in text. Cells were counted with a Counter Counter Z1 Particle counter. For growth curves, 300,000 cells were plated on a 10 cm dish and grown for approximately 72 hrs Cells were harvested using trypsin and recovered in 4 ml of media, and the total cell number was determined. 300,000 cells were plated in a new 10 cm dish. At specified times, extra cells were plated in

order to obtain protein and DNA samples for analysis. Population doublings were determined by the following formula: PD = original PD + [ln(# cells at passage/#cells seeded)/ln(2)] using Excel.

Calcium phosphate transfection of 293T cells

One day prior to transfection, 2 x 10^6 293T cells were plated in 10 cm dishes. Cells were transfected with 10 μg of the appropriate plasmid using $CaPO_4$ co-precipitation. For each plate, 428 μl H_20, 62 μl 2M $CaCl_2$, and 10 μg plasmid DNA was mixed with an equal amount of 2X HBS (50 mM HEPES pH 7.05, 10 mM KCl, 12 mM dextrose, 280 mM NaCl, 1.5 mM Na_2PO_4) while lightly vortexing. Media was refreshed 5-8 hrs after transfection. 48 hrs after transfection, cells were harvested in media, counted, washed with PBS, and resuspended in 200-500 μl of lysis buffer (50 mM Tris-HCl pH 7.4, 1% Triton X-100, 0.1% SDS, 150 mM NaCl, 1 mM EDTA, 1 mM DTT, 1 mM PMSF, with a completemini-protease inhibitor tablet [Roche] per 10 ml). The NaCl concentration was raised to 400 mM (this step was removed for the salt-sensitive TRF2/TIN co-IPs), and the lysate was incubated on ice for 20 min. The NaCl concentration was reduced in half with an equal volume of cold water, and cell debris was removed by centrifugation at 13K for 10 min at 4°C.

Immunoprecipitation

For immunoprecipitation of proteins expressed by transient transfection in 293T cells, transfection and harvesting was performed as above. 50 μL of 2X Laemmli buffer was added to 50 μL of lysate and set aside as the "Input." Antibody (2 μL of affinity purified and commercial antibodies, 10 μL of crude serum) was added to 400 μL of lysate. Samples were nutated at 4°C for 5 hrs. 60 μL of a Protein G sepharose slurry (50% [v/v] Protein-G sepharose [Amersham] in PBS in 1 mg/ml BSA) were added, and samples were nutated at 4°C for an additional 60 min. Beads were washed 3 times at 4°C with lysis buffer, and immunoprecipitated protein was eluted with 60 μL 2X Laemmli buffer. Samples were boiled for 5 min before loading onto SDS-PAGE gels.

Retroviral gene delivery

One day prior to transfection, 1 x 10^6 Phoenix packaging cells (293T derived cell lines) were plated in 10 cm dishes. For infection of mouse cells, Phoenix ecotropic cells were used. For infection of human cells, Phoenix amphotropic cells were used. Phoenix cells were transfected with 20 μg of the appropriate plasmid DNA by $CaPO_4$ co-precipitation (described above). The media was refreshed 5-8 hrs later, and again 24 hrs later. 36 hrs after

transfection, media was filtered through a 0.4 μm filter and polybrene was added to a final concentration of 4 μg/mL. Fresh media was added to the virus producing cells. This procedure was repeated 3 additional times at 12 hr intervals. If appropriate, 12 hrs after the final infection, fresh media was added containing antibiotics for selection (puromycin 2 μg/ml, hygromycin 90 μg/ml) for 4-5 days until uninfected control cells were completely dead.

Lentiviral gene delivery

293T cells were transfected using calcium phosphate with 3 μg each of helper plasmids (pMDLg/RRE, pRSV-rev, and pCMV-VSVG) and 7 μg of lentiviral vector (pLenti6/Ubc/V5, Invitrogen) carrying the appropriate transgene per 10 cm dish. Fresh media was added 5-8 hrs after transfection. 72 hrs after changing the media, virus-containing media was collected in a 50 ml conical tube and centrifuged for 5 min at 1K rpm at 4°C. The virus was filtered through a 0.4 μm filter and polybrene was added to a final concentration of 4 μg/ml. $2x10^5$ MEFs were plated for each infection, the day before infection. Half of the filtered virus was used for the initial infection. Remaining virus was kept on ice and used for a second infection 12 hrs later. 12 hrs after the second infection, virus-containing medium was replaced with fresh medium. The following day, media was replaced with

media containing 6 μg/ml blasticidin. After four days of selection, blasticidin concentration was dropped to 2.5 μg/ml, and cells were selected for an additional 7 days.

Isolation of clonal lines

$TRF2^{F/-}$ MEFs expressing TRF2 alleles were plated at low density (500-2000 cells/10 cm dish) and grown for approximately 2 weeks until clonal populations were visible under the light microscope. Clonal populations of cells were isolated by trypsinizing cells in cloning cylinders. Clonal populations were transferred to a well of a 96 well plate. When the cells reached confluence in the well, the clonal population was expanded.

Expression of Cre recombinase

Cre was introduced into MEFs using pMMP Hit & Run Cre-GFP retrovirus[104] or pWZL-Cre retrovirus (containing the hygromycin resistance gene) using the retroviral infection technique described above.

shRNA

shRNAs were made in pSUPER-retro (Oligo-Engine) and retroviral infections were performed as described above. The sequences of the shRNA targets are as follows:

Tank1 sh1; 5’-GGCAGTGGCAGTAACAATT-3’

Tank1 sh3; 5’-GAGGTTGTGAGTCTGTTAT-3’

Tank1 sh4; 5’-GCGCTGATCCTACGTTAGT-3’

Tank1 sh5; 5’-GCGTCGCTCTCAGCATCAT-3’

ATM sh3; 5’-GGAAGTCAAGGAACAACTA-3’

Whole cell lysates and western blots

For whole cell lysates, cells were harvested, washed with PBS, counted and resuspended in 2X Laemmli buffer at a concentration of 5000 cells/µl. Lysates were boiled for 5 min and DNA was sheared through a 28-gauge insulin syringe. Protein samples were separated by SDS-PAGE and blotted onto nitrocellulose membranes. Membranes were blocked in 5% milk in PBST (0.5% Tween-20 in PBS) for 30 min at RT and nutated with primary antibodies in 0.1% milk in PBST overnight at 4°C. Membranes were washed 3 times in PBST, nutated in secondary antibody in 0.1% milk in PBST for 45 min at RT, and washed 3 times with PBST at RT. ECL (Amersham) was applied to membranes for 5 min before exposure to film.

Chromatin immunoprecipitation (ChIP)

Cells were washed with PBS, fixed in 1% formaldehyde in PBS for 60 min at RT, washed in PBS, and lysed in 1% SDS, 50 mM Tris-HCl pH 8.0, 10 mM EDTA at a density of $1x10^7$ cells/ml. Lysates were sonicated on ice for 10 cycles of 20 seconds each (0.5 seconds on/0.5 seconds off) on power setting 5 on a Misonix Sonicator 3000. Two 50 µl aliquots of lysates were set aside at 4°C to represent "Total" DNA. 200 µl of lysate was diluted with 1.2 ml 0.01% SDS, 1.1% Triton X-100, 1.2 mM EDTA, 16.7 mM Tris-HCl pH 8.0, and 150 mM NaCl. Antibody (20 µl crude serum or 4 µl affinity purified antibody or anti-c-myc 9E10, see antibody section below for specifics) was added and cells were nutated overnight at 4°C. 30 µl protein G sepharose beads (Amersham; blocked with 30 µg BSA and 5 µg sheared *E. coli* DNA) was added and samples were nutated for an additional 30 min at 4°C. Beads were pelleted by centrifugation and pellets were washed with 0.1% SDS, 1% Triton X-100, 2 mM EDTA pH 8.0, 20 mM Tris-HCl pH 8.0, 150 mM NaCl. The second wash was the same except with 500 mM NaCl. Subsequent washes were with 0.25 M LiCl, 1% NP-40, 1% Na-deoxycholate, 1 mM EDTA pH 8.0, 10 mM Tris-HCl pH 8.0, 1 mM EDTA. Chromatin was eluted from beads with 500 µl 1% SDS, 0.1M Na_2CO_3. 450 µl 1% SDS, 0.1M Na_2CO_3 was added to the "Total" fractions, and these

were subsequently processed along with the rest of the samples. 20 µl 5M NaCl was added and samples were incubated for 4 hr at 65°C to reverse cross-links. At this point, 20 µl 1M Tris-HCl pH 6.5, 10 µl 0.5 M EDTA, and 20 µg DNase free RNase A was added and samples were incubated at 37°C for 30 min 40 µg proteinase K was added and samples were digested for 60 min at 37°C and extracted with phenol. 20 µg of glycogen was added and samples were mixed. 1 ml ethanol was added and DNA was precipitated overnight at -20°C. Precipitated DNA was dissolved in 100 µl H_20, denatured at 95°C for 5 min, and blotted onto Hybond membranes in 2X SSC (0.3M NaCl, 0.03M Sodium citrate). Membranes were treated with 1.5M NaCl, 0.5 N NaOH for 10 min and then with 1 M NaCl, 0.5 M Tris-HCl pH 7.0 for 10 min Hybridization was performed with a γ^{32}-P end-labeled $[CCCTAA]_4$ probe as described for in gel hybridization of genomic DNA. Membranes were washed 4 times in 2X SSC and exposed overnight to a PhosphorImager screen. Screens were developed using a STORM 820 Phosphorimager (Molecular Dynamics). ImageQuant software was used to quantify the percent of total telomeric DNA that was precipitated by each antibody.

Co-IP of TRF1 and TRF2 from BJ-hTERT cells

Cells were retrovirally infected with FLAG-tagged TRF1 or vector alone and were expanded on 15-cm plates. At confluency, cells were trypsinized, collected, washed in 10x pellet volume PBS, washed in 10x pellet volume resuspension buffer (10 mM Tris-HCl (pH 7.4), 60 mM NaCl, 5 mM $MgCl_2$, 0.5 mM EDTA, and 0.1 mM EGTA), and resuspended in 10x pellet volume lysis buffer (resuspension buffer with 0.2% Nonidet P-40, 1 mM dithiothreitol, 0.5 mM phenylmethylsulfonyl fluoride, and a complete protease inhibitor mixture tablet (Roche)). The cell lysate was kept on ice for 10 min with occasional mixing, and the nuclei were collected by centrifugation, washed in resuspension buffer, and then resuspended in 3x pellet volume nuclear extraction buffer (20 mM Tris-HCl (pH 7.4), 400 mM NaCl, 0.5 mM EDTA, 0.2% Nonidet P-40, 1 mM dithiothreitol, 0.5 mM phenylmethylsulfonyl fluoride, and a complete protease inhibitor mixture tablet). The nuclear extract was kept on ice for 30 min with occasional vortexing, the lysate (derived from 3 x 10^8 cells) was centrifuged, and the supernatant was diluted with an equal volume of water. The diluted supernatant was incubated with 100 μl (settled volume) of bovine serum albumin-blocked Sepharose 6B beads for 30 min at 4°C, centrifuged, removed from the beads, incubated with 100 μg/ml ethidium bromide for 20

min on ice (yielding the IP input), and then incubated with 100 µl (settled volume) of bovine serum albumin-blocked FLAG beads overnight at 4°C. Beads were washed four times with 1 ml wash buffer (20 mM Tris-HCl (pH 7.4), 200 mM NaCl, 0.2 mM EDTA, 0.1% Nonidet P-40, 15% glycerol, and 0.5 mM phenylmethylsulfonyl fluoride) and then incubated with 120 µl elution buffer (wash buffer with 0.2 mg/ml FLAG peptide).

Preparation of genomic DNA

Cells were harvested by trypsinization and washed with PBS. 0.5 X 10^6 cells for MEFs and 1 x 10^6 cells for BJ-hTERTs were resuspended in 50 µl PBS and incubated at 50°C for 5 min. Using pipette tips with the ends cut off, 50 µl of 2% agarose (prewarmed to 50°C) was added to each sample, mixed, and incubated for 5 min at 50°C. The 100 µl mixture was added to the Bio-Rad plug cast, incubated at RT for 5 min and at 4°C for 15 min. Solidified plugs were incubated in 0.5 ml Proteinase K digestion buffer (10 mM Tris-HCl pH 7.9, 250 mM EDTA pH 8.0, 0.2% sodium deoxycholate, 1% sodium lauryl sarcosine, and 1 mg/ml fresh Proteinase K) overnight at 50°C. Plugs were washed three times with TE for one hr each at RT with nutation. Plugs were washed for 1 additional hr at RT with TE containing 1 mM PMSF and stored at 4°C in this final wash. Prior to digestion, plugs were washed for 1

hr in fresh TE and 20 min in H_20. Plugs were equilibrated for 1 hr in the appropriate restriction enzyme buffer at RT. Each plug was then digested with 60 units of MboI for MEFs and 60 units of MboI and 60 units AluI for human cells overnight at 37°C. Plugs were washed with TE for 1 hr and equilibrated in 0.5X TBE for 30 min.

In gel hybridization to detect telomeric DNA from MEFs

DNA from MEFs was fractionated on a CHEF-DRII PFGE (Biorad) in a 1% agarose gel in 0.5X TBE for 24 hrs at 6 V/cm at 14°C. Gels were stained with ethidium bromide and photographed. Gels were dried and then prehybridized in Church Mix (0.5M Na_2HPO_4 pH 7.2, 1 mM EDTA, 7% SDS, 1% BSA) for 1 hr at 50°C. Hybridization was performed overnight at 50°C in Church Mix with 4 ng of a γ-32P-ATP end-labeled probe, $[CCCTAA]_4$ (See below for labeling protocol). The gel was washed at 55°C: 3 times for 30 min each in 4X SSC and one time for 30 min in 4X SSC, 0.1% SDS and exposed to a PhosphorImager screen. Subsequently, the gel was denatured in 0.5 M NaOH, 1.5 M NaCl for 30 min, neutralized with two 15min washes in 0.5 M Tris-HCl pH 7.5, 3 M NaCl, prehybridized in Church mix for 1 hr at 55°C, and hybridized with the same probe as above overnight at 55°C. The gel was washed and exposed as above.

Southern blot to detect telomeric DNA from human cells

DNA was separated on a 0.7% agarose gel in 0.5X TBE with ethidium bromide by running for 1 hr at 30 V and then running until the orange G front was at the bottom of the gel (approximately overnight at 45V). Gel was photographed. Gel was then run until the 1.3 kb marker was almost at the bottom of the gel and then photographed with a ruler next to the markers. Gel was gently shaken in Depurination solution (0.25M HCl) for 30 min, Denaturation solution (1.5 M NaCl; 0.5 M NaOH) for 30 min twice, and Neutralization solution (1 M Trish pH 7.4, 1.5M NaCl) for 30 min twice. Gel was then blotted onto a Hybond filter overnight in 20X SSC. Blot was cross-linked, rinsed in H_20, and prehybridized and probed as in the in gel hybridization protocol above.

γ-^{32}P end-labeling of oligonucleotides with T4 polynucleotide kinase

2 µl H_20, 1 µl 10X T4 DNA PNK buffer (NEB), 1 µl 10 U/µl T4 DNA PNK (NEB), 1 µl 50 ng/µl $[CCCTAA]_4$ oligonucleotide and 5 µl 10.0 mCi/ml γ-^{32}P (NEN) were mixed and incubated for 45 min at 37°C. 80 µl TES (10 mM Tris-HCl pH 8.0, 10 mM EDTA pH 8.0, 0.01% SDS) were added to stop the reaction. The probe was loaded onto a 3 ml G25 Sephadex column equilibrated with TNES (10 mM Tris-HCl pH 7.4, 10 mM EDTA, 100 mM

NaCl, 1% SDS). The column was washed with 700 µl TNES and the probe was eluted with 600 µl TNES.

Metaphase spreads

Cells were grown to approximately 40% confluence on 10 cm dishes and incubated for 1-2 hrs in 0.1 µg/ml colcemide (Sigma). Cells were harvested by trypsinization, centrifuged at 1K for 5 min, and resuspended in 0.075M KCL prewarmed to 37°C. Cells were incubated at 37°C for 15 min with occasional inversion. Cells were centrifuged at 1K for 5 min and supernatant was decanted. Cells were resuspended by tapping in the remaining (~200 µl) supernatant. 500 µl of cold 3:1 methanol:glacial acetic acid fixative was added dropwise while cells were mixed gently on a vortexer (<1000 rpm). Another 500 µl fixative was added slowly while cells were being mixed. Tubes were then filled to 10 mL with the fixative and stored at 4°C overnight or longer. Cells were centrifuged at 1K rpm for 5 min and supernatant was decanted. Cells were resuspended in the remaining fixative (~300 µl) and dropped from approximately 6 inches onto glass slides, which had been soaked in cold water. Slides were washed with fresh fixative and placed on a humidified heating block set to 70°C for 1 min. Spreading efficiency was checked under a light microscope. Slides were dried

overnight.

Fluorescence in situ hybridization (FISH)

Metaphases were harvested as described above. Slides were washed in PBS and dehydrated in an ethanol series: 5 min each 70%, 85%, 100%, and air-dried. Slides were incubated with FITC-TelC 5'-$[CCCTAA]_3$-3' PNA probe (Applied Biosystems) in 80 μl of hybridization mix (10 mM Tris-HCl pH 7.2, 70% deionized formamide, 0.5% blocking reagent [Boehringer Mannheim]) under a coverslip, placed on a 70°C heating block for 3 min, and then incubated in the dark for two hrs at RT. Slides were washed twice for 15 min each in Wash I (70% formamide, 10 mM Tris-HCl pH 7.2, 0.1% BSA). Slides were then washed three times for 5 min each in Wash II (0.1M Tris-HCl pH 7.2, 0.15M NaCl, 0.08% Tween-20). DAPI was added to the second wash. Slides were dehydrated in an ethanol series: 5 min each 70%, 95%, 100%, air dried, and mounted.

Immunofluorescence (IF)

Cells were plated in dishes on coverslips. Cells were rinsed with PBS, fixed with 2% paraformaldehyde in PBS for 10 min at RT and then washed twice with PBS for 5 min Cells were either stored in PBS with the addition of 0.02% azide or processed immediately. Cells were permeabilized with 0.5%

NP40. If extraction was desired, prior to fixation, cells were treated with Triton X-100 extraction buffer (0.5% Triton X-100, 20 nM HEPES-KOH pH 7.9, 50 mM NaCl, 3 mM $MgCl_2$, 300 mM sucrose). Extracted cells were fixed with 3% paraformaldehyde, 2% sucrose for 10 min at RT, and washed twice with PBS. If extraction was performed, Triton X-100 buffer was used for permeabilization instead of 0.5% NP-40. After permeabilization, cells were washed three times with PBS and blocked with PBG (0.2% (w/v) cold water fish gelatin (Sigma), 0.5% (w/v) BSA (Sigma) in PBS) for 30 min at RT. Cells were incubated with primary antibody diluted in PBG overnight at 4°C, washed 3 times with PBG at RT, incubated with secondary antibody diluted 1:250 in PBG for 45 min at RT, and washed 3 times with PBS. To the second PBS wash 0.1 μg/ml 4,6-diamidino-2-phenylindole (DAPI) was added. Coverslips were sealed onto glass sides with embedding media (ProLong Gold Antifade Reagent, Invitrogen).

IF-FISH

Cells were plated in dishes with coverslips. Cells were rinsed with PBS, fixed with 2% paraformaldehyde in PBS for 10 min at RT, washed twice with PBS for 5 min each. Cells were either stored in PBS with the addition of 0.02% azide or processed immediately. Coverslips were blocked for 30

min in blocking solution (1 mg/ml BSA, 3% goat serum, 0.1% Triton X-100, 1 mM EDTA in PBS) and incubated for 1 hr in primary antibody diluted in blocking solution. Cover slips were washed 3 times 5 min each in PBS before incubation in secondary antibody diluted in blocking solution. Cover slips were washed 3 times 5 min each in PBS, dehydrated in an ethanol series: 5 min each 70%, 95%, 100%, and air dried. Coverslips were transferred (cells facing up) to glass slides and 80 µl of FITC-TelC 5'-$[CCCTAA]_3$-3' (Applied Biosystems) probe at 1:1000 in hybridizing solution (70% formamide, 0.5% blocking reagent [Boehringer Mannheim], 10 mM Tris-HCl pH 7.2) was added. Slides were placed on a heating block set to 70°C for 5 min and incubated in the dark for 2 hrs – overnight. Coverslips were washed twice for 15 min in 70% formamide, 10 mM Tris-HCl pH 7.2 and three times for 5 min in PBS. DAPI was added to the second PBS wash. Cover slips were sealed on glass slides with embedding media.

Microscopy and image processing

Images were captured using an Axioplan II Zeiss microscope with a Hamamatsu CCD digital camera using Improvision OpenLab software. Images were merged in OpenLab and processed with Adobe Photoshop.

Gel filtration

Nuclear extract from HeLaS3 cells (10 ml, 8 mg protein/ml) was dialyzed overnight at 4 °C against BC150/40% glycerol (20 mM Tris (pH 7.3), 150 mM KCl, 0.2 mM EDTA, 40% glycerol, 0.025% Nonidet P-40, and 0.5 mM dithiothreitol) and cleared by ultracentrifugation at 25,000 rpm for 30 min. The dialyzed sample (5 ml) was loaded to a Sephacryl S-300 (Amersham Biosciences) column (2.5 cm x 70 cm, 350 ml of packed volume) that was equilibrated with BC150/20% glycerol. Proteins were fractionated with BC150/20% glycerol at a linear flow rate of 25 ml/h, and 5-ml fractions were collected. Blue dextran (2 MDa) appears at the end of the void volume (approximately one-third of column volume), and bovine serum albumin (67 kDa) appears at approximately two-thirds of the column volume).

Far western analysis

Two micrograms of purified protein derived from insect cells or bacterial cells, or lysate from 70 µl/500 µl induced bacterial culture were subjected to SDS-PAGE and then blotted onto nitrocellulose. The blots were incubated in blocking buffer (10 mM HEPES (pH 7.5), 50 mM NaCl, 10 mM $MgCl_2$, 0.1 mM EDTA, 1 mM dithiothreitol, 10% glycerol, and 5% milk) for 3 hr at 4°C. Following the blocking step, the blots were probed overnight at 4°C with ^{35}S-labeled in vitro translated protein prepared using the TNT T7-

coupled reticulocyte lysate system (Promega) (a 50 μl reaction mixture in 5 ml of blocking buffer). The next morning, the blots were washed five times every 30 min in wash buffer (10 mM HEPES (pH 7.5), 50 mM NaCl, 10 mM $MgCl_2$, 0.1 mM EDTA, 1 mM dithiothreitol, 10% glycerol, and 0.25% milk) and then incubated with Amplify (Amersham Biosciences) for 10 min. The blots were exposed on a PhosphorImager screen overnight. For the modified far western experiment, the blots were incubated with 4 μg of baculovirus-derived TIN2 in 5 ml of blocking buffer after the blocking step, washed three times every 5 min in wash buffer, and processed as described above.

In vitro PARP assay

4 μg of proteins purified from baculovirus-infected insect cells or *Escherichia coli* cells (GST-mTRF1) were incubated with with [^{32}P]-NAD^+ (1.3 μM) at 25 °C for 30 min. The reactions were stopped by adding ice-cold trichloroacetic acid to 25%. After 10 min on ice, the proteins were collected by microcentrifugation (10 min at 14,000 rpm at 4 °C). The pellets were rinsed gently with ice-cold 5% trichloroacetic acid and dissolved in sample loading buffer (1 M Tris-base, 12% SDS, 0.2 M dithiothreitol, and 0.1% bromphenol blue). The samples were separated by SDS-PAGE and analyzed by autoradiography and Coomassie blue staining.

Antibodies Used

ID	Antigen	Type	Applications	Origin
371	hTRF1 (baculo-FL)	Rb, poly	Western 1:2000	de Lange
647	hTRF2 (baculo-FL)	Rb, poly	Western 1:1000	Zhu/de Lange lab
765	hRap1 (baculo-FL)	Rb, poly	Western 1:2000	Li/de Lange
864	hTIN2 (baculo-FL)	Rb, poly	Western 1:2000	Ye/ de Lange
1150	hTPP1 (GST-1-250)	Rb, poly	ChIP 1:350	Ye/de Lange
978	hPOT1 (baculo-FL)	Rb, poly	Western 1:1000	Loayza/de Lange
465	hTankyrase1 (baculo-FL)	Rb, poly	IF 1:1000 Western 1:1000	Ye/de Lange
644	mTRF1 (peptide)	Rb, poly	IF 1:2000 ChIP 1:350	Karlseder/de Lange
1254	mTRF2 (GST-FL)	Rb, poly	IF 1:10000 Western 1:10000 ChIP 1:350	Celli/de Lange
1252	mRap1 (GST-FL)	Rb, poly	IF 1:10000 Western 1:10000 ChIP 1:350	Celli/de Lange
1447	mTIN2 (GST-FL)	Rb, poly	IF 1:2000 Western 1:2000 ChIP 1:350	Donigian/de Lange
αmPOT1a	mPOT1a (GST-FL)	Mo, mono	IF 1:1000	Hockemeyer/de Lange
1221	mPOT1a (peptide)	Rb, poly	ChIP 1:350	Hockemeyer/de Lange

ID	Antigen	Type	Applications	Origin
1223	mPOT1b (peptide)	Rb, poly	ChIP 1:350	Hockemeyer/de Lange
9E10	c-Myc peptide	Mo, mono	IF 1:1000 Western 1:1000	Calbiochem
9E10	c-Myc peptide	Mo, mono	IF 1:5000	Sigma
M2	Flag peptide	Mo, mono	IF 1:10000 Western 1:10000	Sigma
HA.11	HA peptide	Mo, mono	Western 1:1000	Covance
GTU88	γTubulin (peptide)	Mo, mono	Western 1:5000	Sigma
α53BP1	53BP1 (peptide)	Rb, poly	IF 1:1000	Novus
MAT3	ATM	Mo, mono	Western 1:5000	Sigma
αChk2	Chk2	Mo, mono	Western 1:500	BD Transduction Lab

Rb: Rabbit; Mo: mouse; poly: polyclonal; mono: monoclonal

REFERENCES

1. **Ancelin, K., M. Brunori, S. Bauwens, C. E. Koering, C. Brun, M. Ricoul, J. P. Pommier, L. Sabatier, and E. Gilson**. 2002. Targeting assay to study the cis functions of human telomeric proteins: evidence for inhibition of telomerase by TRF1 and for activation of telomere degradation by TRF2. Mol Cell Biol **22**:3474-3487.
2. **Bae, N. S., and P. Baumann**. 2007. A RAP1/TRF2 complex inhibits nonhomologous end-joining at human telomeric DNA ends. Mol Cell **26**:323-334.
3. **Barnett, M. A., V. J. Buckle, E. P. Evans, A. C. Porter, D. Rout, A. G. Smith, and W. R. Brown**. 1993. Telomere directed fragmentation of mammalian chromosomes. Nucleic Acids Res **21**:27-36.
4. **Baumann, P., and T. R. Cech**. 2001. Pot1, the putative telomere end-binding protein in fission yeast and humans. Science **292**:1171-1175.
5. **Bianchi, A., S. Smith, L. Chong, P. Elias, and T. de Lange**. 1997. TRF1 is a dimer and bends telomeric DNA. Embo J **16**:1785-1794.
6. **Bianchi, A., R. M. Stansel, L. Fairall, J. D. Griffith, D. Rhodes, and T. de Lange**. 1999. TRF1 binds a bipartite telomeric site with extreme spatial flexibility. Embo J **18**:5735-5744.
7. **Bilaud, T., C. Brun, K. Ancelin, C. E. Koering, T. Laroche, and E. Gilson**. 1997. Telomeric localization of TRF2, a novel human telobox protein. Nat Genet **17**:236-239.
8. **Bodnar, A. G., M. Ouellette, M. Frolkis, S. E. Holt, C. P. Chiu, G. B. Morin, C. B. Harley, J. W. Shay, S. Lichtsteiner, and W. E.**

Wright. 1998. Extension of life-span by introduction of telomerase into normal human cells. Science **279**:349-352.

9. **Broccoli, D., A. Smogorzewska, L. Chong, and T. de Lange**. 1997. Human telomeres contain two distinct Myb-related proteins, TRF1 and TRF2. Nat Genet **17**:231-235.
10. **Celli, G., and T. de Lange**. 2005. DNA processing not required for ATM-mediated telomere damage response after TRF2 deletion. Nat Cell Biol **7**:712-718.
11. **Celli, G. B., E. Lazzerini Denchi, and T. de Lange**. 2006. Ku70 stimulates fusion of dysfunctional telomeres yet protects chromosome ends from homologous recombination. Nat Cell Biol **8**:885-890.
12. **Cesare, A. J., N. Quinney, S. Willcox, D. Subramanian, and J. D. Griffith**. 2003. Telomere looping in P. sativum (common garden pea). Plant J **36**:271-279.
13. **Chang, P., M. K. Jacobson, and T. J. Mitchison**. 2004. Poly(ADP-ribose) is required for spindle assembly and structure. Nature **432**:645-649.
14. **Chang, W., J. N. Dynek, and S. Smith**. 2003. TRF1 is degraded by ubiquitin-mediated proteolysis after release from telomeres. Genes Dev **17**:1328-1333.
15. **Chen, Y., Y. Yang, M. van Overbeek, J. R. Donigian, P. Baciu, T. de Lange, and M. Lei**. 2008. A shared docking motif in TRF1 and TRF2 used for differential recruitment of telomeric proteins. Science **319**:1092-1096.

16. **Chi, N. W., and H. F. Lodish**. 2000. Tankyrase is a Golgi-Associated Mitogen-activated Protein Kinase Substrate that Interacts with IRAP in GLUT4 vesicles. J Biol Chem **275**:38437-38444.

17. **Chong, L., B. van Steensel, D. Broccoli, H. Erdjument-Bromage, J. Hanish, P. Tempst, and T. de Lange**. 1995. A human telomeric protein. Science **270**:1663-1667.

18. **Cohen, S., G. ME, G. O. Lovrecz, N. Bache, P. J. Robinson, and R. R. Reddel**. 2007. Protein Composition of Catalytically Active Human Telomerase from Immortal Cells. Science **315**:1850-1853.

19. **Colgin, L. M., K. Baran, P. Baumann, T. R. Cech, and R. R. Reddel**. 2003. Human POT1 Facilitates Telomere Elongation by Telomerase. Curr Biol **13**:942-946.

20. **Compton, S. A., J. H. Choi, A. J. Cesare, S. Ozgur, and J. D. Griffith**. 2007. Xrcc3 and Nbs1 are required for the production of extrachromosomal telomeric circles in human alternative lengthening of telomere cells. Cancer Res **67**:1513-1519.

21. **Cook, B. D., J. N. Dynek, W. Chang, G. Shostak, and S. Smith**. 2002. Role for the related poly(ADP-Ribose) polymerases tankyrase 1 and 2 at human telomeres. Mol Cell Biol **22**:332-342.

22. **Counter, C. M., A. A. Avilion, C. E. LeFeuvre, N. G. Stewart, C. W. Greider, C. B. Harley, and S. Bacchetti**. 1992. Telomere shortening associated with chromosome instability is arrested in immortal cells which express telomerase activity. Embo J **11**:1921-1929.

23. **Crabbe, L., R. E. Verdun, C. I. Haggblom, and J. Karlseder**. 2004. Defective telomere lagging strand synthesis in cells lacking WRN helicase activity. Science **306**:1951-1953.

24. **Cristofari, G., and J. Lingner**. 2006. Telomere length homeostasis requires that telomerase levels are limiting. EMBO J **25**:565-574.

25. **Cross, S. H., R. C. Allshire, S. J. McKay, N. I. McGill, and H. J. Cooke**. 1989. Cloning of human telomeres by complementation in yeast. Nature **338**:771-774.

26. **d'Adda di Fagagna, F., M. P. Hande, W. M. Tong, D. Roth, P. M. Lansdorp, Z. Q. Wang, and S. P. Jackson**. 2001. Effects of DNA nonhomologous end-joining factors on telomere length and chromosomal stability in mammalian cells. Curr Biol **11**:1192-1196.

27. **d'Adda di Fagagna, F., P. M. Reaper, L. Clay-Farrace, H. Fiegler, P. Carr, T. Von Zglinicki, G. Saretzki, N. P. Carter, and S. P. Jackson**. 2003. A DNA damage checkpoint response in telomere-initiated senescence. Nature **426**:194-198.

28. **d'Adda di Fagagna, F., S. H. Teo, and S. P. Jackson**. 2004. Functional links between telomeres and proteins of the DNA-damage response. Genes Dev **18**:1781-1799.

29. **de Lange, T**. 2005. Shelterin: the protein complex that shapes and safeguards human telomeres. Genes Dev **19**:2100-2110.

30. **de Lange, T., L. Shiue, R. M. Myers, D. R. Cox, S. L. Naylor, A. M. Killery, and H. E. Varmus**. 1990. Structure and variability of human chromosome ends. Mol Cell Biol **10**:518-527.

31. **De Rycker, M., R. N. Venkatesan, C. Wei, and C. M. Price**. 2003. Vertebrate tankyrase domain structure and sterile alpha motif (SAM)-mediated multimerization. Biochem J **372**:87-96.

32. **Dimitrova, N., and T. de Lange**. 2006. MDC1 accelerates nonhomologous end-joining of dysfunctional telomeres. Genes Dev **20**:3238-3243.

33. **Dokal, I., J. Bungey, P. Williamson, D. Oscier, J. Hows, and L. Luzzatto**. 1992. Dyskeratosis congenita fibroblasts are abnormal and have unbalanced chromosomal rearrangements. Blood **80**:3090-3096.

34. **Donigian, J. R., and T. de Lange**. 2007. The role of the poly(ADP-ribose) polymerase tankyrase1 in telomere length control by the TRF1 component of the shelterin complex. J Biol Chem **282**:22662-22667.

35. **Dynek, J. N., and S. Smith**. 2004. Resolution of sister telomere association is required for progression through mitosis. Science **304**:97-100.

36. **Fairall, L., L. Chapman, H. Moss, T. de Lange, and D. Rhodes**. 2001. Structure of the TRFH dimerization domain of the human telomeric proteins TRF1 and TRF2. Molecular Cell **8**:351-361.

37. **Feng, J., W. D. Funk, S. S. Wang, S. L. Weinrich, A. A. Avilion, C. P. Chiu, R. R. Adams, E. Chang, R. C. Allsopp, J. Yu, L. S, W. MD, C. B. Harley, W. H. Andrews, C. W. Greider, and B. Villeponteau**. 1995. The RNA component of human telomerase. Science **269**:1236-1241.

38. **Glover, T. W., M. F. Arlt, A. M. Casper, and S. G. Durkin**. 2005. Mechanisms of common fragile site instability. Hum Mol Genet **14 Spec No. 2**:R197-205.

39. **Glover, T. W., C. Berger, J. Coyle, and B. Echo**. 1984. DNA polymerase alpha inhibition by aphidicolin induces gaps and breaks at common fragile sites in human chromosomes. Hum Genet **67**:136-142.

40. **Greider, C. W., and E. H. Blackburn**. 1985. Identification of a specific telomere terminal transferase activity in Tetrahymena extracts. Cell **43**:405-413.

41. **Greider, C. W., and E. H. Blackburn**. 1987. The telomere terminal transferase of Tetrahymena is a ribonucleoprotein enzyme with two kinds of primer specificity. Cell **51**:887-898.

42. **Griffith, J. D., L. Comeau, S. Rosenfield, R. M. Stansel, A. Bianchi, H. Moss, and T. de Lange**. 1999. Mammalian telomeres end in a large duplex loop. Cell **97**:503-514.

43. **Hanish, J. P., J. L. Yanowitz, and T. de Lange**. 1994. Stringent sequence requirements for the formation of human telomeres. Proc Natl Acad Sci USA **91**:8861-8865.

44. **Harley, C. B., A. B. Futcher, and C. W. Greider**. 1990. Telomeres shorten during ageing of human fibroblasts. Nature **345**:458-460.

45. **Hayflick, L**. 1965. The limited in vitro lifetime of human diploid cell strains. Exp Cell Res **37**:614-636.

46. **Hockemeyer, D., J. P. Daniels, H. Takai, and T. de Lange**. 2006. Recent expansion of the telomeric complex in rodents: Two distinct POT1 proteins protect mouse telomeres. Cell **126**:63-77.

47. **Hockemeyer, D., W. Palm, T. Else, J. P. Daniels, K. K. Takai, J. Z. Ye, C. E. Keegan, T. de Lange, and G. D. Hammer**. 2007. Telomere protection by mammalian POT1 requires interaction with TPP1. Nat Struct Mol Biol **14**:754-761.

48. **Hockemeyer, D., A. J. Sfeir, J. W. Shay, W. E. Wright, and T. de Lange**. 2005. POT1 protects telomeres from a transient DNA damage

response and determines how human chromosomes end. EMBO J. **24**:2667-2678.

49. **Houghtaling, B. R., L. Cuttonaro, W. Chang, and S. Smith**. 2004. A dynamic molecular link between the telomere length regulator TRF1 and the chromosome end protector TRF2. Curr Biol **14**:1621-1631.

50. **Hsu, H. L., D. Gilley, E. H. Blackburn, and D. J. Chen**. 1999. Ku is associated with the telomere in mammals. Proc Natl Acad Sci USA **96**:12454-12458.

51. **Hsu, H. L., D. Gilley, S. A. Galande, M. P. Hande, B. Allen, S. H. Kim, G. C. Li, J. Campisi, T. Kohwi-Shigematsu, and D. J. Chen**. 2000. Ku acts in a unique way at the mammalian telomere to prevent end joining. Genes Dev **14**:2807-2812.

52. **Huffman, K. E., S. D. Levene, V. M. Tesmer, J. W. Shay, and W. E. Wright**. 2000. Telomere shortening is proportional to the size of the G-rich telomeric 3'-overhang. J Biol Chem **275**:19719-19722.

53. **Iwano, T., M. Tachibana, M. Reth, and Y. Shinkai**. 2004. Importance of TRF1 for functional telomere structure. J Biol Chem **279**:1442-1448.

54. **Kaminker, P. G., S. H. Kim, R. D. Taylor, Y. Zebarjadian, W. D. Funk, G. B. Morin, P. Yaswen, and J. Campisi**. 2001. TANK2, a new TRF1-associated PARP, causes rapid induction of cell death upon overexpression. J Biol Chem **276**:35891-35899.

55. **Karlseder, J., D. Broccoli, Y. Dai, S. Hardy, and T. de Lange**. 1999. p53- and ATM-dependent apoptosis induced by telomeres lacking TRF2. Science **283**:1321-1325.

56. **Karlseder, J., K. Hoke, O. K. Mirzoeva, C. Bakkenist, M. B. Kastan, J. H. Petrini, and T. de Lange**. 2004. The telomeric protein TRF2 binds the ATM kinase and can inhibit the ATM-dependent DNA damage response. PLoS Biol **2**:E240.

57. **Karlseder, J., L. Kachatrian, H. Takai, K. Mercer, S. Hingorani, T. Jacks, and T. de Lange**. 2003. Targeted deletion reveals an essential function for the telomere length regulator Trf1. Mol Cell Biol **23**:6533-6541.

58. **Karlseder, J., A. Smogorzewska, and T. de Lange**. 2002. Senescence induced by altered telomere state, not telomere loss. Science **295**:2446-2449.

59. **Kelleher, C., I. Kurth, and J. Lingner**. 2005. Human protection of telomeres 1 (POT1) is a negative regulator of telomerase activity in vitro. Mol Cell Biol **25**:808-818.

60. **Kim, N. W., M. A. Piatyszek, K. R. Prowse, C. B. Harley, M. D. West, P. L. Ho, G. M. Coviello, W. E. Wright, S. L. Weinrich, and J. W. Shay**. 1994. Specific association of human telomerase activity with immortal cells and cancer. Science **266**:2011-2015.

61. **Kim, S. H., C. Beausejour, A. R. Davalos, P. Kaminker, S. J. Heo, and J. Campisi**. 2004. TIN2 mediates functions of TRF2 at human telomeres. J Biol Chem **279**:43799-43804.

62. **Kim, S. H., P. Kaminker, and J. Campisi**. 1999. TIN2, a new regulator of telomere length in human cells. Nat Genet **23**:405-412.

63. **Kipling, D., and H. J. Cooke**. 1990. Hypervariable ultra-long telomeres in mice. Nature **347**:400-402.

64. **Kishi, S., X. Z. Zhou, Y. Ziv, C. Khoo, D. E. Hill, Y. Shiloh, and K. P. Lu**. 2001. Telomeric protein Pin2/TRF1 as an important ATM target in response to double strand DNA breaks. J Biol Chem **276**:29282-29291.

65. **Konishi, A., and T. de Lange**. 2008. Cell cycle control of telomere protection and NHEJ revealed by a ts mutation in the DNA binding domain of TRF2. Genes Dev. **in press**

66. **Lazzerini Denchi, E., and T. de Lange**. 2007. Protection of telomeres through independent control of ATM and ATR by TRF2 and POT1. Nature **448**:1068-1071.

67. **Lei, M., A. J. Zaug, E. R. Podell, and T. R. Cech**. 2005. Switching human telomerase on and off with hPOT1 protein in vitro. J Biol Chem **280**:20449-20456.

68. **Lenain, C., S. Bauwens, S. Amiard, M. Brunori, M. J. Giraud-Panis, and E. Gilson**. 2006. The Apollo 5' exonuclease functions together with TRF2 to protect telomeres from DNA repair. Curr Biol **16**:1303-1310.

69. **Li, B., and T. de Lange**. 2003. Rap1 affects the length and heterogeneity of human telomeres. Mol Biol Cell **14**:5060-5068.

70. **Li, B., S. Oestreich, and T. de Lange**. 2000. Identification of human Rap1: implications for telomere evolution. Cell **101**:471-483.

71. **Lillard-Wetherell, K., A. Machwe, G. T. Langland, K. A. Combs, G. K. Behbehani, S. A. Schonberg, J. German, J. J. Turchi, D. K. Orren, and J. Groden**. 2004. Association and regulation of the BLM helicase by the telomere proteins TRF1 and TRF2. Hum Mol Genet **13**:1919-1932.

72. **Lingner, J., T. R. Hughes, A. Shevchenko, M. Mann, V. Lundblad, and T. R. Cech**. 1997. Reverse transcriptase motifs in the catalytic subunit of telomerase. Science **276**:561-567.

73. **Liu, D., M. S. O'Connor, J. Qin, and Z. Songyang**. 2004. Telosome, a mammalian telomere-associated complex formed by multiple telomeric proteins. J Biol Chem **279**:51338-51342.

74. **Liu, D., A. Safari, M. S. O'Connor, D. W. Chan, A. Laegeler, J. Qin, and Z. Songyang**. 2004. PTOP interacts with POT1 and regulates its localization to telomeres. Nat Cell Biol **6**:673-680.

75. **Liu, Y., J. Y. Masson, R. Shah, P. O'Regan, and S. C. West**. 2004. RAD51C is required for Holliday junction processing in mammalian cells. Science **303**:243-246.

76. **Loayza, D., and T. de Lange**. 2003. POT1 as a terminal transducer of TRF1 telomere length control. Nature **424**:1013-1018.

77. **Loayza, D., H. Parsons, J. Donigian, K. Hoke, and T. de Lange**. 2004. DNA binding features of human POT1: A nonamer 5'-TAGGGTTAG-3' minimal binding site, sequence specificity, and internal binding to multimeric sites. J Biol Chem **279**:13241-13248.

78. **Machwe, A., L. Xiao, and D. K. Orren**. 2004. TRF2 recruits the Werner syndrome (WRN) exonuclease for processing of telomeric DNA. Oncogene **23**:149-156.

79. **Makarov, V. L., Y. Hirose, and J. P. Langmore**. 1997. Long G tails at both ends of human chromosomes suggest a C strand degradation mechanism for telomere shortening. Cell **88**:657-666.

80. **Marcand, S., E. Gilson, and D. Shore**. 1997. A protein-counting mechanism for telomere length regulation in yeast. Science **275**:986-990.

81. **Marrone, A., and I. Dokal**. 2004. Dyskeratosis congenita: molecular insights into telomerase function, ageing and cancer. Expert Rev Mol Med **6**:1-23.

82. **McElligott, R., and R. J. Wellinger**. 1997. The terminal DNA structure of mammalian chromosomes. EMBO J **16**:3705-3714.

83. **Mitchell, J. R., E. Wood, and K. Collins**. 1999. A telomerase component is defective in the human disease dyskeratosis congenita. Nature **402**:551-555.

84. **Morales, C. P., S. E. Holt, M. Ouellette, K. J. Kaur, Y. Yan, K. S. Wilson, M. A. White, W. E. Wright, and J. W. Shay**. 1999. Absence of cancer-associated changes in human fibroblasts immortalized with telomerase. Nat Genet **21**:115-118.

85. **Moyzis, R. K., J. M. Buckingham, L. S. Cram, M. Dani, L. L. Deaven, M. D. Jones, J. Meyne, R. L. Ratliff, and J. R. Wu**. 1988. A highly conserved repetitive DNA sequence, (TTAGGG)n, present at the telomeres of human chromosomes. Proc Natl Acad Sci USA **85**:6622-6626.

86. **Munoz-Jordan, J. L., G. A. Cross, T. de Lange, and J. D. Griffith**. 2001. t-loops at trypanosome telomeres. Embo J **20**:579-588.

87. **Muramatsu, Y., H. Tahara, T. Ono, T. Tsuruo, and H. Seimiya**. 2008. Telomere elongation by a mutant tankyrase 1 without TRF1 poly(ADP-ribosyl)ation. Exp Cell Res **314**:1115-1124.

88. **Murti, K. G., and D. M. Prescott**. 1999. Telomeres of polytene chromosomes in a ciliated protozoan terminate in duplex DNA loops. Proc Natl Acad Sci USA **96**:14436-14439.

89. **Nakamura, T. M., G. B. Morin, K. B. Chapman, S. L. Weinrich, W. H. Andrews, J. Lingner, C. B. Harley, and T. R. Cech**. 1997. Telomerase catalytic subunit homologs from fission yeast and human. Science **277**:955-959.

90. **Nasir, L., P. Devlin, T. Mckevitt, G. Rutteman, and D. J. Argyle**. 2001. Telomere lengths and telomerase activity in dog tissues: a potential model system to study human telomere and telomerase biology. Neoplasia **3**:351-359.

91. **O'Connor, M. S., A. Safari, D. Liu, J. Qin, and Z. Songyang**. 2004. The human Rap1 protein complex and modulation of telomere length. J Biol Chem **279**:28585-28591.

92. **Olovnikov, A. M**. 1973. A theory of marginotomy. The incomplete copying of template margin in enzymic synthesis of polynucleotides and biological significance of the phenomenon. J Theor Biol **41**:181-190.

93. **Opresko, P. L., C. Von Kobbe, J. P. Laine, J. Harrigan, I. D. Hickson, and V. A. Bohr**. 2002. Telomere binding protein TRF2 binds to and stimulates the Werner and Bloom syndrome helicases. J Biol Chem **277**:41110-41119.

94. **Philippe, C., P. Coullin, and A. Bernheim**. 1999. Double telomeric signals on single chromatids revealed by FISH and PRINS. Ann Genet **42**:202-209.

95. **Raices, M., R. E. Verdun, S. A. Compton, C. I. Haggblom, J. D. Griffith, A. Dillin, and J. Karlseder**. 2008. C. elegans telomeres contain G-strand and C-strand overhangs that are bound by distinct proteins. Cell **132**:745-757.

96. **Savage, S. A., N. Giri, G. M. Baerlocher, N. Orr, P. M. Lansdorp, and B. P. Alter**. 2008. TINF2, a component of the shelterin telomere protection complex, is mutated in dyskeratosis congenita. Am J Hum Genet **82**:501-509.

97. **Sbodio, J. I., and N. W. Chi**. 2002. Identification of a tankyrase-binding motif shared by IRAP, TAB182, and human TRF1 but not mouse TRF1. NuMA contains this RXXPDG motif and is a novel tankyrase partner. J Biol Chem **277**:31887-31892.

98. **Sbodio, J. I., H. F. Lodish, and N. W. Chi**. 2002. Tankyrase-2 oligomerizes with tankyrase-1 and binds to both TRF1 (telomere-repeat-binding factor 1) and IRAP (insulin-responsive aminopeptidase). Biochem J **361**:451-459.

99. **Schwartz, M., E. Zlotorynski, and B. Kerem**. 2006. The molecular basis of common and rare fragile sites. Cancer Lett **232**:13-26.

100. **Seimiya, H., Y. Muramatsu, T. Ohishi, and T. Tsuruo**. 2005. Tankyrase 1 as a target for telomere-directed molecular cancer therapeutics. Cancer Cell **7**:25-37.

101. **Seimiya, H., Y. Muramatsu, S. Smith, and T. Tsuruo**. 2004. Functional subdomain in the ankyrin domain of tankyrase 1 required for poly(ADP-ribosyl)ation of TRF1 and telomere elongation. Mol Cell Biol **24**:1944-1955.

102. **Seimiya, H., and S. Smith**. 2002. The telomeric poly(ADP-ribose) polymerase, tankyrase 1, contains multiple binding sites for telomeric repeat binding factor 1 (TRF1) and a novel acceptor, 182-kDa tankyrase-binding protein (TAB182). J Biol Chem **277**:14116-14126.

103. **Sfeir, A. J., W. Chai, J. W. Shay, and W. E. Wright**. 2005. Telomere-end processing the terminal nucleotides of human chromosomes. Mol Cell **18**:131-138.

104. **Shampay, J., and E. H. Blackburn**. 1988. Generation of telomere-length heterogeneity in Saccharomyces cerevisiae. Proc Natl Acad Sci USA **85**:534-538.

105. **Silver, D. P., and D. M. Livingston**. 2001. Self-excising retroviral vectors encoding the Cre recombinase overcome Cre-mediated cellular toxicity. Mol Cell **8**:233-243.

106. **Smith, S., and T. de Lange**. 1999. Cell cycle dependent localization of the telomeric PARP, tankyrase, to nuclear pore complexes and centrosomes. J Cell Sci **112**:3649-3656.

107. **Smith, S., and T. de Lange**. 2000. Tankyrase promotes telomere elongation in human cells. Curr Biol **10**:1299-1302.

108. **Smith, S., I. Giriat, A. Schmitt, and T. de Lange**. 1998. Tankyrase, a poly(ADP-ribose) polymerase at human telomeres. Science **282**:1484-1487.

109. **Smogorzewska, A., and T. de Lange**. 2002. Different telomere damage signaling pathways in human and mouse cells. Embo J **21**:4338-4348.

110. **Smogorzewska, A., J. Karlseder, H. Holtgreve-Grez, A. Jauch, and T. de Lange**. 2002. DNA Ligase IV-Dependent NHEJ of Deprotected Mammalian Telomeres in G1 and G2. Curr Biol **12**:1635.

111. **Smogorzewska, A., B. van Steensel, A. Bianchi, S. Oelmann, M. R. Schaefer, G. Schnapp, and T. de Lange**. 2000. Control of human telomere length by TRF1 and TRF2. Mol Cell Biol **20**:1659-1668.

112. **Song, K., D. Jung, Y. Jung, S. G. Lee, and I. Lee**. 2000. Interaction of human Ku70 with TRF2. FEBS Lett **481**:81-85.

113. **Sprung, C. N., G. Afshar, E. A. Chavez, P. Lansdorp, L. Sabatier, and J. P. Murnane**. 1999. Telomere instability in a human cancer cell line. Mutat Res **429**:209-223.

114. **Sprung, C. N., G. E. Reynolds, M. Jasin, and J. P. Murnane**. 1999. Chromosome healing in mouse embryonic stem cells. Proc Natl Acad Sci USA **96**:6781-6786.

115. **Stansel, R. M., T. de Lange, and J. D. Griffith**. 2001. T-loop assembly in vitro involves binding of TRF2 near the 3' telomeric overhang. EMBO J **20**:5532-5540.

116. **Sutherland, G. R**. 1991. Chromosomal fragile sites. Genet Anal Tech Appl **8**:161-166.

117. **Takai, H., A. Smogorzewska, and T. de Lange**. 2003. DNA damage foci at dysfunctional telomeres. Curr Biol **13**:1549-1556.

118. **Tauchi, H., J. Kobayashi, K. Morishima, D. C. van Gent, T. Shiraishi, N. S. Verkaik, D. vanHeems, E. Ito, A. Nakamura, E. Sonoda, M. Takata, S. Takeda, S. Matsuura, and K. Komatsu**. 2002. Nbs1 is essential for DNA repair by homologous recombination in higher vertebrate cells. Nature **420**:93-98.

119. **Undarmaa, B., S. Kodama, K. Suzuki, O. Niwa, and M. Watanabe**. 2004. X-ray-induced telomeric instability in Atm-deficient mouse cells. Biochem Biophys Res Commun **315**:51-58.

120. **van Overbeek, M., and T. de Lange**. 2006. Apollo, an Artemis-related nuclease, interacts with TRF2 and protects human telomeres in S phase. Curr Biol **16**:1295-1302.

121. **van Steensel, B., and T. de Lange**. 1997. Control of telomere length by the human telomeric protein TRF1. Nature **385**:740-743.

122. **van Steensel, B., A. Smogorzewska, and T. de Lange**. 1998. TRF2 protects human telomeres from end-to-end fusions. Cell **92**:401-413.

123. **Verdun, R. E., and J. Karlseder**. 2006. The DNA damage machinery and homologous recombination pathway act consecutively to protect human telomeres. Cell **127**:709-720.

124. **Vulliamy, T., A. Marrone, F. Goldman, A. Dearlove, M. Bessler, P. J. Mason, and I. Dokal**. 2001. The RNA component of telomerase is mutated in autosomal dominant dyskeratosis congenita. Nature **413**:432-435.

125. **Walne, A. J., T. Vulliamy, A. Marrone, R. Beswick, M. Kirwan, Y. Masunari, F. H. Al-Qurashi, M. Aljurf, and I. Dokal**. 2007. Genetic heterogeneity in autosomal recessive dyskeratosis congenita with one subtype due to mutations in the telomerase-associated protein NOP10. Hum Mol Genet **16**:1619-1629.

126. **Wang, F., E. R. Podell, A. J. Zaug, Y. Yang, P. Baciu, T. R. Cech, and M. Lei**. 2007. The POT1-TPP1 telomere complex is a telomerase processivity factor. Nature **445**:506-510.

127. **Wang, R. C., A. Smogorzewska, and T. de Lange**. 2004. Homologous recombination generates T-loop-sized deletions at human telomeres. Cell **119**:355-368.

128. **Watson, J. D**. 1972. Origin of concatemeric T7 DNA. Nat New Biol **239**:197-201.

129. **Wu, L., A. S. Multani, H. He, W. Cosme-Blanco, Y. Deng, J. M. Deng, O. Bachilo, S. Pathak, H. Tahara, S. M. Bailey, Y. Deng, R. R. Behringer, and S. Chang**. 2006. Pot1 deficiency initiates DNA damage checkpoint activation and aberrant homologous recombination at telomeres. Cell **126**:49-62.

130. **Xin, H., D. Liu, M. Wan, A. Safari, H. Kim, W. Sun, M. S. O'Connor, and Z. Songyang**. 2007. TPP1 is a homologue of ciliate TEBP-beta and interacts with POT1 to recruit telomerase. Nature **445**:559-562.

131. **Yamaguchi-Iwai, Y., E. Sonoda, M. S. Sasaki, C. Morrison, T. Haraguchi, Y. Hiraoka, Y. M. Yamashita, T. Yagi, M. Takata, C. Price, N. Kakazu, and S. Takeda**. 1999. Mre11 is essential for the maintenance of chromosomal DNA in vertebrate cells. Embo J **18**:6619-6629.

132. **Yamaguchi, H., R. T. Calado, H. Ly, S. Kajigaya, G. M. Baerlocher, S. J. Chanock, P. M. Lansdorp, and N. S. Young**. 2005. Mutations in TERT, the gene for telomerase reverse transcriptase, in aplastic anemia. N Engl J Med **352**:1413-1424.

133. **Ye, J. Z., and T. de Lange**. 2004. TIN2 is a tankyrase 1 PARP modulator in the TRF1 telomere length control complex. Nat Genet **36**:618-623.

134. **Ye, J. Z., J. R. Donigian, M. Van Overbeek, D. Loayza, Y. Luo, A. N. Krutchinsky, B. T. Chait, and T. de Lange**. 2004. TIN2 binds TRF1 and TRF2 simultaneously and stabilizes the TRF2 complex on telomeres. J Biol Chem **279**:47264-47271.

135. **Ye, J. Z., D. Hockemeyer, A. N. Krutchinsky, D. Loayza, S. M. Hooper, B. T. Chait, and T. de Lange**. 2004. POT1-interacting protein PIP1: a telomere length regulator that recruits POT1 to the TIN2/TRF1 complex. Genes Dev **18**:1649-1654.

136. **Zhou, X. Z., and K. P. Lu**. 2001. The Pin2/TRF1-Interacting Protein PinX1 Is a Potent Telomerase Inhibitor. Cell **107**:347-359.

137. **Zhu, X. D., B. Kuster, M. Mann, J. H. Petrini, and T. de Lange**. 2000. Cell-cycle-regulated association of RAD50/MRE11/NBS1 with TRF2 and human telomeres. Nat Genet **25**:347-352.

138. **Zhu, X. D., L. Niedernhofer, B. Kuster, M. Mann, J. H. Hoeijmakers, and T. de Lange**. 2003. ERCC1/XPF Removes the 3' Overhang from Uncapped Telomeres and Represses Formation of Telomeric DNA-Containing Double Minute Chromosomes. Mol Cell **12**:1489-1498.

139. **Zou, L., and S. J. Elledge**. 2003. Sensing DNA damage through ATRIP recognition of RPA-ssDNA complexes. Science **300**:1542-1548.